UNITED NATIONS UNIVERSITY

UNU-GTP

ORKUSTOFNUN

Meyjarauga hot spring, Hveravellir, Kjölur, Central Iceland

Samuel Ikinya Ng'ang'a

WELLBORE STABILITY – PRINCIPLES AND ANALYSIS IN GEOTHERMAL WELL DRILLING

Report 2
November 2018

UNITED NATIONS UNIVERSITY
UNU-GTP
Geothermal Training Programme

Orkustofnun, Grensasvegur 9,
IS-108 Reykjavik, Iceland

Reports 2018
Number 2

WELLBORE STABILITY – PRINCIPLES AND ANALYSIS IN GEOTHERMAL WELL DRILLING

MSc Thesis
Master of Science in Sustainable Energy Engineering
Iceland School of Energy
Reykjavik University

by

Samuel Ikinya Ng'ang'a
Kenya Electricity Generating Company Ltd
P.O Box 785-20117
Naivasha
Kenya
snganga@kengen.co.ke

United Nations University
Geothermal Training Programme
Reykjavík, Iceland
Published in November 2018

ISBN 978-9979-68-479-4 (PRINT)
ISBN 978-9979-68-480-0 (PDF)
ISSN 1670-7427

This MSc thesis has also been published in June 2018 by the
Iceland School of Energy
Reykjavik University

INTRODUCTION

The Geothermal Training Programme of the United Nations University (UNU) has operated in Iceland since 1979 with six-month annual courses for professionals from developing countries. The aim is to assist developing countries with significant geothermal potential to build up groups of specialists that cover most aspects of geothermal exploration and development. During 1979-2018, 694 scientists and engineers from 61 developing countries have completed the six month courses, or similar. They have come from Africa (39%), Asia (35%), Latin America (14%), Europe (11%), and Oceania (1%). There is a steady flow of requests from all over the world for the six-month training and we can only meet a portion of the requests. Most of the trainees are awarded UNU Fellowships financed by the Government of Iceland.

Candidates for the six-month specialized training must have at least a BSc degree and a minimum of one-year practical experience in geothermal work in their home countries prior to the training. Many of our trainees have already completed their MSc or PhD degrees when they come to Iceland, but many excellent students with only BSc degrees have made requests to come again to Iceland for a higher academic degree. From 1999, UNU Fellows have also been given the chance to continue their studies and study for MSc degrees in geothermal science or engineering in co-operation with the University of Iceland. An agreement to this effect was signed with the University of Iceland. A similar agreement was also signed with Reykjavik University in 2013. The six-month studies at the UNU Geothermal Training Programme form a part of the graduate programme.

It is a pleasure to introduce the 58th UNU Fellow to complete the MSc studies under a UNU-GTP Fellowship. Samuel Ikinya Ng'ang'a, Mechanical Engineer from the Kenya Electricity Generating Company, Ltd. - KenGen in Kenya, completed the six-month specialized training in *Drilling Technology* at UNU Geothermal Training Programme in October 2014. His research report was entitled: *Cementing processes in geothermal well drilling: application and techniques.* After two years of geothermal work for KenGen at the Olkaria geothermal field in Kenya, he came back to Iceland for MSc studies at Iceland School of Energy, Reykjavik University in July 2016. In April 2018, he defended his *MSc thesis* in *Sustainable Energy Engineering* presented here, entitled: *Wellbore stability – principles and analysis in geothermal well drilling*. His studies in Iceland were financed by the Government of Iceland through a UNU-GTP Fellowship from the UNU Geothermal Training Programme. We congratulate Samuel on the achievements and wish him all the best for the future. We thank Iceland School of Energy, Reykjavik University, for the co-operation, and his supervisors for the dedication.

Finally, I would like to mention that Samuel's MSc thesis with the figures in colour is available for downloading on our website *www.unugtp.is*, under publications.

With warmest greetings from Iceland,

Lúdvík S. Georgsson, Director
United Nations University
Geothermal Training Programme

ACKNOWLEDGEMENTS

I wish to express my gratitude to the Government of Iceland, the United Nations University, Geothermal Training program (UNU-GTP) and Kenya Electricity Generating Company, Ltd. (KenGen) for granting me this study opportunity and supporting my stay in Iceland.

I am thankful to the UNU-GTP staff: Director, Lúðvík S. Georgsson, Deputy Director Ingimar G Haraldsson, Thórhildur Ísberg, Markús A.G. Wilde and Málfríður Ómarsdóttir, for their pleasant encouragement, support and guidance during my studies.

Special thanks to my supervisors Dr. Juliet Newson and the late Björn Már Sveinbjörnsson for their selfless guidance, input and support in the writing of this report. I am grateful to Sverrir Thórhallsson for dedicating his time to read the report, meetings and providing professional advice.

Am indebted to my colleagues from KenGen, fellows at UNU-GTP, my friends and classmates at Iceland school of energy for their support and providing information to complete this report.

Sincere gratitude to my family for the inspiration, motivation and moral support throughout the duration of my studies.

Thank you God for making everything possible.

DEDICATION

I dedicate this work to my beloved wife, daughter and son.

ABSTRACT

Drilling a stable geothermal well that experiences least drilling challenges is key to delivering a successful well that meets the set objective of either being a production or reinjection well. Wellbore instabilities encountered during drilling can add to the overall cost of the well by consumption of more materials and extension of well completion time. Olkaria geothermal field in Kenya is a high temperature field and wells are designed with 20" surface casing, 13⅜" anchor casing, 9⅝" production casing and the production section is lined with 7" perforated liner. Drilling progress is affected by various downhole challenges such as loss of drilling fluid circulation and borehole wall collapse that lead to stuck drilling string, problems in landing casings and liners and in extreme cases loss of irretrievable part of drill string and abandonment of the well. Well sections with less drilling problems affecting drilling progress have high percentage of time spent on drilling activity but wells that encountered downhole challenges have less drilling time compared to other activities that do not add to the well depth.

Geothermal wells in Olkaria at well pad OW-731 and well RN-33 in Reykjanes Iceland have been used in this report. Reassessment of minimum casing setting depths for 3000 m deep Olkaria wells was made according to the The African Union Code of Practice for Geothermal Drilling (2016). The criteria applied for this report was for the formation temperature and pressure to follow the boiling pressure for depth (BPD) curve based on a water level at 700 m and the effective containment pressure resulting to a vertical Production Casing depth of 1450 m. The pressure pivot point is lacking in the directional well indicating need for a deeper production casing setting depth. Minimum stress S_h calculated using Eaton´s formula and overburden stress S_v form the maximum and minimum field stresses used to calculate effective hoop, radial and vertical stresses on the wellbore wall. Maximum compressive hoop stress occurs at 90° and 270° and minimum hoop stress at 0° and 180° in vertical well indicating the direction of minimum and maximum horizontal stresses measured clockwise from North (0° azimuth). In directional wells, the hoop stresses are dependent on the well inclination and azimuth. Directional wells at OW-731 pad are inclined to approximately 20° from the vertical at different azimuths but indicate difference effective stresses. Well RN-33 with an inclination angle of 30° at azimuth of 171° has the highest hoop stresses at 96°/276° followed by OW-731D (200°), OW-731B (225°), OW-731A (135°) and OW-731C (270°) with the least measured clockwise from North (0° azimuth).

Mohr´s circle diagrams using effective stresses at different depths and drilling fluid densities 0, 500, 800, 1000 1200 and 1800 kg/m3, indicate compressive failure that induces wellbore collapse during loss of circulation at all depths. Tensile failure that can result in fracturing occurs in all depths at 1.8 SG because of high radial stresses. Wellbore stability is maintained with drilling fluid density between 0.8-1.2 SG. The average of estimated formation pressure and calculated minimum stress gives a ratio of 0.60 to 0.73 for minimum stress that corresponds to an ECD of 0.60 to 0.93 SG from 750 to 3000 m giving a range of drilling fluid variation.

TABLE OF CONTENTS

LIST OF FIGURES

LIST OF TABLES

LIST OF ABBREVIATIONS

ABI	Acoustic Borehole Imaging
AU	African Union
BHA	Bottom Hole Assembly
BHCT	Bottom Hole Circulating Temperature
BHST	Bottom Hole Static Temperature
BOP	Blow Out Preventer
BPD	Boiling Pressure for Depth
BWOC	By Weight of Cement
DTH	Down the Hole Hammer
FPP	Fracture Propagating Pressure
ECD	Equivalent Circulation Density
ECP	Effective Containment Pressure
ELOT	Extended Leak Off Test
ESD	Equivalent Static Density
FLOT	Formation Leak Off Tests
FPP	Fracture Propagation Pressure
IADC	International Association of Drilling Contractors
KOP	Kick off Point
Lbf	Pounds per foot
LCM	Loss of Circulation Material
LOC	Loss of Circulation
LWD	Logging While Drilling
M.a.s.l	Meters above sea level
mRKB	Meters from Rotary Kelly Bushing
MD	Measured Depth
MDP	Maximum Design Pressure
MWD	Measurement While Drilling
NPT	Non-Productive Time
OD	Outside Diameter
OW	Olkaria Well
PDC	Polycrystalline Diamond Compact
POOH	Pulling Out Of Hole
RIH	Running In Hole
RKB	Rotary Kelly Bushing
ROP	Rate of Penetration
RPM	Revolutions per Minute
SG	Specific Gravity
SPM	Strokes per Minute
TD	Total Depth
TVD	Total Vertical Depth
UCS	Unconfined Compressive Strength
WOC	Wait on Cement
XLOT	Extended Leak Off Test

1. INTRODUCTION

In this thesis, review of wellbore stability is discussed with regard to drilling in the Olkaria geothermal field in Kenya. Data from wells drilled in Olkaria geothermal project are analysed in terms of drilling days taken to complete drilling. The challenges experienced during drilling are partly associated with wellbore stability, contribute to the overall cost of the well and power plant. Analysis takes into account the different well sections (diameters), stability problems or problems encountered during drilling and the contribution to the total Non-Productive Time (NPT) of the total drilling time.

Olkaria geothermal field is located within a volcanic complex in southern part of the Kenyan East African Rift System and has North-South trending normal rifting faults traversing across the field (Munyiri, 2016). The field is classified as high enthalpy geothermal field with temperatures above 200°C below 1000 m. Using the Resource Code proposed by Sanyal (2005), the field can be classified as Code 5 (high temperature) with temperature between 230 and 300°C (Sveinbjörnsson, 2014). Over three hundred wells have been drilled to date in the field supporting over 650 MW of electricity generation (Ouma et al., 2016). The early wells were drilled to a depth of less than 2000 m targeting shallow steam dominated reservoir above the deeper liquid dominated reservoir (Grant and Bixley, 2011). With the expansion to other sectors of the Olkaria Field and need for high productive wells, most of the wells drilled after the year 2007 range from 2000 to 3000 m. Well drilling represents a significant portion of geothermal development cost and accounts for 30 to 50% of the total cost of a geothermal plant (Finger and Blankenship, 2010; European Union, 2015). Improvement of drilling practices have the potential of lowering the well cost. For this analysis of challenges encountered during drilling operations and their solutions is essential. Delay in project completion increases project cost and affects implementation of other related projects (Larson and Gray, 2011).

The geological setting of the geothermal field/reservoir presents various difficulties during drilling that are sometimes amplified by high temperature, pressure, fractures and abrasiveness of the formation being drilled (Finger and Blankenship, 2010). Stability of a well during drilling can be improved if there is no extreme variations in drilling parameters such as ROP drilling pressure or critical operations such as cementing. Wellbore instability can results in loss of drilling fluid circulation, wellbore collapse, drill string sticking, caving and requires measures to counter during drilling. Instability leads to extra operations such as fishing to remove drilling tools, cementing to stabilize collapsing formations, side tracking to change the well course in order to bypass the problem and in extreme cases instability can result in total abandonment of the well (Jiménez et al., 2007). Drilling reports, analyses and logs provide valuable information on the area being drilled and help in better decision making and problem-solving approaches.

Conventional rotary drilling method using tri-cone or Polycrystalline Diamond Compact (PDC) rock bits is mainly used in geothermal drilling. Hammer (air or hydraulic) drilling combining rotary and percussion has the potential to increase the rate of drilling in hard formations but is not often used in deep drilling (European Union, 2015). Tests of using down the hole air hammers (DTH) in Olkaria Field to drill the 17½" Anchor Casing section did not achieve much success. It was tried in two wells and in both wells ended with fishing operation to retrieve broken air hammer pieces in the wells (KenGen, 2013-40A; KenGen, 2014 OW-49). Understanding the downhole conditions during drilling and correlating it to the geothermal field geology aids in predicting the drilling challenges in each borehole section.

Well stability study in a geothermal field such as Olkaria can assist in understanding the interaction between the drill bit, drilling fluids and formation, resulting in proper adjustments of drilling parameters accordingly (Tariq, 2014). Dividing a geothermal well into sections, namely Surface Casing, Anchor Casing, Production Casing and production section, having slotted liners and analysing time allocation for the various activities in the sections gives the indicator of which well section contributes to the highest ratio of Non-Productive Time (NPT) of drilling. Well sections with few drilling problems have high percentage of time spent on drilling activity but wells that encountered downhole challenges have less drilling time compared to other activities that do not add to the well depth. Wells from different parts of the Olkaria Field are compared in this report an effort of highlighting which sectors in the

geothermal field has high likelihood of drilling problems. Well planning and a drilling program incorporates well instability such as well collapse, fractures, and drill string sticking. Such studies also provide an input to build a geo-mechanical model of the field (Schoenball et al., 2016).

Downhole logging of a geothermal well for measurement of parameters during drilling are conducted before running casing/liner or after casing and cementing is completed. Logging before running casing or liner into the well is referred to as open hole logging.). Open hole logging during drilling include caliper, temperature, pressure and resistivity logs (Steingrímsson, 2011; Steingrímsson and Gudmundsson, 2006). After running and cementing of casing, cement bond log (CBL) is carried out for quality evaluation of the cementing job. Well completion logging, simulation and testing is carried out after the final well depth is achieved and running of the liner (Haraldsdóttir, 2016). Logging or measurements also conducted inside the drill string for pressure, temperature and directional surveys as drilling progresses Pressure and temperature logging of a geothermal well during drilling is important especially at casing setting depths. The results are for example used for the cement slurry design in determining the percentages of additives to be used (Nelson, 1990). Pressure pivot point is used in determination of the Production Casing depth (Tulinius, 2016). Logging during the time of drilling is essential when evaluating wellbore stability problems and the data acquired forms an important input in well design (Steingrímsson, 2011).

The caliper log measures the diameter of the well and displays the geometry of the wellbore. Data from caliper tool reveals the layers of rock formations intersected during drilling and their strength by matching it with drill cuttings in lithological logs. Where the well intersects soft formation, the diameter tends to be greater than the bit diameter due to erosion action by drilling fluids. Compact rock formation will record diameter close to the bit diameter. Likewise, collapsing sections of the well recorded as large cavities form indicators of probable instability depths along the wellbore (Steingrímsson, 2011). Other uses of caliper log are estimation of cement volume requirement, depths for casing centralization, casing damages, corrosion and direction of wellbore breakouts (Fjaer et al., 2008). Borehole imaging log (televiewer) is used to record fractures or structures, their inclination and direction encountered during well drilling. The imaging tool records travel time and amplitude of the acoustic (ultrasonic) wave reflected by the borehole wall. Travel time increases with increase in wellbore diameter such as in cavities created by collapsing formation. Change in the wave amplitude indicates fractures and different formation layers (Zoback, 2010). Zones of instability such as borehole breakouts can be clearly detected using image log and the direction in which they are occurring (Fjaer et al., 2008). In this report, caliper and borehole image (televiewer) logs from well RN-33 in Reykjanes Field in Iceland (Níelsson et al., 2014; Árnadóttir et al., 2014) is used to demonstrate downhole instability encountered during drilling.

1.1 Background

Drilling a new well offsets the existing formation balance since drilling involves material removal from the formation. Managing drilling parameters to balance out the forces acting within the wellbore wall is critical to the stability of the well. Achieving full circulation of drilling fluid during drilling improves cutting transport out the borehole but this is not usually the case in geothermal well drilling (Economides et al., 1998). Wellbore stability during drilling is affected by frequent loss of drilling fluid encountered and formation collapse in unconsolidated or loose formation layers and at formation layers boundaries that hinders drilling progress. Without proper fluid circulation and having erosion of the borehole wall, cuttings and formation materials accumulate downhole slowing down drilling rate and create conditions for a stuck drill string. Instabilities during geothermal drilling significantly affect final well cost, as more materials and time have to be spent in mitigating them. Loss of drilling fluid circulation is the main cause of most drilling problems in Olkaria geothermal field (Aadnoy and Looyeh, 2011; Fjaer et al., 2008; Mitchell and Miska, 2011).

Olkaria geothermal field is divided into seven geographical sectors namely Olkaria East, Olkaria Northeast, Olkaria Central, Olkaria Northwest, Olkaria West, Olkaria Southeast and Olkaria Domes (Mbithi, 2016). Figure 1 shows the four sectors of the field from which well data have been used in the report.

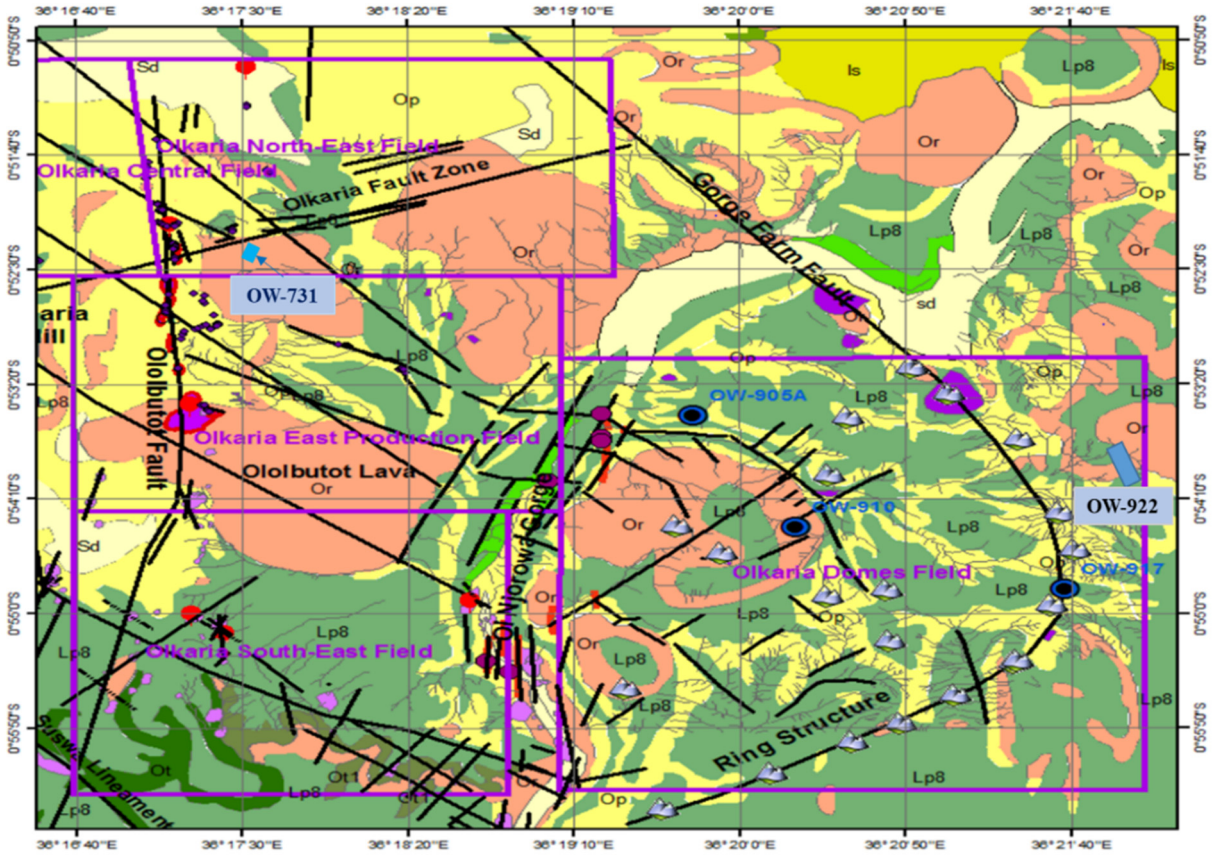

FIGURE 1: Geothermal field sectors in Olkaria, Kenya (Musonye, 2015)

1.2 Problem definition

Geothermal well drilling constitutes the biggest cost of the entire geothermal project. By evaluating drilling activities in a geothermal well, difficulties and challenges can be used in well planning in terms of materials, equipmen8t), tools and how they contribute to the overall cost of a geothermal power project. Understanding of wellbore stability and factors that lead to instability during drilling can be used to manage drilling operations. Table 1 shows the cost of drilling services and materials for twelve wells drilled to 3000 m in Olkaria with the number of working days. The figures show clearly how cost rises significantly with increased number of working days.

TABLE 1: Drilling services and material cost (KenGen, 2017 - Drilling)

Well	Depth (m)	Days	Drilling services costs (USD)	Drilling materials (USD)
OW-925	3000	31	2,158,502	720,089
OW-4V	3000	44	3,117,742	885,563
OW-805D	3000	55	3,166,091	979,285
OW-4A	3000	57	3,951,628	1,058,193
OW-805	3000	61	3,273,093	953,378
OW-731C	3000	62	3,863,965	1,010,200
OW-805C	3000	75	4,212,336	963,035
OW-731B	3000	78	5,062,743	1,043,445
OW-731	3000	85	4,665,167	1,286,361
OW-731A	3000	96	6,058,783	1,432,111
OW-731D	3010	106	6,280,338	1,504,342
OW-922	3000	157	8,988,290	1,613,206

The main contributors to delays in well drilling progress are wellbore instabilities during drilling as discussed in this report. Five wells drilled at same well pad OW-731 had various wellbore instabilities during drilling which affected their completion and well costs. The drilling progress, pressure and temperature logs of well OW-922 that took the highest number of days (157 days) to complete due to wellbore instabilities during drilling is included in this report. Because of loss of circulation, collapsing formations and tight hole (creep), many hours/days were spent in reaming, circulation and waiting on cement.

1.3 Thesis objectives

The main objective of this thesis is to review and analyse wellbore instability concerns in geothermal well drilling in the Olkaria geothermal field. A review is given on wellbore stability in geothermal drilling in terms of Equivalent Circulation Density (ECD), pore pressure gradient and formation strength. The objective is to obtain geomechanic models to use while drilling, so it would be possible to prevent instability problems, reduce NPT and drilling cost. The main topics addressed in this work are:

- Main causes of wellbore instability;
- Mechanical failure - stresses at the wellbore walls;
- Drilling fluid circulation and well stability;
- Instabilities Case studies of wells;
- Stress analysis of vertical and directional wells;
- Compare available drilling data and practices in Iceland.

2. REVIEW OF WELLBORE STABILITY

Well drilling upsets the formation balance that exists before formation removal through the action of the drill bit. Drilling fluids, either mud, air, aerated mud or foam assists in wellbore support as well as in removal of cuttings generated by drilling. Maintaining the correct flowrates of the drilling fluids influences wellbore stability and lower the chances of formation damages during drilling. This is usually difficult to achieve during geothermal well drilling because of frequent loss of circulation caused by the highly fractured formations encountered in geothermal fields such as Olkaria (Grant and Bixley, 2011). Delivering a cost effective well is related to managing problems encountered during drilling and optimizing the drilling progress (Devereux, 1998; Aadnoy and Looyeh, 2011; Immerstein, 2013)

2.1 Wellbore stability

Incorporating wellbore stability in the drilling program is essential as it highlights the likely sections in the well that have high probability of instability. Considering the geology of the field, diverse formations at different well depths provide a guide of the likely failure mechanisms and ways of avoiding or managing them. Loose hyaloclastite or tuff formations to hard granitic rocks are observed to occur in geothermal fields (Musonye, 2015). Loose formation has a high likelihood of well collapse and zones of drilling fluid circulations while hard formations slow down the drilling progress. In addition to geological aspect of the field, in-situ stresses, pore pressure, temperature, open hole and depth have an impact on geothermal drilling operations. According to Devereux (Devereux, 1998), the following factors influence stability:

- Drilling fluids used;
- Type of rock and properties;
- Rock stresses;
- Drilling practices - connections and tripping;
- Bottom Hole Assembly (BHA).

2.2 Sub-surface condition

According to the African Union Code of Practice for Geothermal Drilling (African Union, 2016), information on the expected well path sub-surface conditions is important in planning for well instability challenges. In addition to pressure, temperature and reservoir fluid properties, the relevant geological information should be assessed including:

a) Lithology and stratigraphy of geological formations;
b) Rock alteration;
c) Compressive strength;
d) Faulting, fracturing and permeability;
e) Unstable formations and water sensitive swelling clays;
f) Fracture pressures from Formation Leak Off Tests FLOTs or from similar formations.

2.3 Formation Leak Off Test (FLOT)

Formation Leak Off Tests (FLOT) is conducted after casing cementing to evaluate formation strength and cement integrity. The test is aimed at ensuring that the formation at the casing shoe is strong enough to contain fluid flow to the higher formations, determine open hole strength for the next drilling phase, establish pressure magnitude that the well can withstand and determine the fracture gradient (earth minimum horizontal stress) (Rabia, 2001).

The FLOT procedure involves drilling 4 to 6 m, below the casing shoe into the formation, shutting in the well and pressurizing it by pumping water (or drilling fluid) at a slow and constant rate. Pressure builds up proportional to increasing volume (or time) giving a straight line in pressure against volume

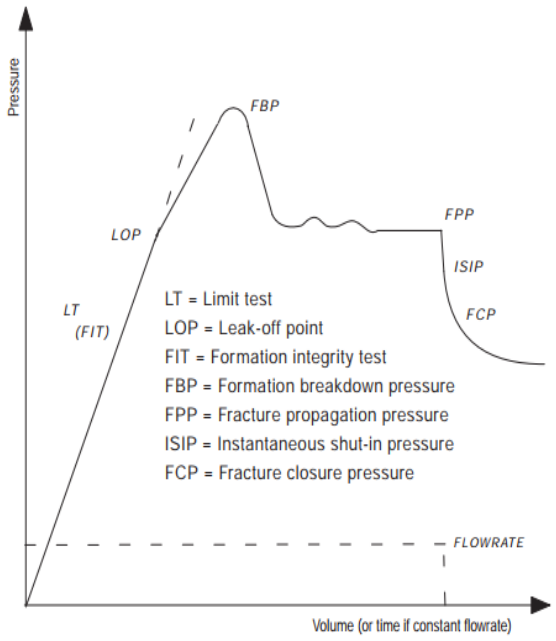

FIGURE 2: Leak Off and Extended Leak Off test graph (Zoback, 2010)

(time). Further increase in pumping time/volume reaches a point where pressure response starts to deviate from the straight line. The point of deviation is referred to as the leak-off point and defines the pressure (formation breakdown pressure) at which fracture starts to form in the formation (Zoback, 2010; (Mitchell and Miska, 2011). The FLOT and XLOT are illustrated in Figure 2.

After the leak off point the leak off test is usually stopped and the pressure drop recorded (Fjaer et al., 2008). The pressure at the leak off point is used to design in conjunction with other factors, the optimal drilling fluid weight for drilling the well section (Mitchell and Miska, 2011). Extended Leak Off Test (XLOT) involves pumping of drilling fluid beyond the leak off point at constant rate and will define the fracture propagation pressure (FPP) (Zoback, 2010). FLOT is recommended in the African code of practice to obtain the formation fracture pressure from nearby wells or other with similar conditions, but actual tests are often omitted.

2.4 Well instability

Well instability can be grouped into two categories namely mechanical related instability and physical-chemical. Mechanical related instability refers to the situation when there is collapse or failure in the wellbore due to stresses, erosion, pressures (surge and swab) and drill string action. Physical-chemical instability involves interactions between drilling fluids and formation that result to swelling or dispersion of the formation. Cases of wellbore instability are associated with stuck drill string, loss of circulation (LOC) tight spots, caving, wellbore collapse and sidetracking. These conditions result in increased cost and NPT of drilling operations (Fjaer et al., 2008).

2.5 Lost circulation

Geothermal formations are generally highly fractured and losses of drilling fluid are experienced during drilling (Grant, 2014). Circulation loss indicates feeder zones in the production section and point to the expected well output but it is not desired in other well sections that are cased and cemented. Losing the drilling fluids increases material cost since more than the planned amount of drilling fluid has to be used. In addition, lost circulation zones present difficulties in cementing work (Nelson, 1990). Healing lost circulation zones involves in extreme cases applying plug cementing to seal off the zones preventing drilling fluid loss into the formation. More cement is used as multiple plugs may have to be pumped that increases both the amount of cement and cementing time required. Waiting on Cement (WOC) contributes to the NPT of the rig (Azar and Samuel, 2007; Finger and Blankenship, 2010; Thórhallsson, 2017).

Lost Circulation Materials (LCM) such as Mica Flakes and Walnut shells provide alternative way of reducing lost circulation by mixing and pumping them together with the drilling fluids during drilling (Nelson, 1990). During drilling of Surface Casing section and Anchor Casing section, highly flocculating agents such as Starch are used to thicken the mud and therefore reducing mudflow into the formation. The other harmful effect of lost circulation is the loss of borehole cleaning ability. Without circulation, transport to surface of drill cuttings is not be possible causing accumulation of cuttings in the well as drilling continues. Loss of circulation creates potential situations for the drill string to be

stuck, borehole wall collapse because of lack of fluid pressure support and well control incidences due to steam flow in case of drilling steam zones (Economides et al., 1998; Mitchell and Miska, 2011).

2.6 Stuck drill string

Stuck drill string is classified as either differential or mechanical, depending on the cause of the condition. Differential sticking is caused by the pressure difference between wellbore and formation that holds the drill string against permeable formation. Mechanical sticking result from various causes that includes key seating, ineffective hole cleaning, under gauge borehole and wellbore instability (Rabia, 2001). Most of the stuck drill string experienced in Olkaria geothermal field drilling are mechanical caused mainly by well instability problems during drilling. The main contributor being loss of drilling fluid circulation that causes drill cuttings to accumulate in the well. Unstable fragmented formations can also collapse onto the BHA restricting its movement (Bourgoyne et al., 1986).

If the wellbore pressure is higher than the formation pressure, the pressure difference between the wellbore and formation can hold the drill string against the wellbore walls resulting in differential sticking. In differential sticking situations, the drill string can neither be rotated nor moved up or down but the well can be circulated with the drilling fluid (Devereux, 1998). Solution to differential sticking includes impact loading (jarring) by sudden loading and unloading of the drill string with the help of energy storing tools (jars) in the BHA and working the drill string immediately when a sticking condition is realized. Other solutions involve the use of soaking agents. Similar solutions are applicable to mechanical sticking. Most important for solving stuck drill string problems is to identify the causes. Having a feel of the well through monitoring and control of the necessary parameters can reduce chances of stuck drill string (Economides et al., 1998).

2.7 Collapsing formation

Having loose formations that are destabilized during drilling in sections of the wellbore results in part of the formation collapsing into the wellbore. Borehole collapse can also occur when the drilling-fluid pressure is too low to maintain the structural integrity of the drilled wellbore wall. The collapsed materials can bury the BHA or form a bridge around drill collars resulting in stuck drill string. The damages caused by collapsing formation sometimes can be irreparable and lead to abandonment of the well (Azar and Samuel, 2007) or cutting of the drilling string and drilling a sidetracked well. This is common in Olkaria geothermal drilling with occurrence of unconsolidated heterogeneous formation zones with low cohesion strength. Once the drill bit intersects these zones, there is high probability of collapse into the well. In addition, drilling fluid movement erode these zones creating cavities that curtail smooth movement of cuttings. Accumulated cuttings fall back once circulation is stopped (Musonye, 2015).

2.8 Well cleaning

The ability to remove cuttings generated by the drilling action and transport them from the well bottom back to surface is mainly dependent on the drilling fluid properties such as density, wellbore diameter and formation properties. Drilling fluid viscosity and flow rates affect its capacity to remove cuttings from the well. Other factors that influence borehole cleaning are drill string rotation, eccentricity, well condition and formation properties (Economides et al., 1998). Inadequate well cleaning results in cuttings settling above the drill collars and creating an obstacle that can prevent the drill string from being Pulled Out Of Hole (POOH). Other problems associated with borehole cleaning are high rate of drill bit wear, reduced Rate Of Penetration (ROP), formation fracturing, high torque and drag on the drill string, difficult in running casing and poor cementing. (Azar and Samuel, 2007). Maintaining correct drilling fluid parameters and drilling practices has the impact of achieving the desired well cleaning and minimize the associated problems (Rabia, 2001). Drilling fluid hydraulics and flow models are used to characterize drilling fluid properties (Baker Hughes, 1995).

3. ROCK MECHANICS IN WELLS

Rock mechanics is concerned with the mechanical behaviour of rocks when subjected to applied force (stress). Rock masses contain fractures and pressurized fluid is usually contained in the fractures and pores in the rock body (Jaeger et al., 2007). Drilling removes natural materials from the formation, creating a new circular free surface, and introduces fluids into the formation. Material removal alters the formation stresses and can initiate failure depending on the mechanical properties of the rock (Economides et al., 1998; Aadnoy and Looyeh, 2011).

Wellbore surface forms a stress concentration field and the forces acting within the well profile from the drilling fluids and formation pressure can result in well collapse and other problems. Wellbore failure occurs when the stress concentrated around the circumference of the well exceeds the formation strength (Zoback, 2010). Knowledge of stress magnitude and direction in a well helps solving problems associated with wellbore instability. The information assists in designing the optimal mud weight, casing setting point, cementing, drill bit performance and many other important parameters of well drilling operation (Zoback et al., 2003).

3.1 Rock properties

Mechanical properties of the rocks influence well response to the applied force. Compressive strength, fracture resistance, ductility due to loading and unloading, porosity and permeability are the rock properties that contribute to wellbore instability problems (Economides et al. 1998; Renpu, 2011).

3.2 Stress

Well drilling activities involve loading and unloading cycles and the stress-strain relationship demonstrates the material response to applied loads (Economides et al., 1998). Stress is force acting over an area and describes the density of forces passing through a given point. It can be resolved into normal stress σ, perpendicular to the surface, and shear stress τ, acting along the plane as illustrated in Figure 3 (Harrison and Hudson, 2000). Normal stress σ, is expressed in Equation 1:

$$\sigma = \frac{F_n}{A} \tag{1}$$

where F_n is the force acting normal to the surface area A, that results to either tensile or compressive stress.

Shear stress, τ results in material slip along the plane as expressed in Equation 2 where $F_p$is equal to the force parallel to the plane (Harrison and Hudson, 2000):

$$\tau = \frac{F_p}{A} \tag{2}$$

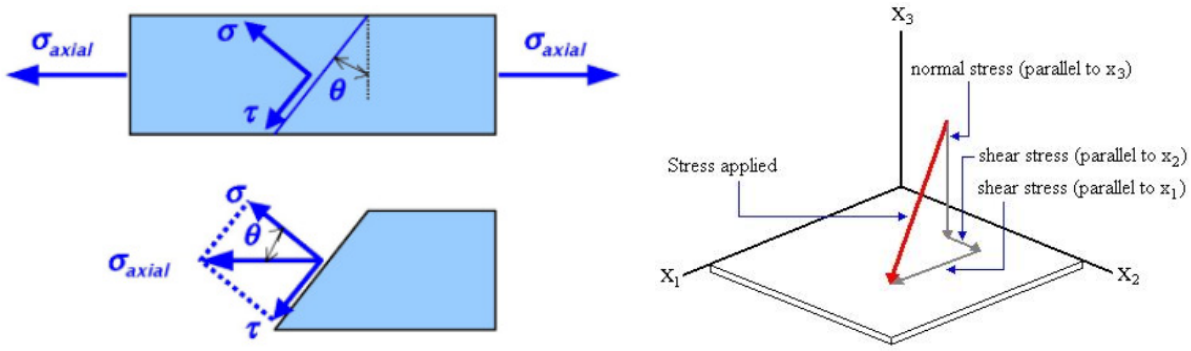

FIGURE 3: Stress acting on a plane from applied force (Aadnoy and Looyeh, 2011; Blanck, 2016)

The existing field stress state (in-situ stress) is used to analyse changes that take place due to drilling activity (Aadnoy and Looyeh, 2011).

3.3 Stress components

In three dimension, nine stress components are required to determine completely stress at a point. The stresses are identified with three planes oriented perpendicular to each other and are represented using a stress tensor (multi-component quantity, each of the components having magnitude and direction) (Fjaer et al., 2008). As illustrated in Figure 4 (Turcotte and Schubert, 2014), equal stresses act in opposite direction on each of the three sides of the cube for it to be in equilibrium. The stress components σ_{xx}, σ_{yy}, and σ_{zz} are normal stresses components and σ_{xy}, σ_{xz}, σ_{yx}, σ_{yz}, σ_{zx}, and σ_{zy} are the shear stress components τ_{ij} as expressed in Equation 3 (Aadnoy and Looyeh, 2011; Fjaer et al., 2008; Turcotte and Schubert, 2014):

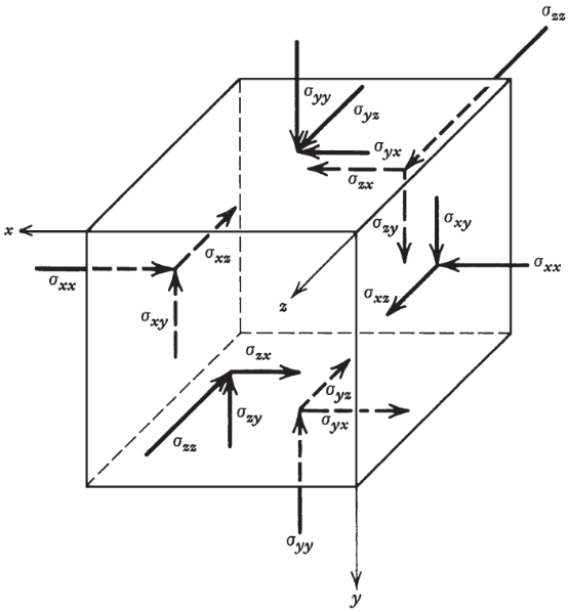

FIGURE 4: Stress components on three perpendicular planes (Turcotte and Schubert, 2014)

$$\sigma_{ij} = \begin{bmatrix} \sigma_{xx} & \sigma_{xy} & \sigma_{xz} \\ \sigma_{yx} & \sigma_{yy} & \sigma_{yz} \\ \sigma_{zx} & \sigma_{zy} & \sigma_{zz} \end{bmatrix} \quad (3)$$

In equilibrium, $\sigma_{xy} = \sigma_{yx}, \sigma_{xz} = \sigma_{zx}, \sigma_{yz} = \sigma_{zy}$, therefore the stress tensor reduces to six independent components, three normal stresses and three shear stresses as expressed in Equation 4 (Fjaer et al., 2008):

$$\sigma_{ij} = \begin{bmatrix} \sigma_{xx} & \sigma_{xy} & \sigma_{xz} \\ \sigma_{xy} & \sigma_{yy} & \sigma_{yz} \\ \sigma_{xz} & \sigma_{yz} & \sigma_{zz} \end{bmatrix} \quad (4)$$

3.4 Principal stresses

Principal stresses are resultant normal stresses in three perpendicular planes in which the shear stress components reduce to zero. The three perpendicular planes define the principal axes of the stress with only normal stresses as shown in Equation 5 (Kearey et al., 2002):

$$\sigma = \begin{bmatrix} \sigma_{11} & \sigma_{12} & \sigma_{13} \\ \sigma_{12} & \sigma_{22} & \sigma_{23} \\ \sigma_{13} & \sigma_{23} & \sigma_{33} \end{bmatrix} = \begin{bmatrix} \sigma_1 & 0 & 0 \\ 0 & \sigma_2 & 0 \\ 0 & 0 & \sigma_3 \end{bmatrix} \quad (5)$$

They represent the maximum, intermediate and minimum stresses denoted by σ_1, σ_2 and σ_3 and are perpendicular to each other (Fjaer et al., 2008). For any induced stress state in rock formation such as in drilling, the maximum and minimum normal stresses occur on the principal stress planes oriented parallel and perpendicular to the wellbore wall (Harrison and Hudson, 2000). One pre-existing principal stress in an area (in situ) is generally normal to the Earth's surface with the other two principal stresses acting in an approximately horizontal plane. To analyse state of stress at depth, field principal stress magnitudes S_v, the vertical stress, S_{Hmax} the maximum principal horizontal stress and S_{hmin}, the minimum principal horizontal stress are considered (Zoback, 2010).

3.4.1 Vertical stresses

The maximum vertical stress at any depth below the Earth's surface is the weight of the overburden (overlying formations). Overburden weight increases with increase in depth and the rock formation must

be able to support it (Turcotte and Schubert, 2014). When drilling into the rock formation, the bottom borehole stresses changes because the borehole fluid pressure is less than the overburden stress that originally acted on the rock and this allows rock expansion (Azar and Samuel, 2007). The magnitude of the principal vertical stress is the integral (sum) of the rock densities from surface to the depth of interest expressed in Equation 6 (Zoback, 2010):

$$S_v = \int_0^z \rho(z) g dz = \rho_1 g h_1 + \rho_2 g h_2 + \rho_3 g h_3 + \cdots + \rho_n g h_n \approx \rho_{av} g z \quad (6)$$

where S_v is the vertical stress, $\rho(z)$ is density as a function of depth, g is acceleration due to gravity, ρ_{av} is the average overburden density and dz or h is the formation thickness.

Overburden pressure is the sum of the rock material and the formation fluids in the pore space. The combined density of the rock and fluid is referred to as the bulk density given by Equation 7 (Rabia, 2001):

$$\rho_b = (1 - \emptyset)\rho_r + \emptyset \rho_f \quad (7)$$

where ρ_b is the bulk density, $\emptyset$ is the porosity, ρ_r is the rock density and ρ_f is the fluid density. Equation 8 therefore gives the overburden pressure in terms of bulk density (Rabia, 2001):

$$P_{ob} = \rho_b g h = \left[(1 - \emptyset)\rho_r + \emptyset \rho_f\right] g h \quad (8)$$

3.4.2 Horizontal stresses

The two horizontal principal stresses are maximum and minimum horizontal stresses perpendicular to the vertical stress. Their relative magnitudes are related to the tectonic setting that yields different faulting systems. According to Anderson's classification of tectonic stresses (Zoback, 2010) the faulting system active in an area can be either normal, reverse or strike-slip faulting depending on the magnitudes and orientation of the three principal stresses summarized in Table 2 and illustrated in Figure 5.

TABLE 2: Faulting system and associated field stresses (Zoback, 2010)

Faulting system (type)	**Stress**		
	S_1	**S_2**	**S_3**
Normal	S_v	S_{Hmax}	S_{hmin}
Reverse	S_{Hmax}	S_{hmin}	S_v
Strike-slip	S_{Hmax}	S_v	S_{hmin}

- Normal faulting: $S_v > S_{Hmax} > S_{hmin}$;
- Reverse faulting: $S_{Hmax} > S_{hmin} > S_v$;
- Strike-slip: $S_{Hmax} > S_v > S_{hmin}$.

Knowledge of the orientation and magnitudes of the principal stresses is critical while analysing wellbore stability.

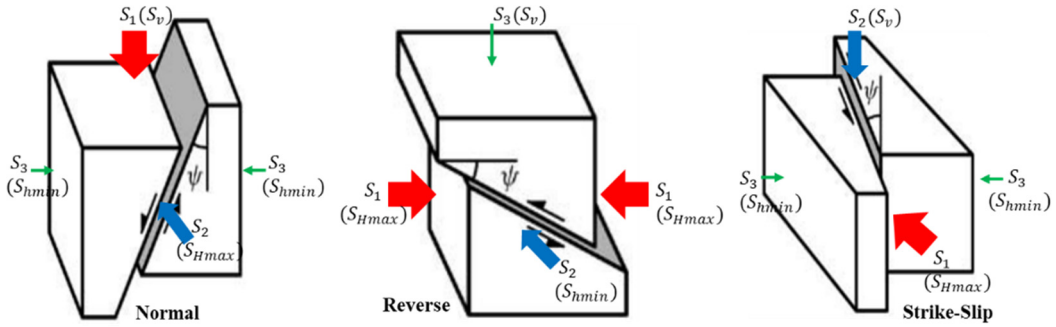

FIGURE 5: Faulting system types (Fjaer et al., 2008)

3.5 Pore (formation) pressure

Pore pressure (P_p) acts on the fluids in the pore spaces of the rock. It is related to the hydrostatic pressure (P_f) and increases with depth in normal conditions at a rate of 10 MPa/km (McNamara, 2017). Hydrostatic pressure is the pressure exerted by a column of fluid expressed in Equation 9 (Rabia, 2001):

$$P_f = \rho g h \tag{9}$$

where P_f is the hydrostatic pressure, ρ the fluid density, g is the gravitational acceleration and h is the height of the fluid column.

The highest possible pressure is equal to the overburden pressure as illustrated in Figure 6 using average vertical stress profile at lithostatic density of 2.6 g/cm^3 (average Earth´s crust density range 2.6-2.8 g/cm^3) and water density at 1g/cm^3 (McNamara, 2017). Three conditions of pore pressure are possible (Rabia, 2001):

1. Normal pore pressure when it is equal to the hydrostatic;
2. Abnormal pore pressure when it is higher than the hydrostatic pressure;
3. Subnormal when it is lower than the hydrostatic pressure.

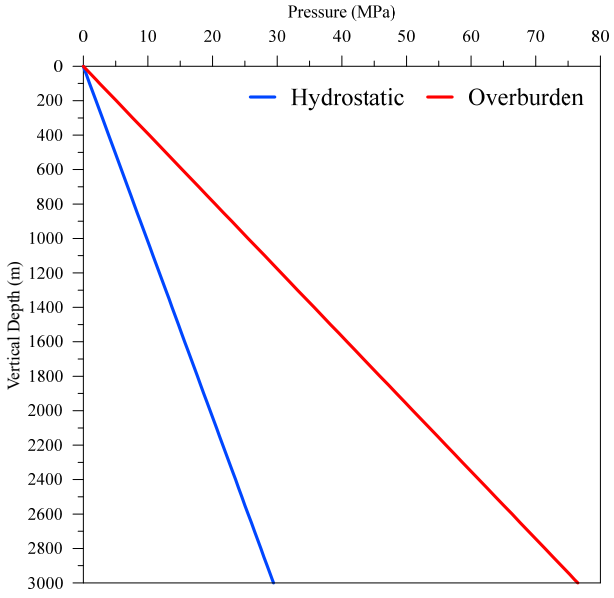

FIGURE 6: Hydrostatic pressure and overburden stress variation with depth (McNamara, 2017)

Pore pressure supports part of the formation load making the effective stress to be the difference between total normal stress and pore pressure in the failure strength of the rock formation expressed in Equation 10 for effective vertical stress:

$$\sigma_v = S_v - P_p \tag{10}$$

where $S_v$is the total overburden load, σ_v the effective vertical stress and P_p is the pore pressure.

Formation pressure reduces during utilization of the reservoir and can result in problems such as casing failure and subsidence. It can also affect near well porosity and permeability (Economides et al., 1998; Fjaer et al., 2008; Aadnoy and Looyeh, 2011; Bourgoyne et al., 1986)).

3.6 Stress around the wellbore

Drilling a circular wellbore and use of drilling fluid disturbs the existing stable formation and can lead to wellbore instability and borehole failure. Wellbore creates a new rock surface and new stress field that concentrates stress around the wellbore wall. If the concentrated stress exceeds the formation strength, failure will occur. The magnitude of the stress and the formation properties determine the nature of failure that can occur in the well (Aadnoy and Looyeh, 2011; Harrison and Hudson, 2000; Zoback, 2010)

In anisotropic condition, the principal stresses are not equal giving rise to existence of shear stresses. Kirsch Equations (Mitchell and Miska, 2011; Zoback, 2010) equations are used to express stress around wellbore wall. Stresses converge and align parallel and perpendicular to the wellbore wall as a free surface that cannot resist shear stresses due to removal of support material (Economides et al., 1998; Zoback, 2010).

3.6.1 Vertical well

In a vertical well, the vertical principal stress is parallel to the wellbore axis with the two horizontal principal stresses in the rock mass aligning perpendicular to the borehole wall as illustrated in Figure 7. Horizontal principal stresses converge in the direction of minimum horizontal stress S_{hmin} direction increasing compressive stress but diverge in the direction of maximum horizontal stress S_{Hmax}, decreasing compressive stress. Increased compressive stresses can result in borehole breakouts if the shear strength at the borehole wall exceeds the rock's shear strength. Decrease in compressive stresses creates conditions for tensile stress that can result in tensile failure (fracture) of the borehole wall (Zoback, 2010; Tariq, 2014; Schoenball et al., 2016). Equations 11-14 (Zoback, 2010; Economides et al., 1998) express effective stresses around vertical borehole wall:

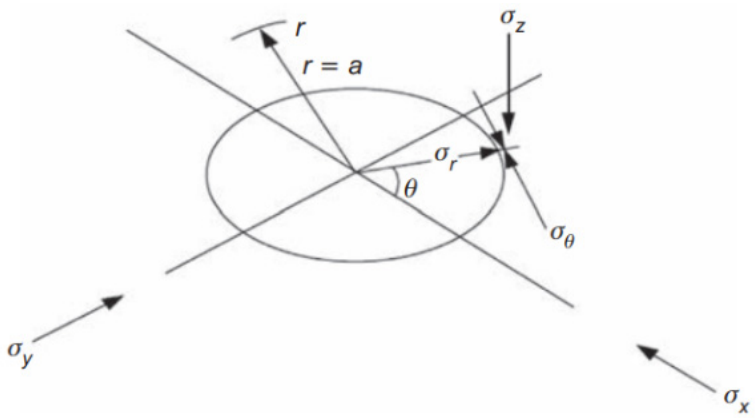

FIGURE 7: Stresses acting on a vertical borehole wall (Mitchell and Miska, 2011)

$$\sigma_{rr} = \frac{1}{2}(S_{Hmax} + S_{hmin} - 2P_p)\left(1 - \frac{a^2}{r^2}\right) + \frac{1}{2}(S_{Hmax} - S_{hmin})\left(1 - \frac{4a^2}{r^2} + \frac{3a^4}{r^4}\right)cos2\theta + \frac{a^2}{r^2}(P_f - P_p) \quad (11)$$

$$\sigma_{\theta\theta} = \frac{1}{2}(S_{Hmax} + S_{hmin} - 2P_p)\left(1 + \frac{a^2}{r^2}\right) - \frac{1}{2}(S_{Hmax} - S_{hmin})\left(1 + \frac{3a^4}{r^4}\right)cos2\theta - \frac{a^2}{r^2}(P_f - P_p) - \sigma^{\Delta T} \quad (12)$$

$$\sigma_{zz} = S_v - 2\vartheta(S_{Hmax} - S_{hmin})\frac{a^2}{r^2}cos2\theta - P_p - \sigma^{\Delta T} \quad (13)$$

$$\tau_{r\theta} = \frac{1}{2}(S_{Hmax} - S_{hmin})\left(1 + \frac{2a^2}{r^2} - \frac{3a^4}{r^4}\right)sin2\theta \quad (14)$$

where S_{Hmax} = maximum horizontal stress, S_{hmin}= minimum horizontal stress, S_v= vertical stress, ϑ = Poison's Ratio, θ = angle measured clockwise from the direction of σ_{Hmax}, $\sigma_{\theta\theta}$ is the effective hoop stress and σ_{rr} is the effective radial stress. Stress $\sigma^{\Delta T}$ is the thermal stress induced by temperature difference, P_f is drilling fluid pressure and P_p is the pore pressure (Zoback, 2010; Aadnoy and Looyeh, 2011).

At $r = a$, Equation 12 simplifies to Equation 15 (Economides et al., 1998; Renpu, 2011; Zoback, 2010):

$$\sigma_{\theta\theta} = \sigma_{\theta\theta} = S_{hmin} + S_{Hmax} - 2(S_{Hmax} - S_{hmin})cos2\theta - 2P_p - (P_f - P_p) - \sigma^{\Delta T} \quad (15)$$

At $r = a$, and $\theta = \frac{\pi}{2}$, Equation 15 reduces to Equation 16:

$$\sigma_{\theta\theta} = 3S_{Hmax} - S_{hmin} - 2P_p - (P_f - P_p) - \sigma^{\Delta T}, \quad (16)$$

At $r = a$, and $\theta = 0$, Equation 15 reduces to Equation 17:

$$\sigma_{\theta\theta} = 3S_{hmin} - S_{Hmax} - 2P_p - (P_f - P_p) - \sigma^{\Delta T} \quad (17)$$

At $r = a$ for both $\theta = 0$ *and* $\theta = \frac{\pi}{2}$, Equation 11 reduces to Equation 18 indicating radial pressure is uniform around the wellbore:

$$\sigma_{rr} = \left(P_f - P_p\right) = \Delta P \tag{18}$$

For vertical stress at the borehole wall $r = a$, Equation 13 reduces to Equation 19 (Zoback, 2010):

$$\sigma_{zz} = S_v - 2\vartheta(S_{Hmax} - S_{hmin})cos2\theta - P_p - \sigma^{\Delta T} \tag{19}$$

When $r > 3a \; or \; 4a$, $\frac{a^2}{r^2} \approx 0$ and $\frac{a^4}{r^4} \approx 0$ the rock stress approaches in situ field stress given by Equations 20-22 (Economides et al., 1998; Renpu, 2011):

$$\sigma_{rr} \approx \frac{1}{2}\left[\left(S_{Hmax} + S_{hmin} - 2P_p\right) + (S_{Hmax} - S_{hmin})cos2\theta\right] \tag{20}$$

$$\sigma_{\theta\theta} \approx \frac{1}{2}\left[\left(S_{Hmax} + S_{hmin} - 2P_p\right) - (S_{Hmax} - S_{hmin})cos2\theta\right] - \sigma^{\Delta T} \tag{21}$$

$$\sigma_{zz} = S_v - P_p - \sigma^{\Delta T} \tag{22}$$

At $\theta = 0$, $\sigma_{rr} \approx S_{Hmax}$ and $\sigma_{\theta\theta} \approx S_{hmin}$ and at $\theta = \frac{\pi}{2}$, $\sigma_{rr} \approx S_{hmin}$ and $\sigma_{\theta\theta} \approx S_{Hmax}$.

The difference between hoop stresses at $\theta = 0 \; and \; \theta = \frac{\pi}{2}$ (Equations 16 and 17) shows that at the wellbore wall the field stresses increases by a factor of 4 as expressed in Equation 23 (Zoback, 2010):

$$\sigma_{\theta=90} - \sigma_{\theta=0} = 4(S_{Hmax} - S_{hmin}) \tag{23}$$

Stresses S_{hmin}, S_{Hmax} and S_v, can be estimated using Equations 24-26 (Economides et al., 1998):

$$S_v = 1.1H - \alpha P_p \tag{24}$$

$$S_{hmin} = \frac{\vartheta}{1 - \vartheta}(S_v) \tag{25}$$

$$S_{Hmax} = \frac{S_v + S_{hmin}}{2} \tag{26}$$

Equations 15-18 give the effective (difference between total stress and pore pressure) radial, hoop and vertical stresses at the borehole wall. Effective stress applies to normal stresses only because fluids cannot transmit shear stress when they are not in motion (Aadnoy and Looyeh, 2011). Shear stress $\tau_{r\theta}$ reduces to zero at the borehole wall. When wellbore pressure is lower than formation fluid pressure (actively loaded) as in underbalance drilling and loss of circulation or wellbore pressure is higher than formation fluid pressure (passively loaded) in overbalance drilling, formation failure can take place if the formation strength is exceeded (Economides et al., 1998).

3.6.2 Directional well

In a directionally drilled well, the field principal stresses are not aligned to the well axis. Well breakout is dependent on the orientation of the well in relation to the existing field stress magnitude and direction. Vertical and horizontal stresses orientation change when the borehole axis is inclined. The stresses have to be transformed to the well orientation with respect to the in situ stresses, well inclination and azimuth as shown in Figure 8 (Zoback, 2010; Mitchell and Miska, 2011).

The far field stresses, vertical S_v, maximum horizontal S_H and minimum horizontal S_h stresses are resolved into three normal stresses σ_x, σ_y and σ_z and three shear stresses τ_{xy}, τ_{xz} and τ_{yz} with respect to coordinate system x (vertical down), y (perpendicular) and z (parallel). The stress transformation is based on the borehole inclination angle φ from the vertical and, geographical azimuths α as expressed in Equations 27-32 (Mitchell and Miska, 2011; Renpu, 2011; Aadnoy and Looyeh, 2011):

$$\sigma_x = (S_H cos^2\alpha + S_h sin^2\alpha)cos^2\varphi + \sigma_v sin^2\varphi \tag{27}$$

$$\sigma_y = (S_H sin^2\alpha + S_h cos^2\alpha) \tag{28}$$

$$\sigma_z = (S_H cos^2\alpha + S_h sin^2\alpha)sin^2\varphi + S_v cos^2\varphi \tag{29}$$

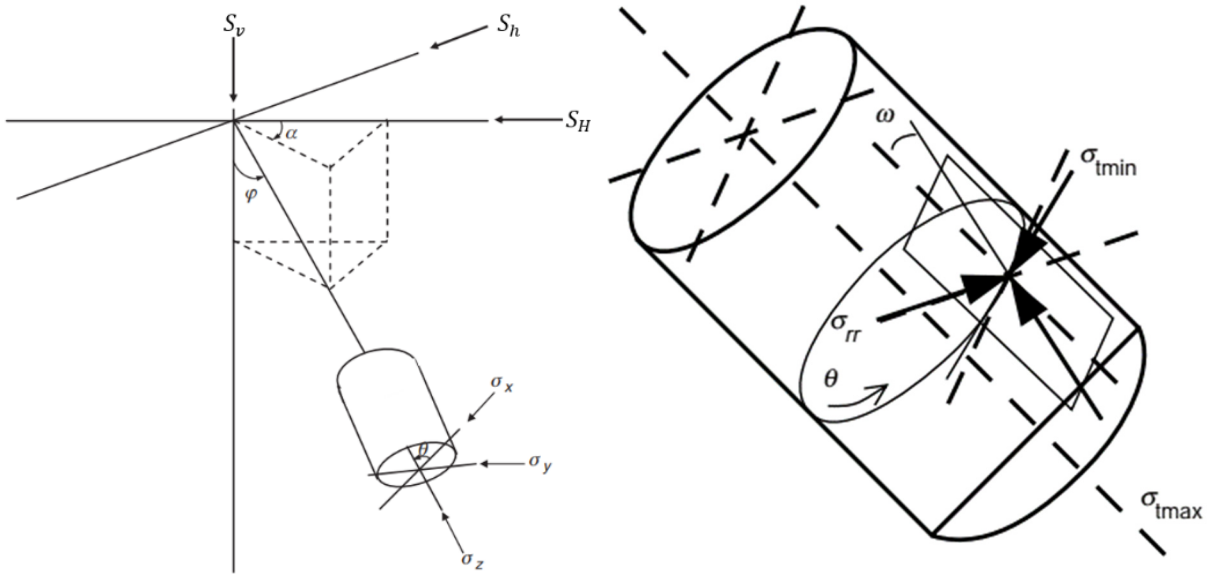

FIGURE 8: Stresses on a wellbore wall in directionally drilled well
(Mitchell and Miska, 2011; Zoback, 2010)

$$\tau_{yz} = \frac{1}{2}(S_h - S_H)sin2\alpha sin\varphi \quad (30)$$

$$\tau_{xz} = \frac{1}{2}(S_H cos^2\alpha + S_h sin^2\alpha - S_v)sin2\varphi \quad (31)$$

$$\tau_{xy} = \frac{1}{2}(S_h - S_H)sin2\alpha cos\varphi \quad (32)$$

The transformed stresses are then converted into three normal σ_{rr} $\sigma_{\theta\theta}$ and σ_{zz} and three shear stresses $\tau_{r\theta}$, τ_{rz} and $\tau_{\theta z}$ based on the circular cylindrical coordinate system rotated at angle θ around the borehole wall. The resultant stresses are expressed in Equations 33-37 (Renpu, 2011; Zoback, 2010; Mitchell and Miska, 2011; Aadnoy and Looyeh, 2011):

$$\sigma_{rr} = \Delta P = (P_f - P_p) \quad (33)$$

$$\sigma_{\theta\theta} = \left(\sigma_x + \sigma_y - \Delta P\right) - 2\left(\sigma_x - \sigma_y\right)cos2\theta - 4\tau_{xy}sin2\theta \quad (34)$$

$$\sigma_{zz} = \sigma_z - 2\vartheta\left(\sigma_x - \sigma_y\right)cos2\theta - 4\vartheta\tau_{xy}sin2\theta \quad (35)$$

$$\tau_{r\theta} = \tau_{rz} = 0 \quad (36)$$

$$\tau_{\theta z} = 2\left(\tau_{yz}cos\theta - \tau_{xy}sin\theta\right) \quad (37)$$

where $\Delta P = \left(P_f - P_p\right)$ = effective fluid pressure acting on the wellbore wall (difference between fluid pressure P_f and pore pressure, P_p).

The principal effective stresses acting along the borehole are calculated from the normal and shear stresses resolved in the circular system giving radial stress σ_{rr} acting normal to the wall and two tangential (hoop) stresses σ_{tmax} and σ_{tmin}. These stresses define the maximum normal stresses in the plane (direction) where shear stresses reduces to zero. Failure either compressive or tensile occurs if the principal stresses exceeds the borehole wall strength (Zoback, 2010; Mitchell and Miska, 2011). The effective principal stresses are expressed in Equations 38-40:

$$\sigma_1 = \sigma_r = \Delta P = (P_f - P_p) \quad (38)$$

$$\sigma_2 = \sigma_{\theta max} = \frac{1}{2}\left(\sigma_{zz} + \sigma_{\theta\theta} + \sqrt{(\sigma_{zz} - \sigma_{\theta\theta})^2 + 4\tau_{\theta z}^2}\right) \quad (39)$$

$$\sigma_3 = \sigma_{\theta min} = \frac{1}{2}\left(\sigma_{zz} + \sigma_{\theta\theta} - \sqrt{(\sigma_{zz} - \sigma_{\theta\theta})^2 + 4\tau_{\theta z}^2}\right) \quad (40)$$

The stresses are rearranged to reflect maximum σ_1, intermediate σ_2 and minimum σ_3 principal effective stress (Renpu, 2011). For tensile failure (fracturing), radial stress σ_r (Equation 38) becomes the maximum principal stress and the minimum hoop $\sigma_{\theta min}$stress (Equation 40) gives the minimum effective principal stress. For compressive failure (collapse), maximum hoop $\sigma_{\theta max}$stress (Equation 39) becomes the maximum stress and radial stress represents the minimum stress (Mitchell and Miska, 2011).

3.6.3 Thermal induced stresses

Thermal induced stresses are generated when changes in temperature occur in the rock formation. Geothermal reservoirs are highly fractured and fractures control fluid flow within the reservoir. Drilling fluid is usually at lower temperature than the formation in geothermal drilling making the formation surrounding borehole walls to contract due to cooling effect of drilling fluid depending on the circulation rate. Cooling effect makes the formation to contract creating tensile (negative) stresses around the wellbore. When circulation of drilling fluid is stopped, the borehole wall will gradually heat up. Temperature increase during heat up expands the formation creating compressive (positive) stresses both tangential and axial to the borehole wall (Zoback, 2010; Fjaer et al., 2008).

Increase in tensile stresses increases chances of borehole wall fracture and thereby reducing the magnitude of compressive stresses that result in shear failure. Compressive stresses create wellbore collapse and therefore the tendency of wellbore collapse is reduced with cooling effect of drilling fluid. According to Fjaer et al (2008), cooling acts as a strengthening of the borehole against collapse and cooling of the mud can therefore be a practical approach to mitigate stability problems. Thermal stresses are dependent rocks coefficient of thermal expansion, elastic modulus and temperature difference. It is more significant in hard than soft rocks. Tensile stresses enhance chances of fracturing creating loss of circulation condition but since geothermal formations are usually fractured the effects is minimal if the induced stresses do not exceed the rock strength (Fjaer et al., 2008; Jaeger et al., 2007). In the reservoir section, high enough thermal tensile stresses have the potential of increasing permeability initiating new fracture and expansion of existing fractures (Grant and Bixley, 2011; Siratovich et al., 2015). Drilling fluid density have higher impact on formation tensile stress as compared to thermal stresses which are also time dependent (Zoback, 2010). Thermal stress is expressed in Equation 41 (Zoback, 2010; Turcotte and Schubert, 2014; Fjaer et al., 2008):

$$\sigma^{\Delta T} = \frac{\alpha_t E \Delta T}{1 - \vartheta} \tag{41}$$

where α_t is the linear coefficient of thermal expansion, E the static Young's modulus and ϑ is Poisson's ration. Tensile thermal stresses are taken as negative and are subtracted from compressive stress equations.

According to Jaeger et al. (2007), thermal induced stresses are caused by a combination of change in temperature and mechanical restraint that inhibits free expansion or contraction of the rock (Jaeger et al., 2007). Thermal stresses are not considered in stress analysis in this report due to the assumption that the geothermal field is highly fractured and loss of circulation will be much more controlled by the fractures and drilling fluid hydrostatic pressure as opposed to rock contraction (Grant, 2014).

3.7 Failure modes

Rock failure occurs if the rock is subjected to high stresses exceeding its strength that makes the rock to deform or break thereby reducing its capacity to resist loading. Failure mechanism is analysed and an appropriate compatible failure criterion applied. Shear failure (brittle) takes place in granular materials while clays undergo plastic (ductile) deformation. The failure mechanism likely to create wellbore and near wellbore instability issues are (Economides et al., 1998):

- Shear failure in absence of plastic deformation as in cases of breakout;
- Pore collapse due to deformation and compaction;
- Formation fracturing due to tensile failure;

- Erosion;
- Creep, resulting to reduction in diameter and tight holes.

To predict rock failure, failure criteria are used to develop failure envelopes separating stable and unstable zones (Aadnoy and Looyeh, 2011).

3.7.1 Mohr-Coulomb failure criterion

This criterion relates failure through shear stress to applied force, friction and material cohesion. The model assumes that the intermediate principal stress has no effect on the failure strength and failure depends on the maximum principal stress (σ_1) and the minimum principal stress(σ_3). Failure in compression occurs when maximum shear stress exceeds the formation cohesion and the frictional force (Alidi, 2017). Stress state at a point can be presented graphically using Mohr's Circle drawn in the normal and shear stress plane. In the principal coordinate system, shear stresses reduce to zero and normal stresses are the maximum and minimum principal effective stresses. In this system, the normal and shear stresses are expressed in terms of maximum and minimum principal stresses in Equations 42 and 43 (Jaeger et al., 2007):

$$\sigma = \frac{\sigma_1 + \sigma_3}{2} + \frac{\sigma_1 - \sigma_3}{2} cos2\theta \quad (42)$$

$$\tau = \frac{\sigma_1 - \sigma_3}{2} sin2\theta \quad (43)$$

Plotting a Mohr's Circle illustrated in Figure 9 using the maximum and minimum effective principal stresses, a line tangent to the circle given by Equation 44 (Azar and Samuel, 2007) defines the Mohr-Coulomb failure criterion:

$$\tau = \pm(C + \sigma tan\emptyset) \quad (44)$$

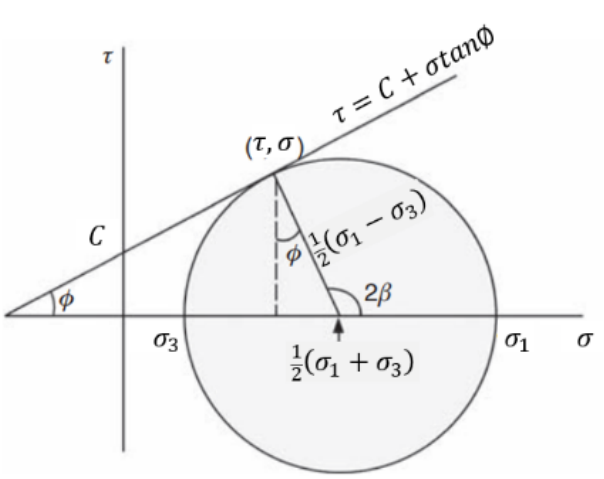

FIGURE 9: Mohr-Coulomb failure criterion (Mitchell and Miska, 2011)

where τ is the shear stress, σ= effective normal stress acting on the rock materials and ∅= internal friction angle.

The gradient of the straight line is equal to the effective normal stress and its intercept gives the value of shear stress when normal stress is zero. Mohr's Circle developed has a diameter equal to the difference between the maximum and the minimum effective stresses at failure (Mitchell and Miska, 2011).The shear stress value occurring when normal stress reduces to zero defines the material cohesion C, the minimum shear stress required to initiate failure. The cohesive strength C, defines the joint strength (degree of cementation of the material). The angle between the line and the normal stress reflects the material internal friction angle (Mitchell and Miska, 2011). The Mohr-Coulomb failure criterion will be the criterion that will be applied in this thesis.

3.7.2 Hoek-Brown criterion

The criterion is applicable more in naturally fractured reservoirs and uses uniaxial compressive stress (UCS) C_0 of intact un-fractured rock formation as the scaling parameter and two dimensionless constants. The constants depend on the rock properties and fracture system. The criterion is expressed in terms of maximum and minimum effective principal stresses in Equation 45 (Hoek et al., 2018; Fjaer et al., 2008; Zoback, 2010):

$$\sigma'_1 = \sigma'_3 + C_0 \left[m_b \frac{\sigma'_3}{C_0} + s \right]^a \quad (45)$$

where a, m_b and s are material constants based on the geological strength index (GSI) (Hoek et al., 2018).

3.7.3 Von Mises criterion

This criterion uses the second deviatoric invariants and the effective average stress to analyse material strength (Immerstein, 2013). For $\sigma_1 > \sigma_2 = \sigma_3$, the invariant J_2 is expressed in Equation 46:

$$\sqrt{J_2} = \frac{1}{\sqrt{3}}(\sigma_1 - \sigma_3) \quad (46)$$

The criterion assumes that failure takes place when the second invariant J_2 of the deviatoric stress reaches a critical value (material yield point).The effective average stress is expressed in Equation 47:

$$\sigma_m - P_p = \frac{1}{3}(\sigma_1 + \sigma_2 + \sigma_3) - P_p \quad (47)$$

The deviatoric invariants are plotted against the effective average stress for various stress conditions σ_1 and confine pressure σ_3 to generate a failure curve (Immerstein, 2013). In Extended Von Mises criterion expressed in Equation 48, the intermediate stress is included to calculate normal and shear stresses (Economides et al., 1998; Aadnoy and Looyeh, 2011):

$$\alpha I_1 + \sqrt{J_2} - K = 0 \quad (48)$$

where, I_1 is the first invariant of the stress tensor and J_2 the second invariant of the stress tensor expressed in Equations 49 and 50 (Economides et al., 1998):

$$J_2 = \frac{1}{6}[(\sigma'_1 - \sigma'_2)^2 + (\sigma'_2 - \sigma'_3)^2 + (\sigma'_3 - \sigma'_1)^2] \quad (49)$$

$$I_1 = \sigma'_1 + \sigma'_2 + \sigma'_3 \quad (50)$$

where α and K are material constants, expressed as in Equations 51 and 52 in relation to internal friction angle $\emptyset$ and cohesion C of the material under consideration. (Economides et al., 1998):

$$\alpha = \frac{2sin\emptyset}{\sqrt{3}(3 - sin\emptyset)} \quad (51)$$

$$K = \frac{6Ccos\emptyset}{\sqrt{3}(3 - sin\emptyset)} \quad (52)$$

The constants are determined from the gradient and the intercept of the failure line plotted as shown in Figure 10. In the first invariant $I_1 = \sigma_m - P_p$ gives effective normal stress $\sigma_m = \frac{1}{3}(\sigma_1 + \sigma_2 + \sigma_3) - P_p$ (Equation 45) and square root of the second invariant $\sqrt{J_2} = \left(\frac{1}{6}[(\sigma'_1 - \sigma'_2)^2 + (\sigma'_2 - \sigma'_3)^2 + (\sigma'_3 - \sigma'_1)^2]\right)^{1/2}$ (Equation 46) gives shear stress root mean square of the deviatoric stress (Renpu, 2011).

3.8 Determination of minimum principal stress

Plotting pressure against time in Leak Off Test (LOT) at constant pumping rates, pressure increases linearly with time. When fractures develops pressure, increase is no longer linearly proportional with time. The point of departure is referred to as the Leak Off Point (LOP). The LOP is approximately equal to the minimum principal stress. Figure 2 in Section 2.3 illustrates the procedure. Data from LOT or Extended Leak Off Test (XLOT) is used to determine with accuracy the magnitude of minimum stress

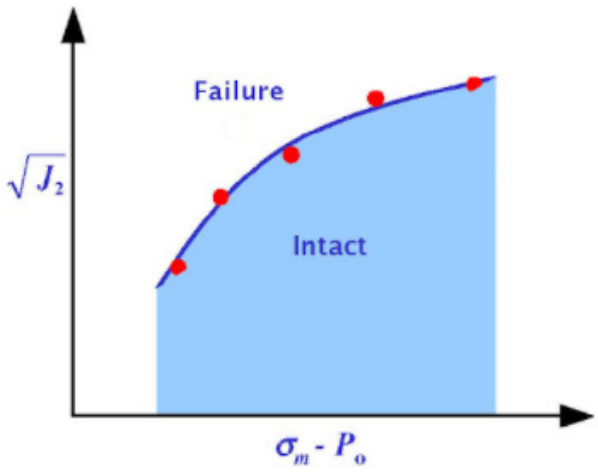

FIGURE 10: Von Mises criterion (Aadnoy and Looyeh, 2011)

(σ_3) that is expressed as the sum of the measured surface pressure (P_0) and pressure in wellbore due to column of wellbore fluid (P_w) expressed in Equation 53 (Zoback, 2010):

$$\sigma_3 = P_0 P_w \tag{53}$$

According to Zoback (Zoback, 2010), hydraulics fractures will develop perpendicular to the orientation of the minimum stress because it is the lower energy configuration. LOT gives the maximum borehole pressure that initiates formation of fractures at the wellbore wall but does not lead to drilling fluid loss. Fluid loss occurs when fracture extends further away from the wellbore wall and intersect permeability features such as fractured formation boundary zones common in geothermal formation. The LOP can be used to design the maximum drilling fluid density that can be used to drill next section below the casing (Zoback, 2010).

3.8.1 Eaton's formula

The minimum principal stress helps in determining the full stress tensor and provides important information for drilling stable wells. Drilling fluid density is kept below minimum principal stress (S_{hmin}) to prevent formation fracturing and inducing loss of circulation. On the other hand, drilling fluid density has to be maintained above pore pressure for ease of well control to avoid a blowout and prevent wellbore collapse especially in uncased section of geothermal wells. The Eaton's (1969) formula (Zoback, 2010) in Equation 54 is one of the formulas used to estimate the minimum principal stress when there is no field data from direct measurements such as LOT and to estimate the pressure required to initiate hydraulic fracture in a rock formation (Zoback, 2010):

$$S_{hmin} = P_p + \frac{\vartheta}{1-\vartheta}\left(S_v - P_p\right) \tag{54}$$

where S_{hmin} is the minimum principal stress, P_p is the pore pressure, S_v is the vertical stress given by the overburden and ϑ is Poisson's Ratio.

The Eaton's formula estimates the pressure required to initiate hydraulic fracture in a rock formation (Fjaer et al., 2008). It is an accurate method of determining formation fracture pressure as it incorporates the overburden pressure, pore pressure and the rock Poisson's Ratio (Mitchell and Miska, 2011). This equation is also used in Code of Practice for casing design to estimate effective containment pressure (African Union, 2016; New Zealand Standard, 2015) to determine the minimum casing depth for drilling of each section of the well. According to Zoback (2010) a constant Poisson's Ratio of 0.25 gives consistent results of the predicted minimum horizontal stress as predicted using Coulomb's Theory. The Eaton's formula is based on the assumption that the only source of horizontal stress comes from the overburden (bilateral constraint) (Zoback, 2010). In this thesis, Eaton's formula (Equation 54) will be used to estimate the minimum horizontal stress.

4. DRILLING OPERATIONS

A geothermal well provides an access to the subsurface geothermal reservoir. It provides a conduit for fluid flows to surface in case of production wells or a means of fluid injection back to the reservoir. The drilling process is carried out in steps structured to ensure delivery of a complete well either production, reinjection, exploration or make-up well (Thórhallsson, 2017).

4.1 Well planning

Well planning encompasses all the activities required to complete a geothermal well and is described in a drilling program report prepared for each well. These include costs, times and description of individual tasks, sequence of how activities follow each other and execution. Planning involves listing, defining, scheduling and budgeting of all activities required to drill the well (Finger and Blankenship, 2010). Choosing a suitable drill rig to undertake the drilling operation is a prerequisite part of well planning (Azar and Samuel, 2007). Planning includes

1. Rig selection;
2. Drilling fluids;
3. Casing program;
4. Cementing;
5. Drill bits;
6. Drill string and Bottom Hole Assembly (BHA);
7. Well control and Health Safety and Environment (HSE);
8. Well logging and sampling program.

4.2 Well design

Physical parameters such as depths and diameters for drill bits and casing strings define the well itself in what is referred to as casing program. Geothermal well design is a process where the purpose and objective of the well, downhole conditions expected during drilling, material and equipment requirement and drilling procedures are specified to ensure delivery of a high integrity well (Ngigi, 2015). The New Zealand Standard NZS 2403:2015 and The African Union Code of Practice for Geothermal Drilling (2016), outlines the ten steps followed during geothermal well design process (New Zealand Standard, 2015; African Union, 2016).

4.3 Drilling equipment

Rotary drill rigs are mainly used in geothermal drilling utilizing either Kelly Drive or top drive. The drilling rig provides rotary power to turn the drill bit, circulation of the drilling fluid to transport drill cuttings up the wellbore, hoisting power to pull (POOH) or run in (RIH) the drill string and casings and control the weight on the drill bit (WOB) during drilling (ENGINE Coordination Action, 2008). A drill rig can be divided into six functional hardware components namely (Azar and Samuel, 2007):

1. Power generation system - AC or DC generators and internal combustion engines (direct drives) which provide power to the hoisting, circulation and rotary systems;
2. Hoisting system - mast (derrick), draw-works, substructure, travelling block, crown block, drilling line;
3. Drilling fluid circulating system - mud tanks and mud pumps, air compressors;
4. Rotary system - rotary table drive, top drive, downhole motors;
5. Well blowout control systems - Blow Out Preventers (BOP) and rotating head;
6. Drilling data acquisition and monitoring system - display, monitor, record, and retrieve information of the ongoing drilling operation. Drilling rate, hook load, weight on bit (WOB), pumping rate/ pressure, torque and rotational speed. The system assist the drilling crew monitoring the drilling progress and in detecting early any drilling problems that may be encountered.

4.4 Casing

Casing strings of different sizes are set at varied depths in a geothermal well. Major considerations of casing design are the well conditions during and after drilling with the objective of ensuring that the casing strings are able to serve the well for as long as possible without failure. Detailed procedure for the casing design and other drilling related issues are described in "The African Union Code of Practice for Geothermal Drilling" which is based on the New Zealand standard. Other authors have described factors such as rock properties, formation fluids and well control and how they are used to determine the setting of safe casing depths. Maximum Design Pressure (MDP), Effective Containment Pressure (ECP), formation integrity and anticipated problem zones need to be assessed when setting up the depth of each of the casing string (Finger and Blankenship, 2010).

Three casing strings, surface, anchor- and production casing are generally used in a high temperature geothermal well and each one is cemented full length back to surface. A perforated (or slotted) liner in used in the production section to support the formation and allow geothermal fluid into or out of the well (Hole, 2006).

4.5 Casing loading forces and failure

Casing strings are designed to withstand any load encountered during drilling and production. The forces that the casing is subjected to include collapse pressure, burst pressure, tension or compression loading.

4.5.1 Collapse pressure

Collapse force is applied from outside the casing by fluid and is usually greatest at the bottom of the casing string where hydrostatic pressure is greatest. The minimum collapse pressure rating is calculated when the casing is empty but surrounded by fluid in the well and no axial loading (Azar and Samuel, 2007). The minimum collapse pressure given by Equation 55 (Mitchell and Miska, 2011) calculates the external pressure that generates the minimum yield stress on the inside wall:

$$F_c = 2\sigma_{yield}\left[\frac{\left({}^{d_o}/_{t}\right) - 1}{\left({}^{d_o}/_{t}\right)^2}\right] \tag{55}$$

where F_c is the collapse pressure, σ_{yield} is the casing material yield strength d_o/t is the ratio of casing outside diameter d_o to thickness t. Collapse pressure gives the difference between external pressure ($mud\ or\ cement\ density\ x\ depth\ x\ acceleration\ due\ to\ gravity$) and internal pressure.

4.5.2 Burst pressure

Burst force occurs on the inside of the casing due to the fluid pressure inside the casing string. Burst force exerted is resisted by the casing wall strength and is subject to casing material yield strength, outside diameter and casing wall thickness as expressed in Equation 56 (Bourgoyne et al., 1986):

$$F_b = \frac{2\sigma_{yield}\, t}{d_{out}} \tag{56}$$

where F_b is the burst pressure, σ_{yield} is the casing material yield strength, t is the material thickness and d_{out} is the casings outside diameter. Burst pressure is the difference between internal pressure and external pressure.

4.5.3 Tension

Tensional force is produced by the casing weight, pressure differential and fluid densities inside and outside the casing. Axial tension loading is largest at the top of the string and decreases, with depth,

toward the bottom of the string. Body yield strength defines the minimum tensional force required to exceed the casing elastic limit. The tensional force, $F_{c,}$ is a product of the casing, material yield strength and cross-sectional area of the casing wall given by Equation 57 (Bourgoyne et al., 1986):

$$F_c = \sigma_{yield} A_s = \frac{\pi}{4} \sigma_{yield} \, (d_{out} - d_{in}) \tag{57}$$

where σ_{yield} is the casing materials yield strength, d_{out}casing outside diameter, d_{in} casing inside diameter and $A_s$is the cross-sectional area.

4.5.4 Casing thermal stress

Temperature changes encountered in a geothermal well especially during heat up and quenching are significant and result to axial stress on the casing string. Equation 58 expresses unconstrained axial strain due to temperature change (Rabia, 2001):

$$\in_z = \alpha_T \Delta T \tag{58}$$

where $\in_z$ is the axial strain, α_T is the thermal coefficient of expansion and ΔT is the temperature change.

Cemented casing strings are usually installed in the well under tension loading. After curing of cement, casings are restrained to freely expand or contract and this subjects them to compressive loading except above the well surface where free expansion or contraction is not restricted. Equation 59 gives the axial stress induced due to temperature changes:

$$\sigma_z = -E \alpha_T \Delta T \tag{59}$$

where σ_z is the axial stress and E is the Young's modulus of the casing steel. The axial force, F_a generated on the casing is expressed given by Equation 60:

$$F_a = -E \alpha_T \Delta T A_s \tag{60}$$

where A_s is the cross-sectional area.

Cyclic thermal loading during the well lifetime is induced by the heating and cooling cycles and can lead to failure through fatigue failure and breakage of the cement to the casing bond (Rabia, 2001).

4.5.5 Buckling failure

Buckling failure is caused by axial (length) compression of the casing that make lateral deflections if the yield strength is exceeded. The equilibrium point dividing the sections where buckling is most likely to occur and the section least affected by buckling is referred to as the neutral point under uniform loading. Above the neutral point, casing is in tension and it is difficult to buckle. Below the neutral point, the upward buoyancy of the fluid, pressure and mechanical loading, place the casing in compression that can cause buckling failure if the yield strength is exceeded. Equation 61 gives the neutral point in the casing (Azar and Samuel, 2007):

$$F_z = P_i A_i - P_o A_o \tag{61}$$

where F_z is the true axial force, P_i is the pressure inside, A_i is the inside cross-sectional area, P_o is the pressure outside and A_o is the outside cross-sectional area.

The right-hand side of Equation 61 is referred to as the stability force ($P_i A_i - P_o A_o$). When axial force F_z is greater than the stability force, the casing is straight; when F_z is less than the stability force, the casing is likely to buckle and when F_z is equal to the stability force, the neutral point has been reached. Axial force varies from point to point depending on the well condition such as during cementing and changes in pressure and temperature. The buoyancy neutral point is usually assumed and is estimated using Equation 62 (Azar and Samuel, 2007):

$$NP = D_t\left(1 - \frac{\rho_{fluid}}{\rho_{steel}}\right) \quad (62)$$

where NP is the neutral point, D_t is the depth, ρ_{fluid} is the density of the fluid and ρ_{steel} is the density of steel.

4.6 Cementing

Cement bonds the casing to the formation by filling the annular space between the casing and the drilled borehole wall. High compressive strength is developed after curing of cement. One of the main objective of cementing casing is zonal isolation through adhesion of the hardened cement to the casings and development of high shear stress resistance required to detach it. Geothermal casings are cemented full length back to the surface to avoid creep and elongation due to thermal expansion when the well is opened for discharge tests or flowing to supply steam to the power plant and other intended uses (Nelson, 1990). Other functions include well support, protection against corrosion and axial load support of the casings. Cement additives such as silica flour, bentonite, loss of circulation material (LCM), accelerators, retarders, fluid loss control, friction reducers and others alter the properties of cement slurry such as density, rheology, fluid loss to meet the downhole conditions of the well and enable flexible pumping of cement slurry (Rabia, 2001).

Loss of circulation is a major challenge in casing cementing of geothermal well. Most of the geothermal formations are highly fractured and they breakdown at low hydraulic pressure. If loss of circulation was encountered during drilling, it is unlikely that cement will fill up the annulus back to surface in the primary cementing job and backfills will be required. Excess cement slurry volume above the theoretically calculated volume between 50 and 200% is usually pumped to cover for the loss into the fractures and fill up eroded well sections (Finger and Blankenship, 2010). Blended cement is used for primary cementing whereas neat (no additives) is used to backfill if cement is not received on surface (Nelson, 1990).

Annular volumes between casing and open hole and between two strings of casing are used to calculate the amount of cement slurry required in for cementing geothermal wells in Olkaria. In Iceland, a caliper log is used to estimate the cement volume required during cementing (Níelsson et al., 2014):

Well parameters affecting cementing operations are (Mitchell and Miska, 2011):

1. Depth affects the cement volume, pressure and the bottom-hole temperatures of the well.
2. Wellbore geometry determines the amount of cement required, running and centring of casings and achievement of uniform sheath of cement around the casing.
3. Bottom Hole Circulating Temperature (BHCT) and Bottom Hole Static Temperature (BHST) assist in deciding the additives (retarder) to be used, the thickening time and development of compressive strength.
4. Formation pressures includes pore pressure, fracture pressure and hole-collapse pressure are important in maintaining wellbore integrity. The Equivalent Static Density (ESD), which refers to the wellbore pressure without circulation, affects the development of compressive strength of cement. Equivalent Circulating Density (ECD) and hydrostatic pressure control cement slurry design to avoid formation fracture and loss of circulation. The ECD should not exceed the fracture gradient of the formation to prevent fractures from developing and maintain the integrity of the wellbore. If the ECD and ESD are below the hole-collapse pressure of the weakest formation in the borehole, cave in of the borehole walls can occur blocking circulation and stuck drill string as illustrated in Equation 63:

$$ECD = \frac{Wellbore\ circulating\ fluid\ pressure}{True\ vertical\ depth} \quad (63)$$

5. Formation composition - presence of swelling clays can result to compatibility challenges with cement.

6. Permeability - formations of high permeability result to high rate of fluid loss (filtration) from cement slurry leading to poor cement bonds. Challenges in displacing cement will be experienced due to high pressures required to displace dehydrated cement.

4.6.1 Cement plug

Cement plug is placed in open to hole help in solving severe loss of circulation of drilling fluid, collapsing formation and stabilizing the well allowing for further drilling. In instances where fishing of drill string is not successful, cement plugs provide stable formation that enables the well to be sidetracked. This requires using directional drilling tools to create a new trajectory away from the original well path and allowing the well to be drilled to the target depth. However, plugging contributes to Non-Productive Time (NPT) of the rig through Waiting on Cement (WOC) for cement to harden and develop sufficient compressive strength (Mitchell and Miska, 2011).

In Olkaria wells, placing of cement plugs is often used to contain well instability problems encountered during drilling. Challenges such as severe losses of drilling fluid circulation and well breakouts affecting drilling progress in cased sections are contained by using cement plugs. In the production zone of geothermal well, use of cement is not viable and is highly discouraged, as it will block the fractures that make up the geothermal fluid path rendering the well unusable later for either production or reinjection. However, severe well instabilities curtails further drilling and may make it necessary to use cement plugs to stabilize as for example experienced at Olkaria in well OW-731D below the production casing (KenGen, 2014-731D).

5. DRILLING FLUIDS HYDRAULICS, FLOW MODELS AND DRILL BITS

The circulation system comprises of fluid (liquid, air or aerated liquid), mud pumps, compressors, flow lines, drill string and mud tanks. The pumps provide power for the fluid to carry the cutting from bottom of the well to the surface and to drive a downhole motor if it is being used to drill. The density, viscosity and flowrates are major parameters that affect the performances of drilling fluids such as cuttings carrying capacity, wellbore stability and support (Mitchell and Miska, 2011; IADC, 2000; Finger and Blankenship, 2010).

In wellbore stability, drilling fluids limit and control formation damages, downhole pressures and transport the generated drill bit cuttings out of the well. Drilling challenges related to incorrect drilling fluids properties include stuck pipe, loss of circulation and wellbore instability (Economides et al., 1998).

The main functions of drilling fluid are (Mitchell and Miska, 2011; IADC, 2000; Finger and Blankenship, 2010):

- To remove and transport drill bit cuttings from the bottom of the hole to the surface;
- Transmit hydraulic horsepower to the drill bit;
- Cool and lubricate the drill string and bit;
- Control sub-surface pressure by providing sufficient hydrostatic pressure in formations penetrated;
- Minimize settling of cuttings when circulation is temporarily stopped;
- Maintain borehole stability by controlling swelling or sloughing formations;
- Allow collection of geological information about the formations being drilled;
- Support part of the drill string and casing weight;
- Ensure maximum logging information;
- Prevent fluid-loss from the borehole through formation of filter cake or pressure reduction in the well.

5.1 Geothermal drilling fluids

For geothermal well drilling, four main types of drilling fluids are used, water based Bentonite Mud, water alone, aerated mud or water, air and foam. Bentonite mud with starch and caustic soda additives to improve viscosity and pH is mainly used in the surface casing drilling and upper section for anchor casing. Water or aerated water is preferred in drilling production section of the well where loss of circulation is highly likely to occur and not seal the feeder zones for the geothermal fluids into the well. Because of high permeability in the production section of a geothermal well, drilling blind (with no circulation returns) is normally undertaken in spite of added risk of getting stuck or other wellbore instability issues if the borehole wall is not mechanically stable (Azar and Samuel, 2007). Alternative to water drilling is aerated water, which reduces the hydrostatic pressure in the borehole for better cutting removal capacity and wellbore cleaning (Hole, 2006).

5.1.1 Aerated and air drilling

Compressed air can be used alone as a drilling fluid or have it injected into the circulation system together with water, mud or foaming agent (detergent) in aerated drilling. Air reduces drilling fluid density and assists to achieve pressure balance or underbalance in the well. Reduced wellbore pressure helps in maintaining drilling fluid circulation returns back to surface improving hole cleaning and prevents accumulation of drill cuttings. This reduces the risk of circulation losses, stuck drill string and wellbore collapse (Hole, 2006).

Aerated drilling fluids subject the formation to less hydrostatic pressure thereby minimizing formation damage especially in the production section of geothermal well. Enhancing circulation of drilling fluid back to surface and reducing loss of circulation improves drilling Rate of Penetration (ROP), increases drill bit life, minimizes formation damage and clogging of fractures and improves wellbore stability

(Hole, 2006). In addition to the air compressor package and detergent injecting pump, a rotating head comprising of stripper rubber that rotates together with the drill string is incorporated on top of the Blow Out Preventer (BOP) stack. The rotating head diverts the circulation fluid return from the annulus around the drill string as it flows up inside the BOP stack to the flow line that takes it away from the rig floor (Economides et al., 1998).

5.2 Drilling hydraulics

For the drilling fluid to fulfil its main functions of transporting drill cuttings and wellbore stability, the flowrates and pressures have to be right. High wellbore pressures can lead to formation fracturing and loss of circulation while very low circulation can reduce the cutting carrying capacity resulting to sticking of the drill string (Mitchell and Miska, 2011). Three well conditions, namely static-no flow, circulating and surge and swab conditions when tripping in or out of the borehole normally occur during drilling operations. Pressures under these conditions are applied to calculate burst and collapse pressures, formation fracture pressure, well control, cement displacement, bit selection and fluid carrying capacity (Bourgoyne et al., 1986).

In static well conditions, pressure is due to the fluid column in the well. Equation 64 gives the exerted force by this fluid column (Bourgoyne et al., 1986):

$$F = pA \tag{64}$$

For incompressible liquids $p = \rho g$h where ρ is the fluid density, g is the gravitational acceleration and h is the height of the fluid column.

For compressible fluids such as air, pressure is expressed using the real gas Equation 65 (Bourgoyne et al., 1986):

$$p = \rho z \frac{RT}{M} \tag{65}$$

where p is the absolute pressure, ρ is gas density, z is the compressibility factor, R is the universal gas constant, T is the absolute temperature and M is the gas molecular weight.

At constant temperature T over the depth rangeΔZ, pressure is expressed in Equation 66 (Bourgoyne et al., 1986):

$$p = p_0 exp\left(\frac{gM\Delta Z}{zRT}\right) \tag{66}$$

where p_0 is the surface pressure at depth Z =0, g =gravitational acceleration, M= gas molecular weight, R=universal gas constant and z= compressibility factor.

5.3 Equivalent Circulation Density (ECD)

During drilling, circulation of drilling fluid requires that the effective (dynamic) fluid pressure in the well be higher than the static pressure ($\rho \times g \times h$). The dynamic (circulating) is referred to as Equivalent Circulation Density (ECD). ECD combines drilling fluid density and pressure drop in the annulus and equals the static drilling fluid weight plus pressure drop in the annulus (Fjaer et al., 2008). Complex drilling fluid such as aerated fluid with foaming agent is usually compared to an equivalent single-fluid column that is open to the atmosphere. The equivalent circulation density, ρ_e is defined using Equation 67 (Bourgoyne et al., 1986):

$$\rho_e = \frac{p}{gZ} \tag{67}$$

Under steady flow, laws of conservation of energy, mass and momentum are applied. The law of conservation of mass states that the net mass rate into any volume V is equal to the mass rate out of the volume. Equation 68 gives the balance of mass for single-phase flow (Mitchell and Miska, 2011):

$$\dot{m} = \rho v_1 A_1 = constant = \rho v_2 A_2 \tag{68}$$

where $\dot{m}$ = mass flow rate in kg/s, ρ= density in kg/m^3, v_1 and v_2 = average velocity in m/s and $A_1 and\ A_2$ = cross-sectional areas in m^2.

The flow rate of an incompressible fluid is the same at all points in the well when there is no leakage or addition either from the surface equipment or from formation. Taking the fluid density to be constant at all points in the well, the mean velocity at any given point is the flow per unit area at that point and it varies from point to point due to well geometry even though the flow rate is the same at all points (Bourgoyne et al., 1986). Therefore, for an incompressible fluid, Equation 68 becomes a volumetric flow rate shown in Equation 69 (Mitchell and Miska, 2011):

$$q = vA \tag{69}$$

where $q = \dot{m}/\rho$= volume flowrate in m^3/s, $v =$ velocity in m/s and A = cross sectional area in m^2.

5.4 Rheological fluid flow models

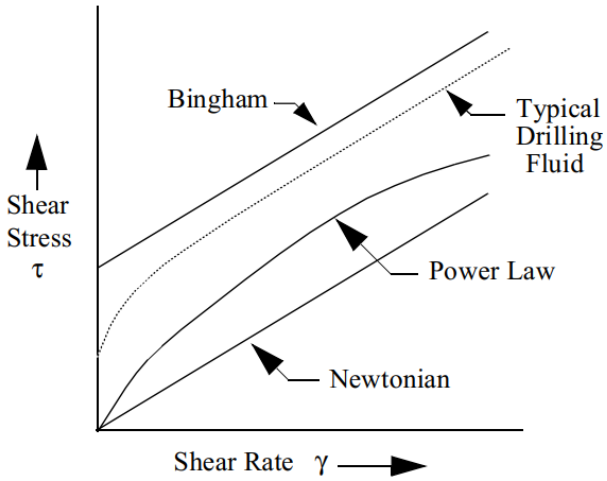

FIGURE 11: Fluid flow models
(Baker Hughes, 1995)

Laminar flow in which fluid move in orderly manner is desired in the annulus during drilling operations. This is because of reduced erosion of the wellbore walls and minimal pressure drop as opposed to turbulent flow in which there is random movement of fluid. Viscosity determines the force requirements in moving drilling fluids and cement slurries in the hydraulic circuit of the drilling process. Fluids are classified as either Newtonian or non-Newtonian. Newtonian fluids are characterized by single viscosity value while Non-Newtonian fluids such as drilling fluids and cement slurries do not have constant viscosity but have an apparent (plastic) viscosity (Baker Hughes, 1995). Figure 11 shows the flow models used to predict flow behaviours of drilling fluids.

Drilling fluids and cement slurries are classified as Non-Newtonian since they consist of solid particles that tend to increase the force (shear stress) required to maintain a particular flow rate (Baker Hughes, 1995; Mitchell and Miska, 2011; Bourgoyne et al., 1986).

5.5 Surge and swab pressures

Surge pressure is the pressure increase in the annulus during Running in Hole (RIH) of the casings and drill string. If the increase is very rapid, pressure can exceed the formation fracture gradient at certain depths. Surge pressure is defined using Equation 70 (Azar and Samuel, 2007):

$$P_e = P_{hi} + D_i \Delta P_{surge} \tag{70}$$

where P_e is the equivalent fluid pressure at some well depth D_i in the annulus P_{hi} is the drilling fluid hydrostatic pressure at D_i and ΔP_{surge} is the surge pressure gradient in the annulus.

Swab pressure is the pressure decrease during tripping out (running out) of the well. The hydrostatic pressure in the well is reduced and if pressure falls below the formation pressure, fluid flow into the well can be experienced. Swab pressure is expressed in Equation 71 (Azar and Samuel, 2007):

$$P_e = P_{hi} - D_i \Delta P_{swab} \tag{71}$$

where P_e is the equivalent fluid pressure at some well depth D_i in the annulus P_{hi} is the drilling fluid hydrostatic pressure at D_i and ΔP_{swab} is the swab pressure gradient in the annulus. (Azar and Samuel, 2007).

5.6 Drill cuttings transport

Drilling fluid has to have the ability to carry drill cuttings from the well bottom to the surface. Proper borehole cleaning is important in order to avoid problems such as borehole fill, excessive bit wear, low penetration rates, high torque and drag, loss of circulation, stuck drill string and excessive hydrostatic pressure that can lead to formation fracture. Cuttings transport depends on the fluid velocity, density and viscosity (Baker Hughes, 1995). Cuttings slip or terminal velocity defines the velocity at which suspended particle will fall back in static fluid conditions.

Gravity and friction forces acting in the opposite direction counter the lift, buoyancy and drag forces on drill cuttings particle. For the drilling fluid to transport cuttings to the surface, its annular average velocity,v_a must exceed the cuttings average slip velocity, v_{sl}. The difference between the annular velocity and slip velocity is the cutting transport velocity, v_t expressed in Equation 72 (Azar and Samuel, 2007):

$$v_t = v_a - v_{sl} \tag{72}$$

The ratio of the cuttings transport velocity and annular velocity is referred to as the cuttings transport ratio,R_t, expressed in Equation 73 (Azar and Samuel, 2007):

$$\frac{v_t}{v_a} = 1 - \frac{v_{sl}}{v_a} = R_t \tag{73}$$

The weight (W) of the drill cutting particle will act downward and is expressed in terms of density (ρ_s) and particle volume (V_s) in Equation 74 (Bourgoyne et al., 1986):

$$W = \rho_s * V_s * g \tag{74}$$

Drilling fluid flow exerts an upward acting force (F) as it flows up in the annulus and combined with buoyant force (F_{bo}) will resist the downward force due to the cutting particle weight. Solid rock particle will displace fluid volume equal to the particle volume (V_s) hence the buoyancy upward force can be expressed in terms of displaced fluid using solid particle volume and fluid density (ρ_f) as in Equation 75 (Bourgoyne et al., 1986):

$$F_{bo} = \rho_f * V_s * g \tag{75}$$

The resultant upward fluid force (F) will be the difference between the cutting particle weight (W) and the buoyancy force (F_{ob}) as in Equation 76 (Bourgoyne et al., 1986).

$$F = W - F_{ob} = \left(\rho_s - \rho_f\right) V_s g \tag{76}$$

6. CASE STUDY – OLKARIA WELLS AND WELL RN-33 IN ICELAND

Olkaria sub-surface stratigraphy comprises of rhyolite with minor inter layers of trachyte and basalts in the uppermost part of the field. Underlying the pyroclastic is the Olkaria basalt with alternating thin tuff formations. Below the basalts, the formation is mainly made up of trachyte that form the main reservoir rock (Otieno, 2016). Figure 12 highlights the inferred stratigraphy of the Olkaria geothermal field.

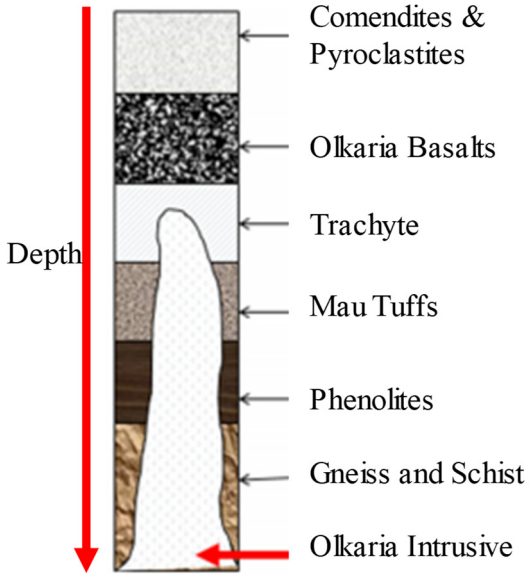

FIGURE 12: Subsurface stratigraphy of Olkaria field in Kenya (Otieno, 2016)

6.1 Olkaria drilling and well design

Geothermal wells in Olkaria are of regular casing program design with a 9⅝" Production Casing and 7" liner (Thórhallsson, 2017). The wells have Surface, Anchor and Production Casings running from surface to respective depths and are fully cemented back to surface. Slotted liner covers the well production section from the Production Casing end to the well bottom.

Majority of the wells drilled in Olkaria are between 2000 and 3000 m, both vertically and directionally drilled. Directional wells have a "J" shaped well profile and are initially drilled vertically to a depth of 400m where the Kick Off Point (KOP) for building the direction angle is established. Angle build up starts at this depth at a rate of 1° for every 10 m drilled targeting a final inclination of about 20° from the vertical. The angle build-up ends at 600m after which drilling proceeds with a straight section hole while maintaining the same inclination by locked drill string to the total drilled depth. After completion, the well bottom has a horizontal displacement of approximately 800 m from the vertical wellhead (Hole, 2006). Summary of the casing sizes, material and depths are depicted in Table 3.

TABLE 3: The wells in Olkaria, Kenya - casings, drill bits and completions of casings (KenGen, 2017 - Drilling)

Casing Size, Steel grade, Weight and Depth					Drill bit diameter (")	Completion
Type	Size (")	Steel grade	Weight (lbf)	Depth interval (m RKB)		
Surface	20	K55	94	0-60	26	Cemented
Anchor	13⅜	K55	54 and 68	300-400	17½	Cemented
Production	9⅝	K55	40 and 47	750-1200	12¼	Cemented
Slotted liner	7	K55	26	~ 1,800-2200	8½	Hanging/sitting

6.2 Drilling days

Comparing the number of drilling days used during drilling, in four sectors for one hundred and fifty wells, Olkaria North East field has higher average well drilling days. analysis of the wells of the wells with the highest (OW-922) and second highest (OW-731D) number of drilling days indicate significant time was spent in addressing drilling challenges in the 8½" section. Table 4 and Figure 13 compare the average, maximum and minimum drilling days taken by drilling contractor to complete one hundred and fifty geothermal wells in four sectors of the Olkaria Field (KenGen, 2017 - Drilling).

TABLE 4: Drilling day's summary of 150 wells in Olkaria, Kenya (KenGen, 2017 - Drilling)

Field Sectors	Number of wells	Drilling days		
		Average	Maximum	Minimum
Olkaria East	33	59	99	40
Olkaria North East	29	66	106	45
Olkaria South East	14	62	76	40
Olkaria Domes	74	58	157	31

6.3 Instability in well OW-922

Borehole instabilities of well OW-922 in Olkaria Domes contributed to extension of the drilling days from planned 55 days to a total of 157 days. Surface and Anchor Casing sections drilling progressed according to the drilling plan. In the production casing, thirty days were spent in efforts to contain wellbore instabilities and stabilize the well at 603 m. The zone required twenty-four cement plug jobs for drilling to resume. Drilling of 8½" production hole progressed well with to the total depth of 3000 m but tight hole conditions were being experienced at depths between 1200m and 1360 m. The zone required extensive reaming and a special dispersant (sodium hexametaphosphate $(NaPO_3)_6$) was procured to contain the swelling clays narrowing the wellbore in this well section and required the use of bentonite based mud. It took a total of sixty-nine additional days from the days the well was drilled to 3000 m to eventually succeed in running the 7" liner and complete the well (KenGen, 2014 - 922; Otieno, 2016).

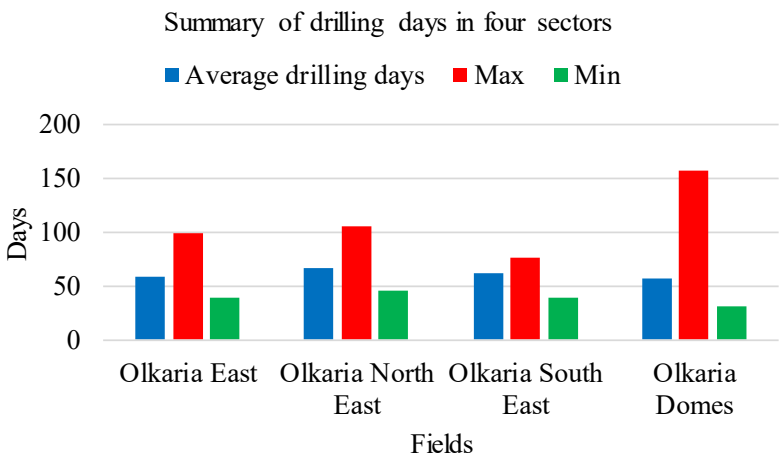

FIGURE 13: Compared drilling days of 150 wells in four fields in Olkaria, Kenya

Comparing four section of the well, contribution of wellbore instability in extension of the total time required to complete the well is evidenced. Taking the major activities from the drilling report of the well and compiling total time accumulation shows the drilling time decreases to less than 50% in each well section. The 8½" hole section had 59% of the total time spent on reaming compared to 22% of drilling time. Summary of the time analyses of the well section are presented in Table 5.

Drilling progress showing instability zones at 603 and 1300 m is shown in Figure 14. The well shows slow temperature recovery after drilling was completed with a temperature below 150°C recorded after 49 days as illustrated in Figure 15.

6.4 Olkaria wells at OW-731 well pad

Well pad 731 in Olkaria North-East Field is at an elevation of about 2220 m a.s.l. and has five wells drilled on it, one drilled vertical, OW-731 and four drilled directionally, namely OW-731A, OW-731B, OW-731C and OW-731D as highlighted in Table 6 and Figure 16 (KenGen, 2017 - Drilling).

TABLE 5: Time analysis of OW-922 well sections showing percentages of drilling time, NPT and other activities (KenGen, 2014 - 922 DDR)

Activity	Time (Hours)	922
26" (0-60 m)		26" hole section 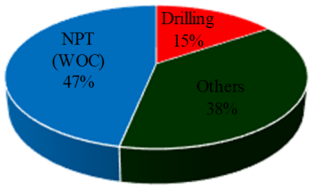
Drilling	12	
NPT (WOC)	36	
Others (casing, cementing, Preparation to spud, Tripping	29	
Total	**77**	
17½" (57-300 m)		17½" hole section 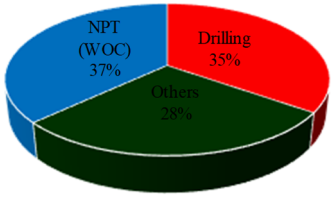
Drilling	48	
NPT (WOC)	51	
Others (casing cementing, tripping, WOW, WHA)	39	
Total	**138**	
12¼" (300- 1199 m)		12¼" hole section 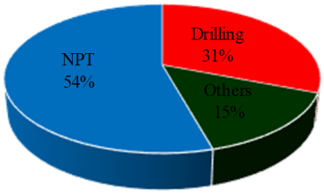
Drilling	410	
NPT (circulating, DOC, reaming, stuck, TOC, WOC, WOI)	719	
Others (casing, cementing, tripping, WHA)	195	
Total	**1324**	
8½"(1199- 3000 m)		8½" hole section 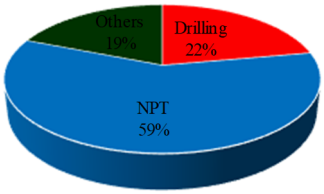
Drilling	499	
NPT (circulating, reaming, dispersant, stuck)	1325	
Others (casing, cementing, survey, WHA, tripping, WHA, WOR)	428	
Total	**2251**	
Grand total	**3790 (157 days)**	

TABLE 6: Orientations of wells at drill pad OW-731 (KenGen, 2017 - Drilling)

Well	Trajectory	Inclination (°)	KOP (m)	Target direction	Elevation (m a.s.l.)
OW-731	Vertical	0	0	Vertical	2215
OW-731A	Directional	20	500	N135°E	2215
OW-731B	Directional	20	400	N225°E	2220
OW-731C	Directional	20	400	N270°E	2220
OW-731D	Directional	20	400	N200°E	2221

Figure 17 indicates the lithology encountered in the wells and location of loss zones in four wells. Drilling parameters (ROP, WOB, torque and pump pressure) from two wells are plotted alongside to correlate the variations with different formation layers and loss of drilling fluid circulation. The vertical well OW- 731 indicates the total loss of drilling fluid circulation experienced during drilling of the 12¼" hole section and part of the17½" hole section. Both sections required backfill cementing to complete casing cementing. Comparing with directional wells OW-731A, the loss of circulation and suspected collapse of wellbore at 400m forced the directional KOP to be move to 500m after conducting cement plug. Large section of the 8½" in OW-731C depicts zones of drilling fluid losses (KenGen, 2017 - Drilling).

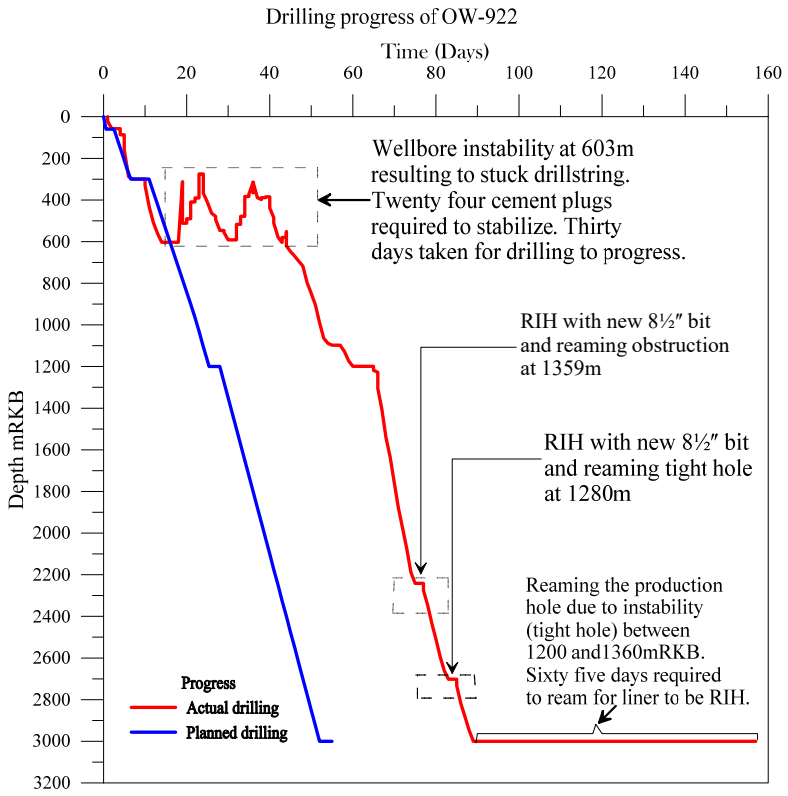

FIGURE 14: Drilling progress of well OW-922 in Olkaria Domes field in Kenya (KenGen, 2014 - 922; KenGen, 2014 - 922 DDR)

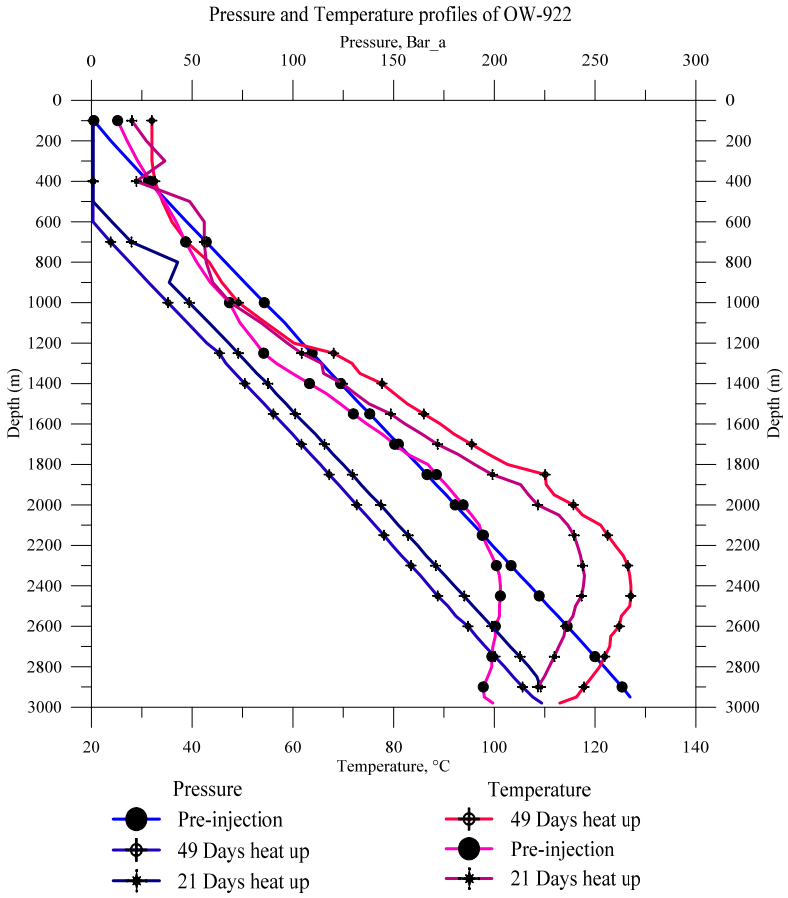

FIGURE 15: Heat up pressure and temperature profiles of well OW-922 in Olkaria, Kenya (KenGen, 2017- Reservoir)

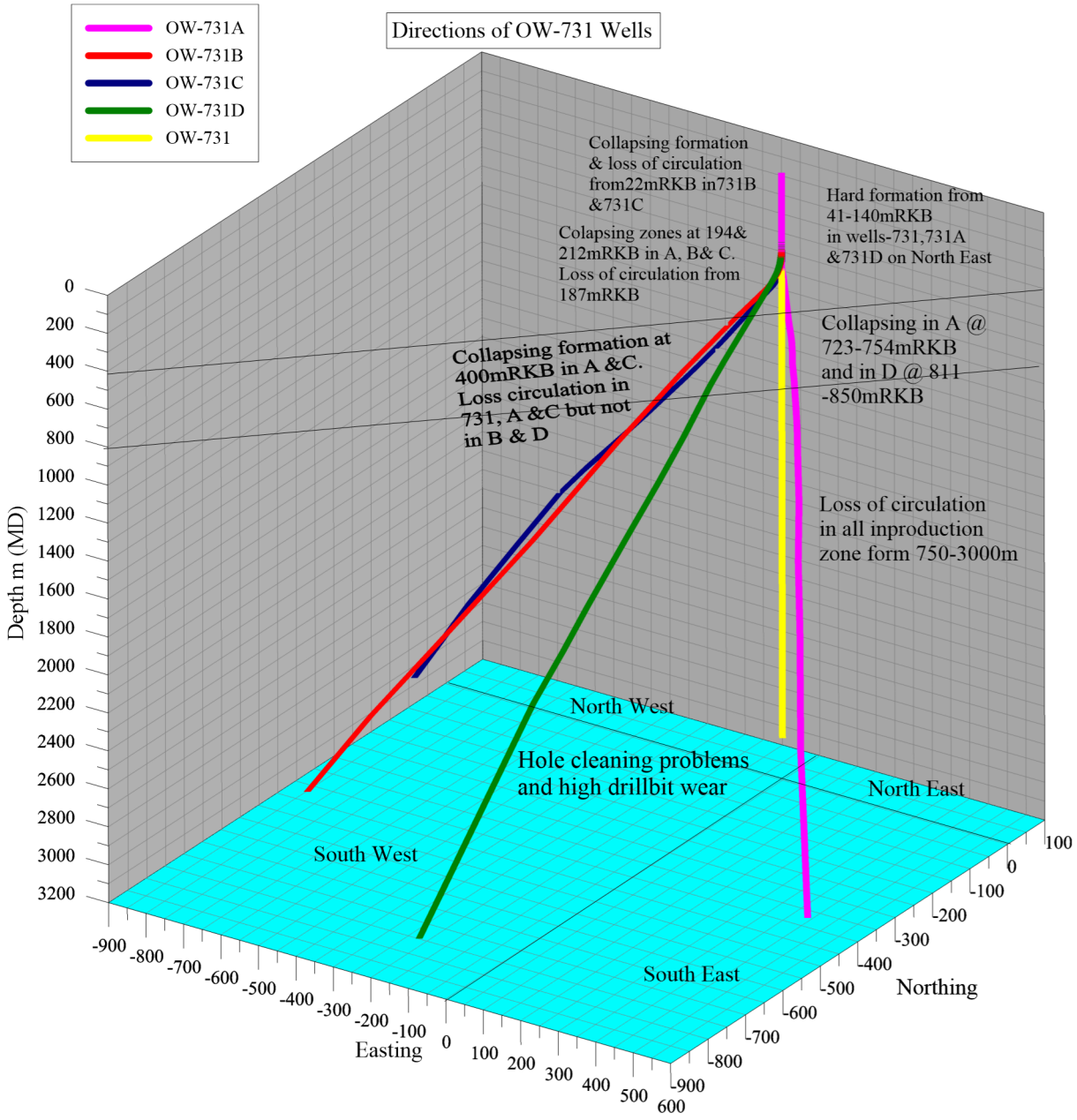

FIGURE 16: Orientations and instability zones in wells at drill pad OW-731

All the wells at OW-731 took more than the planned drilling days of 55 days because of various wellbore instability challenges encountered. Summary of the casing depths, number of drilling days and challenges experienced during drilling of these wells is given in Table 7.

6.4.1 Well OW-731D

Hard formation in surface and part of the anchor casing in addition to cement backfills that were required to complete casing cementing slowed the drilling progress. No challenges were recorded in the production casing section with only change of drill bit noted in the drilling progress. Wellbore instability resulting from loss of circulation and suspected wellbore collapse interrupted drilling progress of the open-hole 8½" section. This contributed to extension of drilling days because of cement plug placement, frequent reaming and circulation of the well. The slotted liner could not be ran to total depth and the bottom of the liners is at 2615m. (KenGen, 2014- 731D). This well took the highest number of days to complete compared to the other wells on this pad. Cumulatively the well took 106 days to complete, 51 days more than the 55 days planned, as depicted in drilling progress, Figure 18. Drilling depths are based on Rotary Kelly bushing (RKB) on the rig floor.

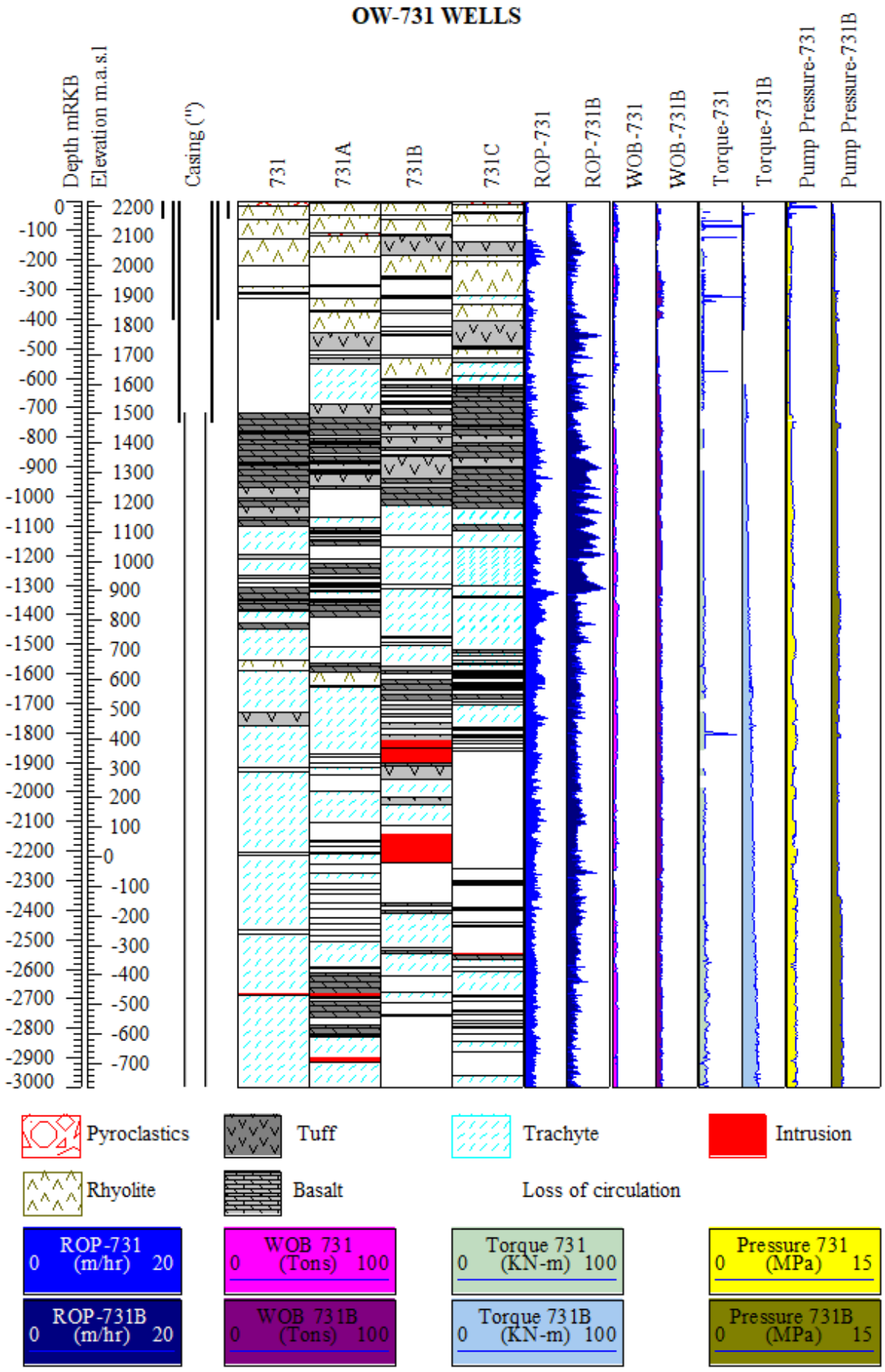

FIGURE 17: Lithology, location of loss zones and drilling parameters of wells at drill pad OW-731 (KenGen, 2011; KenGen, 2013 - 731B)

TABLE 7: Drilling challenges experienced in five wells on Drill pad 731 in Olkaria, Kenya (KenGen, 2017 - Drilling)

Well no.	Section							Challenges in drilling wells at drill pad 731 in Olkaria, Kenya		Total time
	(No)	Bit	Depth	Casing			Depth	Description (drilling depths are based on RKB)	Time	
	(m)	(")	(mRKB)		(")	(m)	(mRKB)		(Days)	(Days)
OW-731	0	26	63	Surface	20	63	0-64	Very hard formation from 41-63 m. Slow drilling progress. Two cement backfills. Extra WOC. Very hard formation from 63-130 m	4 2 10	9
	1	17½	298	Anchor	13⅜	298	64-300	Lost circulation 187-299.5 m. Reaming and circulation to clear cuttings. Six backfill jobs of cement. WOC time.	2 3	27
	2	12¼	722	Production	9⅝	722	300-722	Lost circulation 315-722 m. Reaming, deviation survey and circulation to clean. Loss of cement returns. Six cement backfills required.	4 2	24
	3	8½	3000	Slotted liner	7	3000	722-3000	Lost circulation 1290-1310, 1916-1930, 2206-2212, 2466-2484m	6	25
									SUM	**85**
OW-731A	0	26	57	Surface	20	57	0-57	Very hard formation between 41-63 m.	2	5
	1	17½	294	Anchor	13⅜	294	57-294	Lost circulation 203-294.5 m. Hole clean. problems at 234 m. Collapsing formation at 212 m. Ten plug cement jobs from 234-200 m. Stuck drill string at 212 m. Circulation and reaming to clean the well. Lack of cement returns during casing cementing. Fifteen back fills conducted.	10 1 2 3 1 7 5	38
	2	12¼	754	Production	9⅝	754	294-754	Lost circulation 295.4-372 m. Hole cleaning problem and stuck drill string. Circulation and reaming. Ten plug cement. job from 372-294 m. Change KOP to 500 m Obstruction at 723-754 m, could not run casing. Four cement plugs. Three backfill cement jobs.	2 1 7 3 2 2	30
	3	8½	3000	Slotted liner	7	3000	754-3000	Lost circulation and work on drill-string at 910-926, 974-1072, 1194-1208, 1408-1564, 1638-1644, 1986-1996, 2102-	6	30

Well no.	Section							Challenges in drilling wells at drill pad 731 in Olkaria, Kenya		Total time
	(No)	Bit	Depth	Casing			Depth	Description (drilling depths	Time	
	(m)	(")	(mRKB)		(")	(m)	(mRKB)	are based on RKB)	(Days)	(Days)
								2276, 2322-2400, 2452-2508 and 2700-2824 m .		
									SUM	**96**
OW-731B	0	26	56	Surface	20	56	0-56	Lost circulation 31-56 m. Two backfill cement job due to lack of cement returns. Collapsing well pad, rig down for site repairs and rig up.	1 1 8	12
	1	17½	398	Anchor	13⅜	398	56-398	Collapsing formation from 213-296 m. Thirteen cement plug jobs. Lost circulation 296-396 m. Reaming before running casing. Revision of casing depth from 300 to 400 m. Six backfills required due to lack of cement returns to surface.	4 3 2	26
	2	12¼	751	Production	9⅝	751	398-751	Lack of cement returns in casing cementing. Four backfill required.	1	9
	3	8½	3000	Slotted liner	7	3000	751-3000	Lost circulation 2484-2882 m.	6	31
									SUM	**78**
OW-731C	0	26	57	Surface	20	57	0-575	Collapsing formation at 22 m. Two cement plugs required to stabilize. Two backfills require in casing cementing.	1 1	6
	1	17½	333	Anchor	13⅜	333	57-333	Formation caving at 194 m. Two cement plugs required to stabilize. Lost circulation 84 to 140 m. Three cement backfills required during casing cementing.	1 1 1	15
	2	12¼	751	Production	9⅝	751	333 751	Two cement plug jobs at 400 m to stabilize collapsing formation. Three backfills required in casing cementing.	1 1	12
	3	8½	3000	Slotted liner	7	3000	751-3000	Lost circulation 1304-1340, 1500-1540, 1696-1708, 1810-1850, 1862-2302, 2314-2390, 2402-2440, 2692-2706, 2742-2756, 2818-2846 and 2882-2960 m.	2	31
									SUM	**64**

Well no.	Section							Challenges in drilling wells at drill pad 731 in Olkaria, Kenya		Total time
	(No)	Bit	Depth		Casing		Depth	Description (drilling depths are based on RKB)	Time	
	(m)	(")	(mRKB)			(") (m)	(mRKB)		(Days)	(Days)
OW-731D	0	26	55	Surface	20	55	0-55	Very hard formation. Low drilling rates 25-54 m. Loss of cement returns during casing cementing. Three backfills required.	3 1	6
	1	17½	299	Anchor	13⅜	299	55-299	Very hard formation from 54-140 m. Loss of cement returns during casing cementing. Four backfills required. Reaming before running casing to contain loose formation.	4 1 1	15
	2	12¼	751	Production	9⅝	755	299-755	Loss of cement returns in casing cementing at 755 m. Two backfills required	1	12
	3	8½	3010	Slotted liner	7	2615	755-3010	Lost circulation 786-811 m. Cuttings accumulation problem. Formation caving requiring cement plug to contain and drill ahead. Five cement plugs. Lost circulation 811-849 m. Hole cleaning and steam build up. Ten cement plugs required. Circulation and quenching well. Lost circulation 850-2000 and 2586-2750 m. Partial returns 2000-2586 and 2750-3010 m. Hole cleaning problems as cutting not transported back to surface. High drag between 900-1200 m. Reaming to clear. Obstruction at 1362 and 2552 m. Reaming. Stuck liner at 2006 m Free stuck liner POOH and reaming. Obstruction at 845 m. Liner stops again at 2615 m and didn't go deeper after several attempts Many hours of trips in and out the hole.	1 2 10 6 2 1 1 3 2 26	73
									SUM	106

6.5 Boiling point depth curve (BPD)

Mass and energy balance control fluid flow in a geothermal system. At the reservoir base, fluid is usually in liquid phase. As it flows upward toward the surface, pressure decreases and it separates into two phases, vapour and liquid once the saturation pressure is reached. Below the saturation pressure, fluid

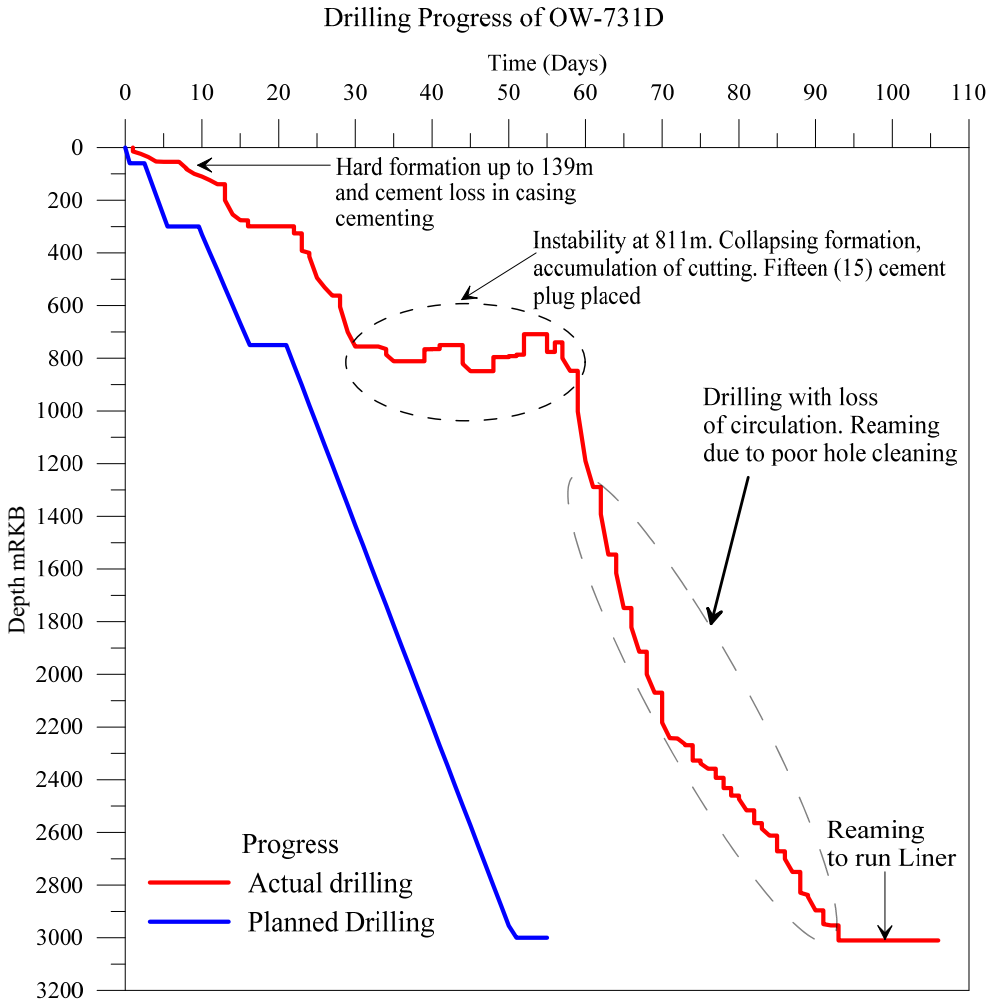

FIGURE 18: Drilling progress of well OW-731D in Olkaria North East field, Kenya (KenGen, 2014- 731D; KenGen, 2014 731D DDR)

temperature is equal to the base liquid temperature. Once boiling has started the temperature depends on the saturation temperature given by Equation 77, which is controlled by the flowing pressure. Pressure gradient at any depth is equal to the geothermal system hydrostatic gradient (Grant and Bixley, 2011):

$$\frac{dP}{dz} = \rho_w g; \quad T = T_{sat}(P) \tag{77}$$

where T =temperature, P = pressure, z= depth, ρ_w= water density, g =acceleration due to gravity and T_{sat}= saturation temperature.

The boiling point depth (BPD) curve is then equal to a static water column pressure determined from the liquid density at saturation temperature at all depths. This gives a good estimate of the initial (natural) state of the reservoir pressure profile (Grant and Bixley, 2011). The BPD curve starting at the water level´s depth of 700m as in wells OW-731 is used to estimate the pore pressure in calculating the minimum principal stress. In well RN-33 the water level depth of 500m is used from the pressure logging data of the well.

6.6 Pressure and temperature in the wells at OW-731

After drilling of the wells at OW-731 and running in a slotted liner, completion tests were carried out. Pre-injection (pressure and temperature logging after drilling completion with no pumping of water into the well), injection tests are normally conducted to confirm the well Injectivity Index. To monitor

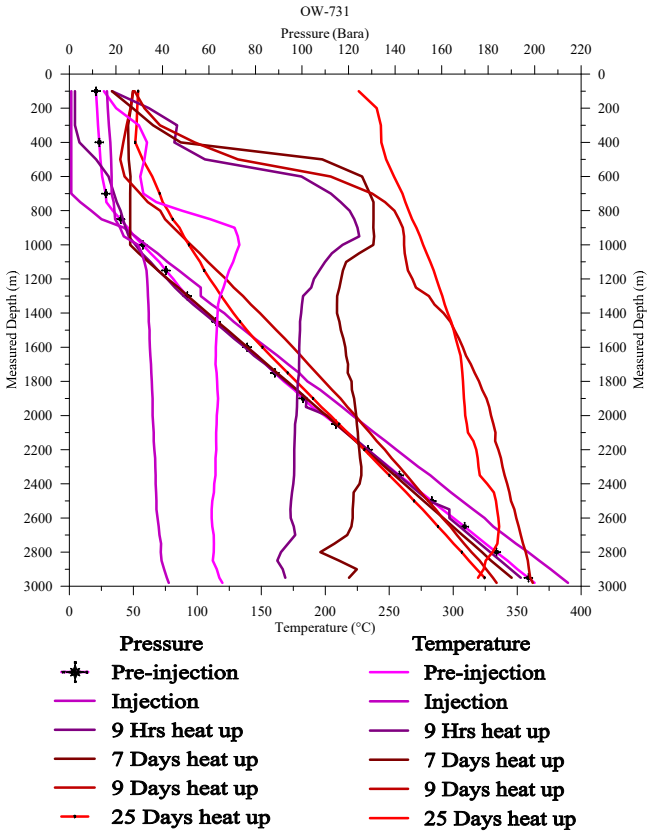

FIGURE 19: Pressure and temperature profiles in well OW-731

temperature recovery of the well, heating up pressure and temperature logging is made at selected time intervals. These tests combined with flow testing are used to evaluate the well productivity. From the pressure logging, water level (table) in the well is easily noticeable with rapid increase of pressure (Grant 2014). The plotted well logging depths are based on the measured depth (MD) recorded during logging.

In the wells at OW-731 well pad, the water level from the pre-injection pressure logging occurs at 700 m. Although in OW-731B and 731D, the water depth is recorded at 850 m and 650 m respectively, the depth of 700m is used as a reference to evaluate the boiling pressure for depth which in this thesis is used as the criteria for the pore pressure in the reservoir. Figures 19-23 show the pressure and temperature plots of the wells from the logging data (KenGen, 2017 - Reservoir).

6.7 Casing depth

The Production Casing depth of the five wells at drill pad OW-731 was set at 750 m (Table 8) and thereafter the open-hole section was drilled to a depth of 3000 m (KenGen, 2014). Using the pressure profiles from vertical well OW-731, the minimum production casing setting depth design is evaluated. Two design methods are compared New Zealand Code of practice for deep geothermal wells (NZS 2403:1991) and African Union code of practice for geothermal drilling (African Union, 2016) which is based on the recently revised New Zealand standard (NZS 2403:2015) (New Zealand Standard, 2015). Both standards start with the conditions on the bottom of the well at 3000 m where the pressure is ~200 bar from the logging pressure data. From this initial point the pressure profile is calculated up to surface by a) assuming saturated steam from final well depth to surface using Equation 77. The point of intersection with the overburden line intersecting the overburden pressure indicates minimum casing depth as per NZS 2403:1991, or b) minimum casing shoe depth is selected where the maximum bottom hole saturated pressure equals the effective containment pressure (ECP) (African Union;, 2016; New Zealand Standard, 1991).

Using the maximum bottom hole pressure of 200 bar, the point of intercept with the minimum fracture pressure sets the minimum casing depth for the production casing at 1450 m (African Union;, 2016). Projecting the steam pressure to the overburden pressure, as per the old New Zealand standard (1991), the minimum casing depth is set at 700 m. Figure 24 shows the minimum casing depth of production for the two design criteria (African Union;, 2016; New Zealand Standard, 1991).

TABLE 8. Design of well RN-33 at the Reykjanes field in Iceland (Níelsson et al., 2014)

Casing	Size (")	Steel grade	Weight (lbf)	Depth (m GL)	Drill bit (")	Depth (mRKB)	Completion
Surface	22½	K-55	-	89.2	26	98.5	Cemented to surface
Anchor	18⅝	K-55	87.5	300.0	21	310.0	Cemented to surface
Production	13⅜	K-55	68.0	947.6	17½	961.0	Cemented to surface
Liner	9⅝	K-55	36.0	2637.2	12¼	2695.0	Slotted

*GL-ground level, Elevation 29.5 m a.s.l.

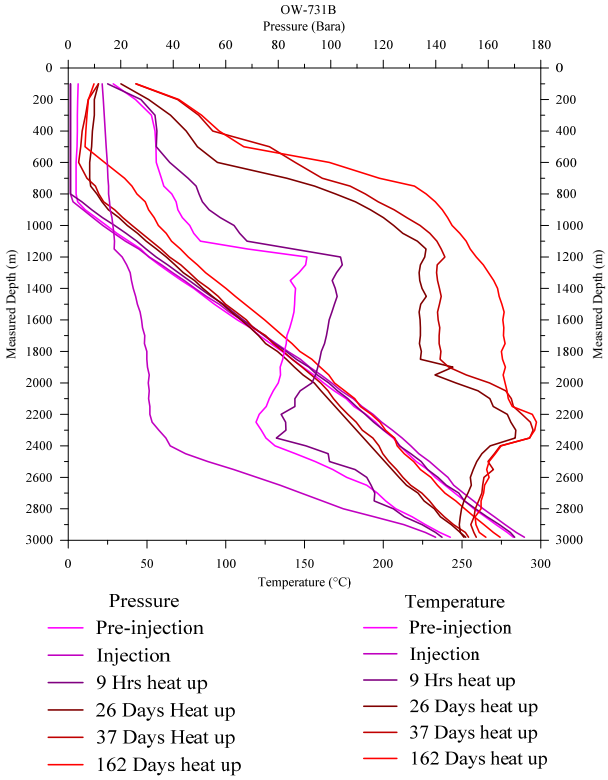

FIGURE 20: Pressure and temperature profiles in well OW-731B

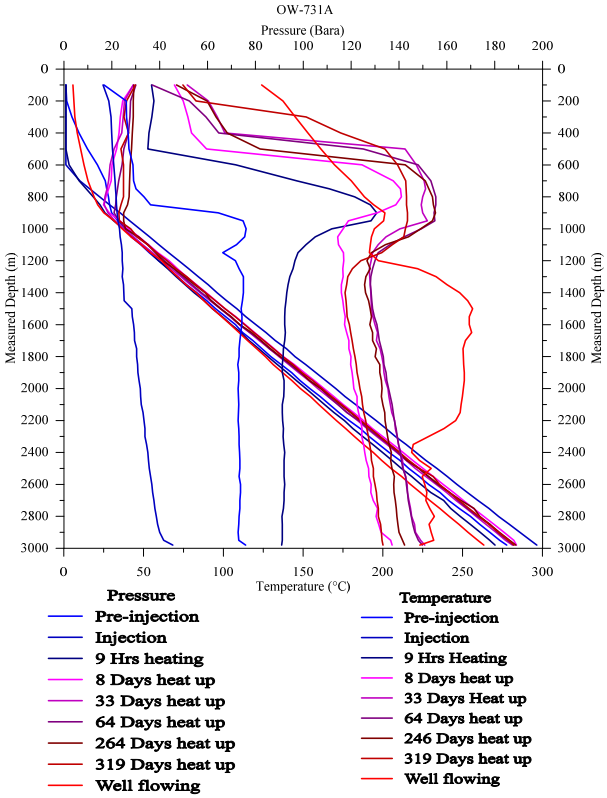

FIGURE 21: Pressure and temperature profiles in well OW-731A

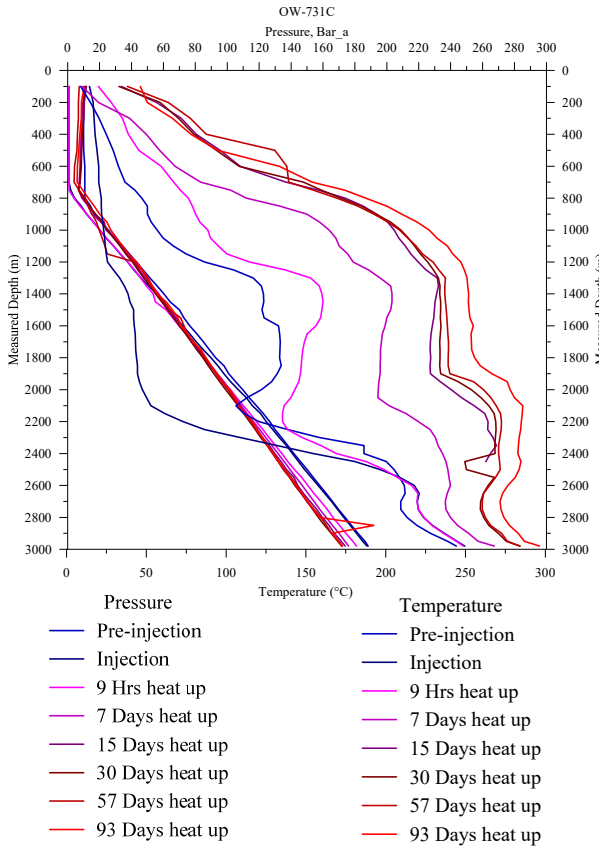

FIGURE 22: Pressure and temperature profiles in well OW-731C

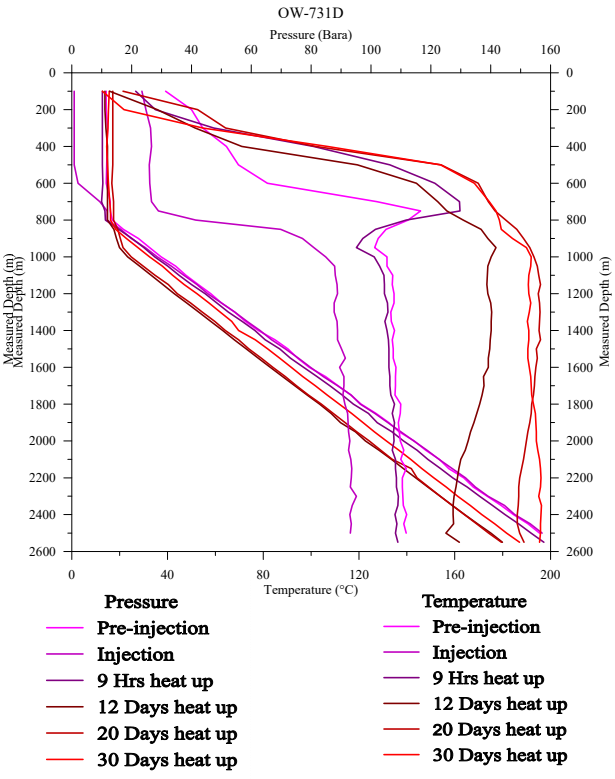

FIGURE 23: Pressure and temperature profiles in well OW-731D

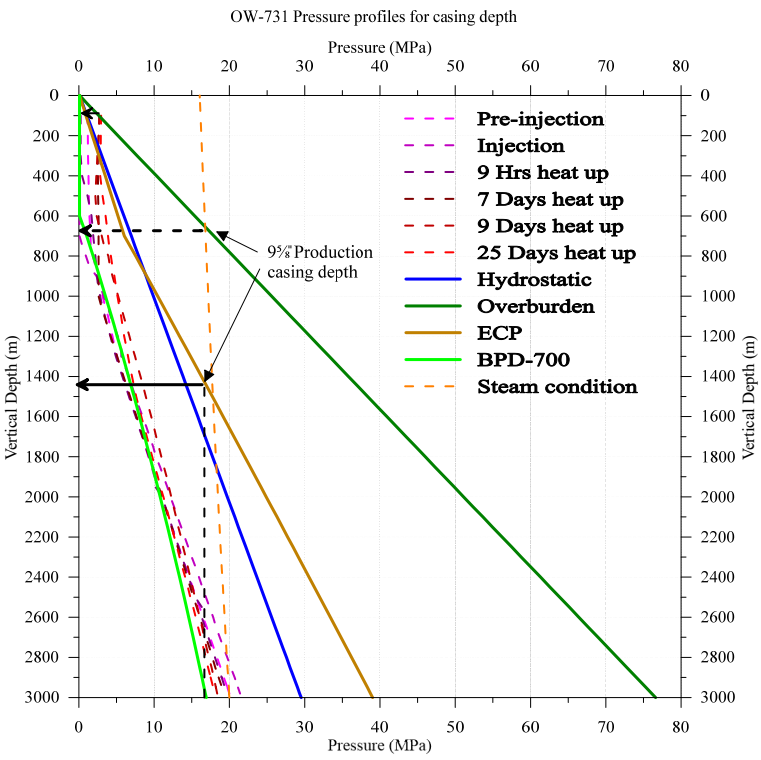

FIGURE 24: Minimum casing depths using BPD and ECP and using steam condition and overburden pressure

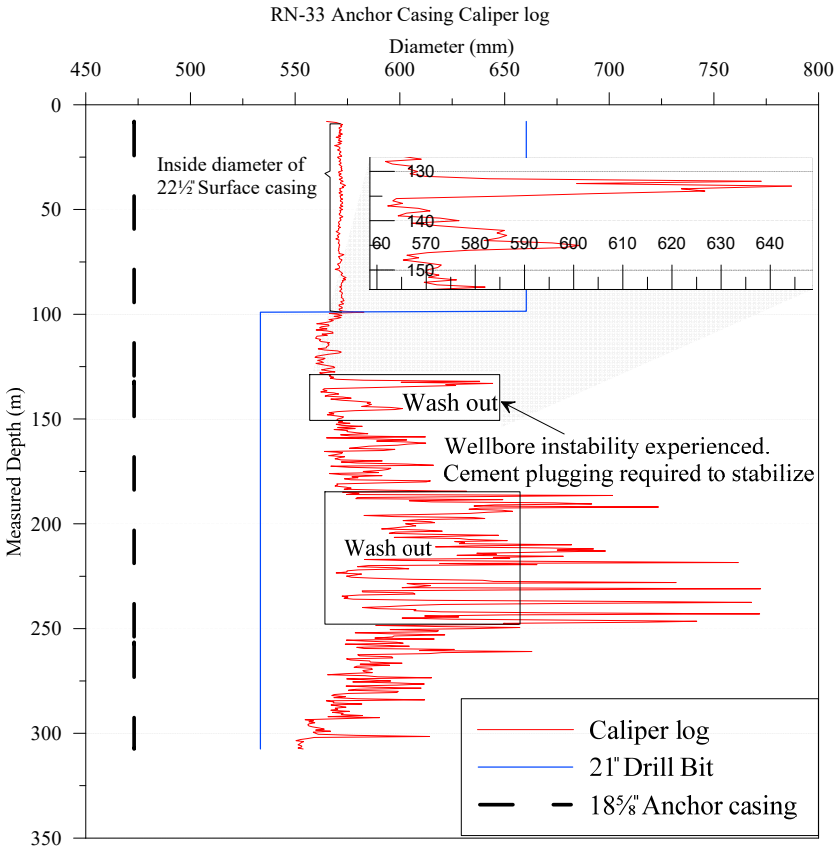

FIGURE 25: Caliper log from the anchor casing section in well RN-33 showing instability at 130 to 135 m and 190 to 250 m (Níelsson et al., 2014)

6.8 Well RN-33 in the Reykjanes field Iceland

Well RN-33 located in Reykjanes geothermal field, Iceland was drilled from July to November 2013. The well was drilled directionally at an inclination of 30° in an azimuth of 171°. The KOP was set at 323 m just below the anchor casing shoe. The well design consists of four sections namely surface, anchor, production and liner, summarized in Table 8 (Níelsson et al., 2014).

Fractured formations and loss of drilling fluid circulation encountered between depth of 47 and 60m created instability conditions during surface hole drilling. Stuck drill string condition was experienced and drilling had to be switched from down the hole hammer drilling (DTH) to rotary drilling with tri-cone bit. Tight hole conditions hindered running of the surface casing and cement was required to stabilize the well. In the Anchor, Production and Liner section, the main challenge was loss of drilling circulation that made cuttings to accumulate at the bottom of the well (Níelsson et al., 2014). Open hole logging was conducted for temperature, Neutrons, gamma ray, resistivity, self-potential and caliper- and acoustic borehole imaging (ABI) (televiewer) (Níelsson et al., 2014).

Caliper logging using four arm XY caliper tool was conducted in the in the Anchor, Production and Liner sections for well geometry and cement estimation. A televiewer log was conducted in the reservoir section to locate permeability structures and feeder zones. Figures 25-27 show caliper logs of anchor, production and liner section of well RN-33

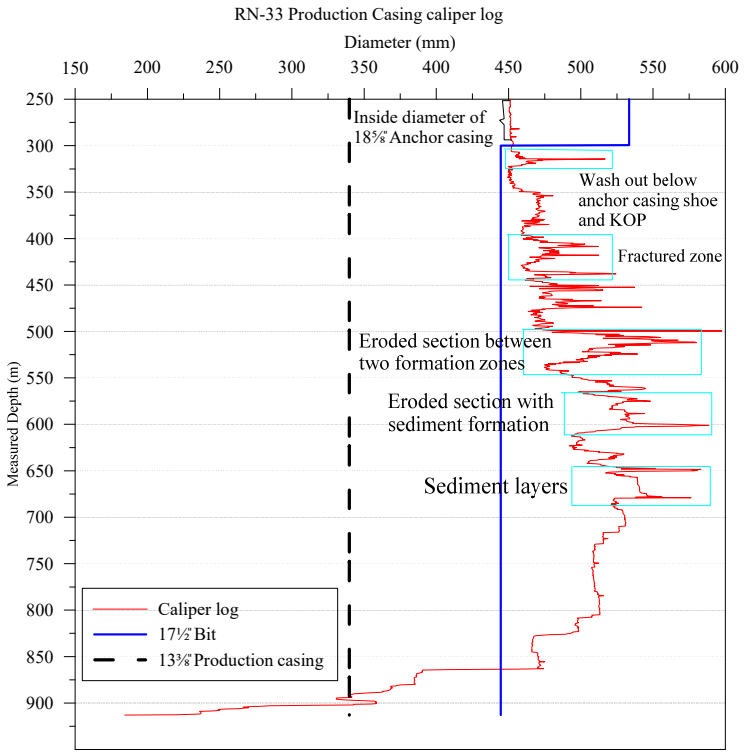

FIGURE 26: Caliper log from the production casing section in well RN-33 showing instability sections at 300, 450, 550 and 650m (Níelsson et al., 2014)

indicating variation of well diameter to the drill bit diameter.

Drilling progress of well RN-33 is shown in Figure 28 with highlight of logging activities carried out at 2520 m during drilling of the well. Note the working days include 23 days of transportation and rig up, which is normally not included on the drilling progress graphs.

The televiewer (ABI) log of liner section showing eroded sections and fractures in the well corresponding to the depths picked during caliper logging are shown in Figure 29. The logs were analysed to show direction of the features observed (Árnadóttir et al., 2014). No feeder zone was located at the broken zone at 2279 m suggesting it as an eroded unstable section of the well that can be affirmed with the pick in the caliper log. The mean direction is 6.09°/ 270.21° clockwise from North (0° azimuth).

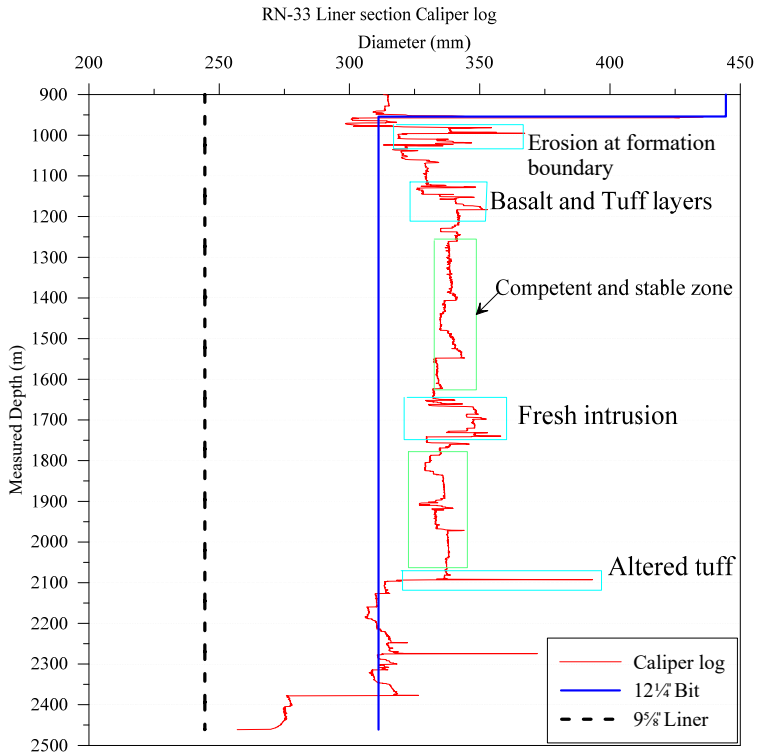

FIGURE 27: Caliper log of the liner section in well RN-33 showing eroded sections at 150, 1550, 1700 and 2250m (Níelsson et al., 2014)

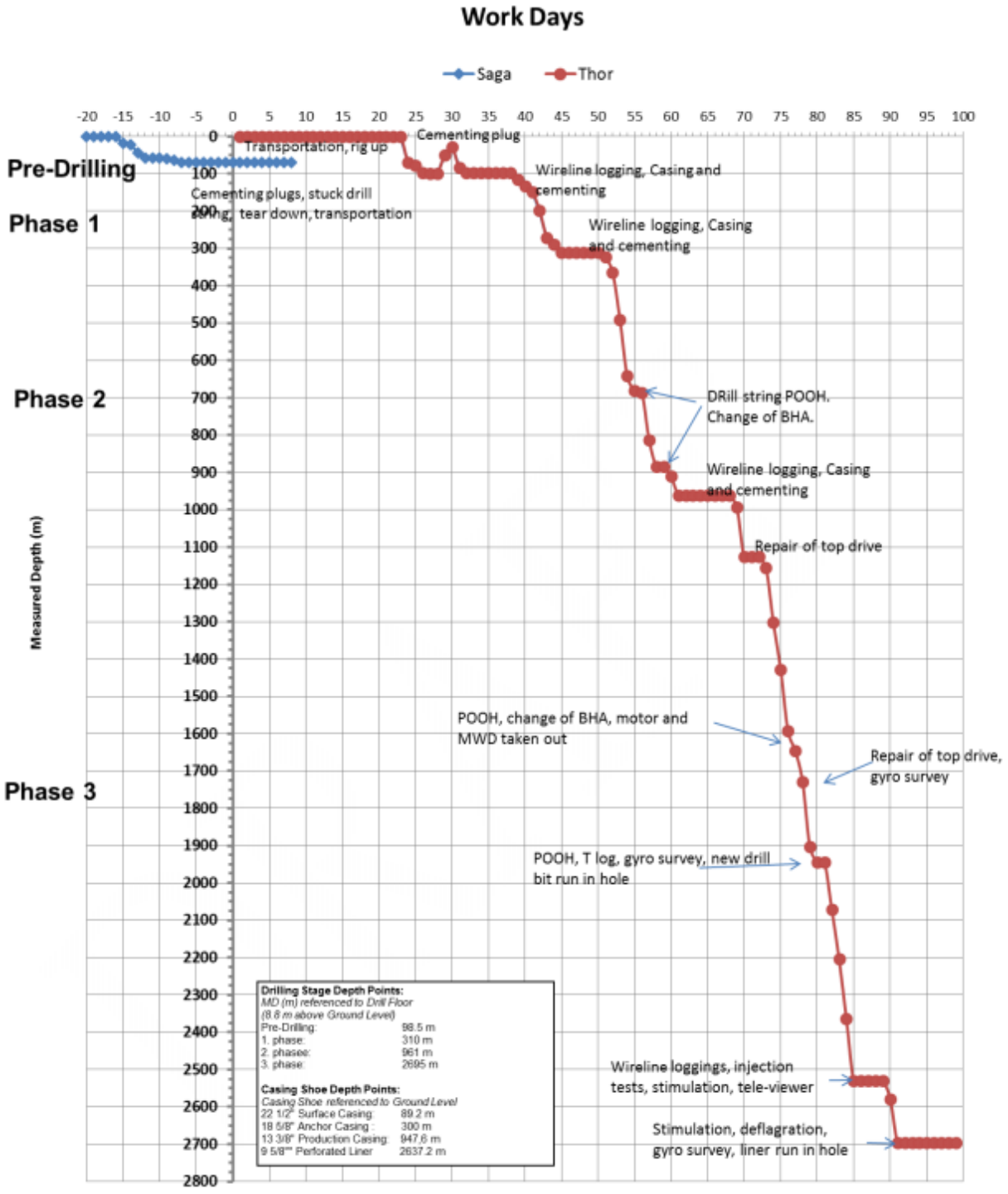

FIGURE 28: Drilling progress of well RN-33 at Reykjanes in Iceland (Níelsson et al., 2014)

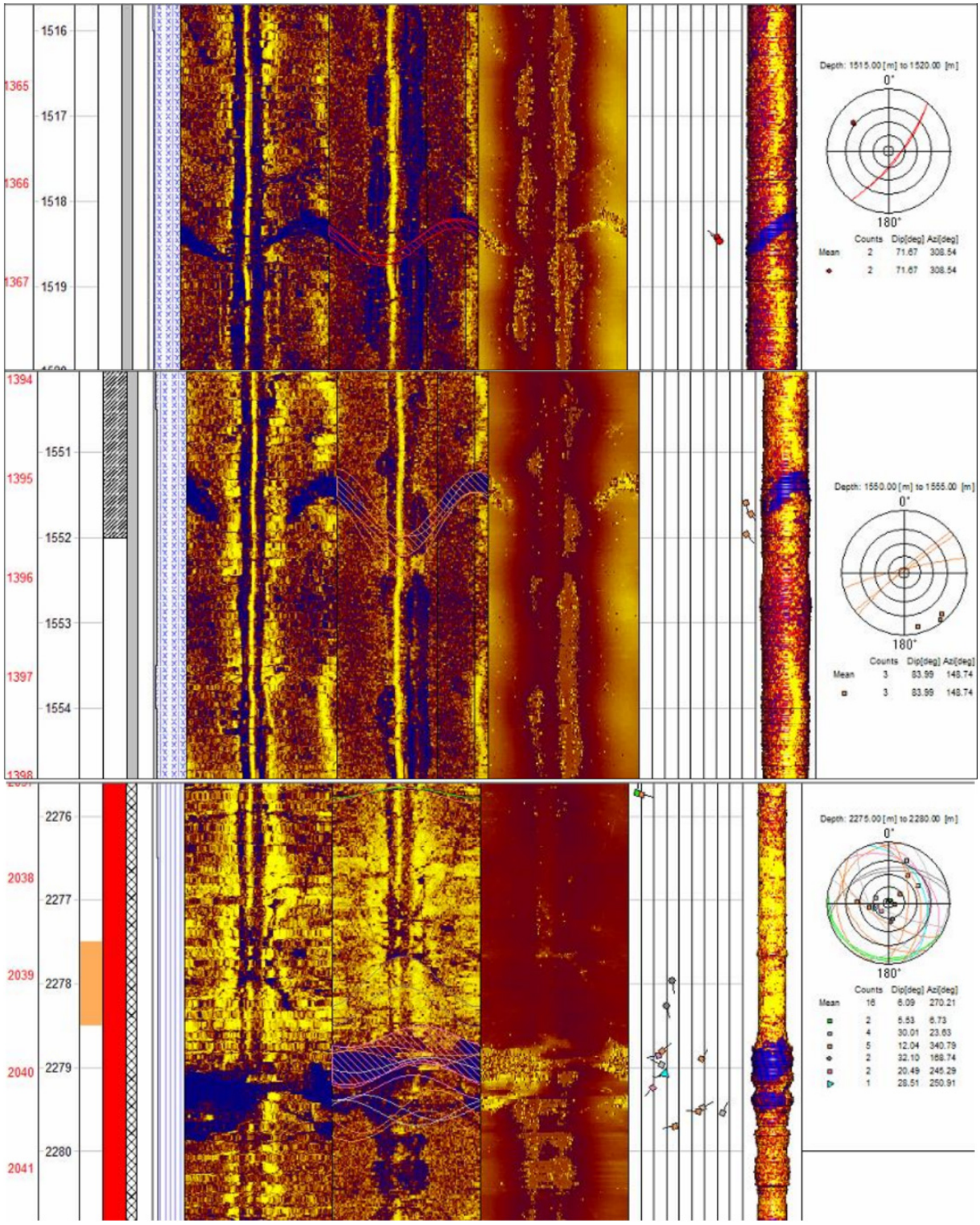

FIGURE 29: Televiewer image from well RN-33 showing fractures at 1518 and 1552m and eroded zone at 2279 (Árnadóttir et al., 2014)

7. STRESS AND STABILITY ANALYSIS

The tectonic setting of Olkaria is in continental East African Rift Valley, a divergent system stretching the lithosphere. It is mainly dominated by normal faulting trending in the N-S, NW-SE, NE-SW, ENE-WSW (Munyiri, 2016). Similarly, well RN-33 is located in the divergent mid- Atlantic rifting system in Iceland (Franzson et al., 2002). Using the Anderson's Faulting Theory (Zoback, 2010), field stresses (in situ) comprises of vertical S_v, maximum horizontal S_H and minimum horizontal S_h stresses. Vertical stress forms the maximum principal compressive stress with magnitude equal to the overburden (lithostatic) stress in normal faulting (Table 2). The maximum (intermediate) horizontal stress has the direction parallel to the faulting direction (N-S) and the minimum horizontal stress perpendicular to faulting direction (Turcotte and Schubert, 2014).

TABLE 9: Rock types and density at drill pad 731 (KenGen, 2017 - Geology)

No.	Depth (mRKB)	Rock (type)	Density (kg/m^3)
1	0 - 450	Rhyolite	2510
2	450 - 630	Basalt	2730
3	630 - 745	Trachyte	2540
4	745 - 1130	Basalt	2730
5	1130 - 3000	Trachyte	2540

The major rock types in the OW-731 area from the well stratigraphy include Rhyolite, Basalts and Trachyte (Otieno, 2016). The depth at which they are located in the well and their respective rock densities are summarised in Table 9. These densities are used in Equation 6 to calculate the overburden at true vertical depths (TVD) in this report to 3000 metres for wells in Olkaria. Well RN-33 has Basalt the most dominant rock formation (Níelsson et al., 2014; Franzson et al., 2001) and basalt density of 2730 Kg/m^3 is used from surface. An average rock Poisson's Ratio of 0:24 (Simiyu, 2000 and 1999) is used in Olkaria and 0.27 (Blanck, 2016) based on the seismic data. Using Eaton's Formula given by Equation 54, the minimum principal stress is calculated that incorporates overburden stress, pore pressure (BPD) and rock Poisson's ratio. The maximum horizonatal stress S_h is approximated by the average of overburden and minimum horizontal. Selected results are presented in Table 10.

TABLE 10: Sample calculation of field stresses

TVD (m)	$\boldsymbol{\rho_r}$ (Kg/m^3)	$\boldsymbol{g}$ (m/s)	$\boldsymbol{S_v = \rho_r * g * h}$ (MPa)	$\boldsymbol{\vartheta}$	BPD (MPa)	$\boldsymbol{S_h = P_p + \frac{\vartheta}{1-\vartheta}(S_v - P_p)}$ (MPa)	$\boldsymbol{S_H = \frac{S_v + S_h}{2}}$ (MPa)
100	2510	9.81	2.46	0.24	0.1	0.85	1.65
500	2730	9.81	13.39	0.24	0.1	4.30	8.84
1000	2570	9.81	25.21	0.24	3.54	10.38	17.80

Transforming the field stresses S_v, S_H, and $S_h$into normal and shear stresses in x, y and z directions using Equations 27 to 32, yields nine stress components that make up the stress tensor (Equation 4). For the vertical well and vertical section of deviated wells, the far field (in situ) stresses form the principal stresses with $S_v = \sigma_z$, $S_H = \sigma_x$ and $S_h = \sigma_y$. The shear stresses $\tau_{xy} = \tau_{xz} = \tau_{yz} = 0$ reducing to zero. The principal stress components are substituted in Equations 15, 18 and 19 without consideration of the thermal stress component to calculate the principal effective stresses acting on a vertical borehole wall. Water density of 1000 kg/m^3 is assumed in calculation of the hydrostatic fluid pressure P_f. The results for selected depths at 0° and 90° clockwise from North (0° azimuth) are presented in Table 11.

In directional well, transformed field stress generates normal stresses σ_x, σ_y and σ_z and shear stresses τ_{xy}, $\tau_{xz}$and τ_{yz} in the x, y and z coordinates (Equations 27 to 32). These form the stress tensor components used to calculate the effective hoop, radial shear and vertical stresses at around the wellbore wall using Equations 33 to 37 in circular coordinates. The principal effective stresses around the wellbore namely maximum, intermediate and minimum stresses are then determined by substituting the circular hoop, vertical and shear in Equations 38, 39 and 40. (Zoback, 2010). The calculated stresses for the various vertical depths based on the well inclination and azimuths from the North for well RN-33 and OW-731D are presented in Table 12 and 13.

TABLE 11: Calculated effective stresses in vertical well OW-731

Depth (m)		60	100	300	500	750	1000	1200	1500	2000	3000
BPD (MPa)		0.10	0.10	0.10	0.10	1.47	3.54	5.10	7.33	10.80	16.92
P_f (MPa)		0.69	1.08	3.04	5.01	7.46	9.91	11.87	14.82	19.72	29.53
Field stress (MPa)											
S_v		1.58	2.56	7.49	13.49	18.79	26.88	30.00	37.48	49.93	74.85
S_H		1.08	1.74	5.02	9.03	13.02	19.10	21.70	27.43	36.89	55.54
S_h		0.59	0.92	2.56	4.56	7.25	11.32	13.40	17.38	23.84	36.23
Transformed stresses in x, y and z coordinates (MPa)											
σ_x		1.08	1.74	5.02	9.03	13.02	19.10	21.70	27.43	36.89	55.54
σ_y		0.59	0.92	2.56	4.56	7.25	11.32	13.40	17.38	23.84	36.23
σ_z		1.58	2.56	7.49	13.49	18.79	26.88	30.00	37.48	49.93	74.85
τ_{xy}		0.00	0.00	0.00	0.00	0.00	0.00	0.00	0.00	0.00	0.00
τ_{xz}		0.00	0.00	0.00	0.00	0.00	0.00	0.00	0.00	0.00	0.00
τ_{yz}		0.00	0.00	0.00	0.00	0.00	0.00	0.00	0.00	0.00	0.00
Effective principal stresses acting on the borehole wall at 0° and 90° (MPa)											
0°	$\sigma_{\theta\theta}$	-0.10	-0.16	-0.48	-0.44	-0.21	1.41	1.53	2.56	4.12	6.70
	σ_{zz}	1.48	2.46	7.39	13.39	17.31	23.34	24.90	30.15	39.14	57.94
	σ_r	0.59	0.98	2.94	4.91	5.98	6.37	6.77	7.49	8.92	12.61
90°	$\sigma_{\theta\theta}$	1.87	3.12	9.37	17.41	22.87	32.53	34.73	42.76	56.31	83.95
	σ_{zz}	1.72	2.87	8.62	15.62	20.20	27.23	29.05	35.17	45.66	67.59
	σ_r	0.59	0.98	2.94	4.91	5.98	6.37	6.77	7.49	8.92	12.61

TABLE 12: Calculated stresses in directional well RN-33 inclined at 30º at an azimuth of 171°

Depth (m)		60	100	300	500	750	1000	1200	1500	2000	2600
BPD (MPa)		0.10	0.10	0.10	1.04	3.15	5.11	6.61	8.76	12.12	15.79
P_f (MPa)		0.69	1.08	3.04	5.01	7.46	9.91	11.87	14.82	19.72	25.61
Field stress (MPa)											
S_v		1.71	2.78	8.13	13.49	20.19	26.88	32.24	40.27	53.66	69.73
S_H		1.17	1.89	5.46	9.34	14.51	19.63	23.70	29.77	39.81	51.75
S_h		0.64	0.99	2.78	5.19	8.83	12.37	15.15	19.27	25.96	33.77
Transformed stresses in x, y and z coordinates (MPa)											
σ_x		1.17	1.89	5.46	10.30	15.82	21.31	25.67	32.20	43.02	55.92
σ_y		0.64	0.99	2.78	5.29	8.97	12.55	15.36	19.52	26.30	34.21
σ_z		1.71	2.78	8.13	12.43	18.73	25.02	30.05	37.58	50.12	65.13
τ_{xy}		0.00	0.00	0.00	0.56	0.76	0.97	1.14	1.41	1.85	2.41
τ_{xz}		0.00	0.00	0.00	-1.84	-2.52	-3.22	-3.79	-4.66	-6.14	-7.98
τ_{yz}		0.00	0.00	0.00	0.32	0.44	0.56	0.66	0.81	1.07	1.39
Circular stress components and principal stresses acting on the borehole wall at 0° and 90° (MPa)											
0°	$\sigma_{\theta\theta}$	-0.05	-0.09	-0.26	-0.47	0.47	1.31	1.93	2.79	4.05	5.32
	σ_{zz}	1.34	2.23	6.70	7.88	11.15	14.53	17.28	21.48	28.64	37.48
	$\tau_{\theta z}$	0.00	0.00	0.00	0.64	0.88	1.12	1.32	1.62	2.14	2.78
	σ_{tmax}	1.34	2.23	6.70	7.93	11.22	14.62	17.39	21.62	28.83	37.72
	σ_{tmin}	-0.05	-0.09	-0.26	-0.52	0.40	1.22	1.82	2.65	3.87	5.08
	σ_r	0.59	0.98	2.94	3.96	4.31	4.80	5.26	6.05	7.60	9.82
90°	$\sigma_{\theta\theta}$	2.09	3.48	10.45	19.57	27.89	36.35	43.18	53.50	70.93	92.14
	σ_{zz}	1.87	3.12	9.37	13.89	19.01	24.29	28.59	35.16	46.36	60.19
	$\tau_{\theta z}$	0.00	0.00	0.00	3.68	5.04	6.44	7.58	9.32	12.29	15.95
	σ_{tmax}	2.09	3.48	10.45	21.38	30.17	39.14	46.40	57.41	76.02	98.74
	σ_{tmin}	1.87	3.12	9.37	12.08	16.73	21.50	25.37	31.26	41.27	53.59
	σ_r	0.59	0.98	2.94	3.96	4.31	4.80	5.26	6.05	7.60	9.82

TABLE 13: Calculated stresses in directional well OW-731D

Depth m	60	100	300	500	750		1000	1200	1500	2000	3000
BPD (MPa)	0.10	0.10	0.10	0.10	1.47		3.54	5.10	7.33	10.80	16.92
P_f (MPa)	0.69	1.08	3.04	5.01	7.46		9.91	11.87	14.82	19.72	29.53
Field stress (MPa)											
S_v	1.58	2.56	7.49	13.49	18.79		26.88	30.00	37.48	49.93	74.85
S_H	1.08	1.74	5.02	9.03	13.02		19.10	21.70	27.43	36.89	55.54
S_h	0.59	0.92	2.56	4.56	7.25		11.32	13.40	17.38	23.84	36.23
Transformed stresses in x, y and z coordinates (MPa)											
σ_x	1.08	1.74	5.02	9.09	13.10		19.21	21.81	27.56	37.07	55.80
σ_y	0.59	0.92	2.56	5.09	7.92		12.23	14.37	18.55	25.37	38.49
σ_z	1.58	2.56	7.49	12.91	18.03		25.86	28.92	36.16	48.23	72.33
τ_{xy}	0.00	0.00	0.00	-1.35	-1.74		-2.35	-2.51	-3.03	-3.94	-5.83
τ_{xz}	0.00	0.00	0.00	-1.60	-2.07		-2.79	-2.98	-3.61	-4.68	-6.93
τ_{yz}	0.00	0.00	0.00	-0.49	-0.63		-0.86	-0.91	-1.10	-1.43	-2.12
Circular stress components and principal stresses acting on the borehole wall at 0° and 90° (MPa)											
0°	$\sigma_{\theta\theta}$	-0.10	-0.16	-0.48	1.06	1.73	4.03	4.33	5.95	8.52	13.21
	σ_{zz}	1.23	2.05	6.16	9.81	12.97	17.84	19.09	23.33	30.58	45.75
	$\tau_{\theta z}$	0.00	0.00	0.00	-0.98	-1.27	-1.71	-1.82	-2.21	-2.87	-4.25
	σ_{tmax}	1.23	2.05	6.16	9.91	13.11	18.05	19.32	23.60	30.95	46.30
	σ_{tmin}	-0.10	-0.16	-0.48	0.96	1.59	3.82	4.11	5.68	8.16	12.67
	σ_r	0.59	0.98	2.94	4.91	5.98	6.37	6.77	7.49	8.92	12.61
90°	$\sigma_{\theta\theta}$	1.87	3.12	9.37	17.07	22.43	31.94	34.10	42.00	55.32	82.48
	σ_{zz}	1.72	2.87	8.62	14.81	19.15	25.81	27.54	33.34	43.28	64.07
	$\tau_{\theta z}$	0.00	0.00	0.00	3.20	4.14	5.59	5.96	7.21	9.37	13.87
	σ_{tmax}	1.87	3.12	9.37	19.34	25.25	35.25	37.62	46.08	60.43	89.92
	σ_{tmin}	1.72	2.87	8.62	12.54	16.33	22.51	24.02	29.25	38.17	56.63
	σ_r	0.59	0.98	2.94	4.91	5.98	6.37	6.77	7.49	8.92	12.61

7.1 Stress variation wellbore

During geothermal well drilling loss of drilling fluid is frequently experienced either full or partial loss of fluid circulation. This reduces the radial effective stress. Plotting effective stress demonstrates how compressive hoop stresses vary with full circulation and when fluid loss is experienced. The hoop stress is tangential to the wellbore and forms one of the principal stresses in a vertical borehole together with the vertical stress and radial stress from drilling fluid. During circulation loss of drilling fluid, the radial effective stress is taken to be zero. Calculated minimum stress S_h is taken to be constant around the wellbore and is used to approximate the formation strength at selected depth.

7.1.1 Vertical well

For vertical well, stress variation indicates maximum compressive stress occurs at $\theta = 90°$ and $270°$ and minimum compressive stresses (tensile) occurs at $\theta = 0°$ and $180°$ clockwise from North (0° azimuth). The minimum compressive hoop stress direction represents the direction of the maximum horizontal field stress while maximum compressive stress minimum horizontal stress direction (Zoback, 2010). With circulation loss, the effective radial stress component that support wellbore wall is lost and this will result in increased compressive stresses. Using fluid density of 1000 Kg/m^3 indicates the effective radial stress is greater than minimum stress making minimum hoop stress is negative (tensile). During circulation loss, there is no support and the minimum hoop stress becomes positive and increases to the minimum horizontal stress level.

Figure 30 show variation of stresses around vertical well OW-731 at 400 m indicating variation of hoop stress with effective radial stress and increase in hoop stress when radial stress component is zero. Variation of the hoop stress has very large amplitude that is four times the difference between maximum hoop and minimum hoop stress. The difference remain constant with loss of circulation but the

magnitude of the stress values increases. The average vertical stress of the vertical stress variation is equal to the overburden stress at the depth of consideration (Zoback, 2010).

7.1.2 Directional well

For directionally drilled wells, stress variation is related to the direction of the well in relation to the field stresses. Plotting effective hoop stress variation for directional wells at OW-731 and RN-33, occurrence of maximum and minimum stresses vary with the well orientation. The principal stresses at the borehole wall are given by maximum stress $\sigma_1 = \sigma_{tmax}$, intermediate $\sigma_2 = \sigma_{tmin}$ and radial stress $\sigma_3 = \sigma_{rr}$ from the drilling fluid as the minimum stress Well RN-33 is oriented at an azimuth of 171° and inclination angle of 30° (Níelsson et al., 2014). The well shows high effective hoop stresses compared to the Olkaria wells that are inclined at 20°. Variation of effective hoop stress at 750 m is depicted in Figure 31.

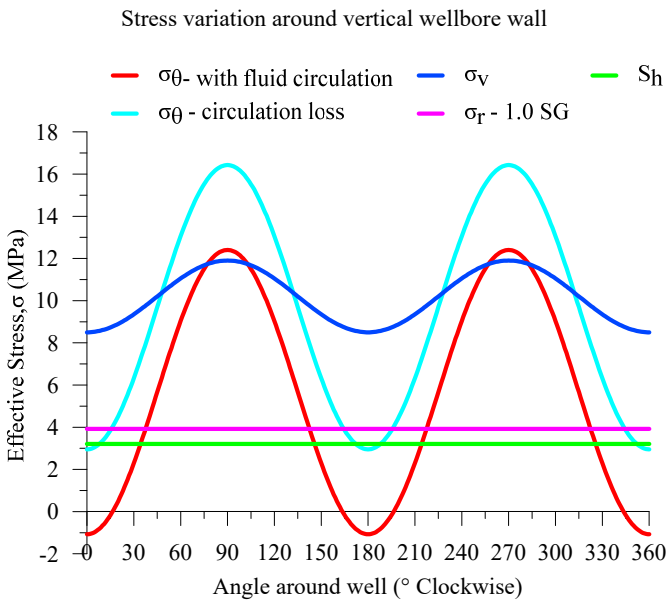

FIGURE 30: Variation of hoop, radial, vertical stresses at 400 m compared with minimum stress

Well OW-731C drilled at an azimuth of 270°N has maximum hoop stresses occurring at 0° and 180° and the magnitude of the stress is lower compared to the other wells. The well also took the least number (64) of days to drill compared to the other wells. Comparing stress difference when there is no fluid in the well, the difference between maximum hoop stress and minimum horizontal stress S_h assumed as the formation strength, the well OW-731C has less as compared to the other wells.

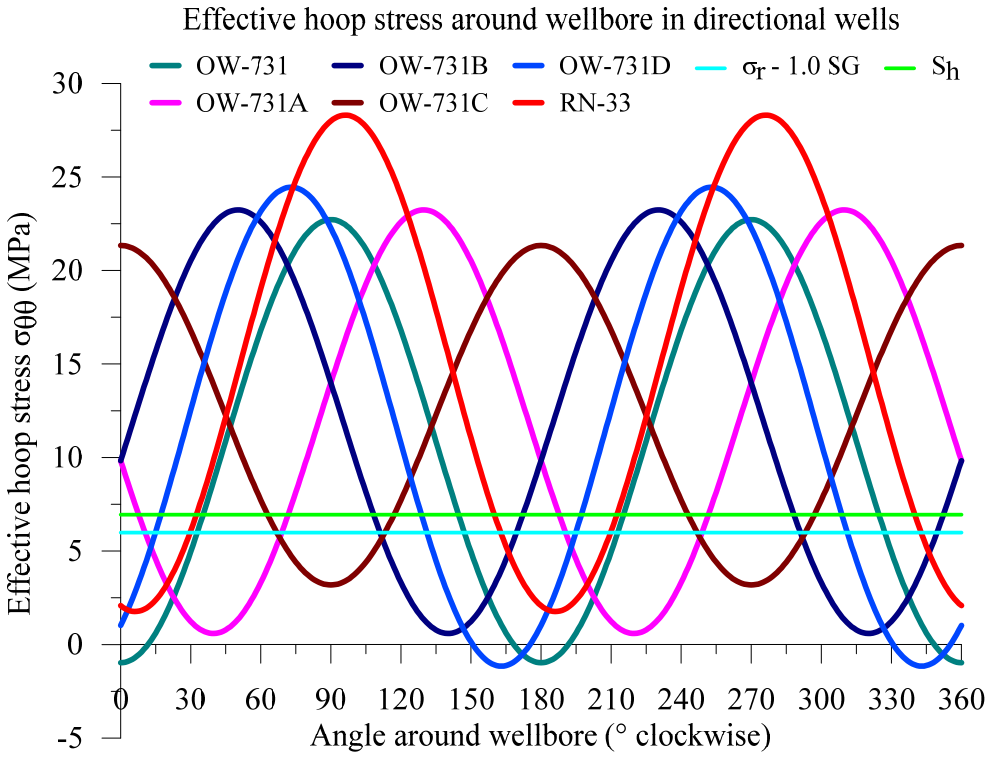

FIGURE 31: Hoop stress variation at 750 m in directional wells

7.2 Wellbore stability

In the wellbore, the compressive hoop stress, $\sigma_{\theta\theta}$ acting tangential will induce collapse of the the wellbore if it exceeds the formation strength. Varying the drilling density varies the effective stresses in the well. Setting fluid density to zero to represent total loss of drilling fluid circulation gives the highest compressive stress. Using drilling fluid densities of 500, 800, 1000, 1200 and 1800 kg/m^3 expressed in specific gravities (SG) of 0.5, 0.8, 1.0, 1.2 and 1.8 when divided with water density of 1000 kg/m^3, compressive stresses decrease with increase in fluid density. Figure 32 indicates variation of effective stresses with varying density from zero.

Using Mohr's circle analysis and applying Mohr-Coulomb failure criterion assuming an internal friction angle of 30°, instability is likely to occur in cases where the circle envelops plots outside the failure line. Setting the minimum value of cohesion at a value given by the maximum shear stress for field stresses$\left(\frac{S_v - S_h}{2}\right) sin90/270°$, stability variation in the well at different depths is shown by the Mohr's circles envelops in Figures 33-39.

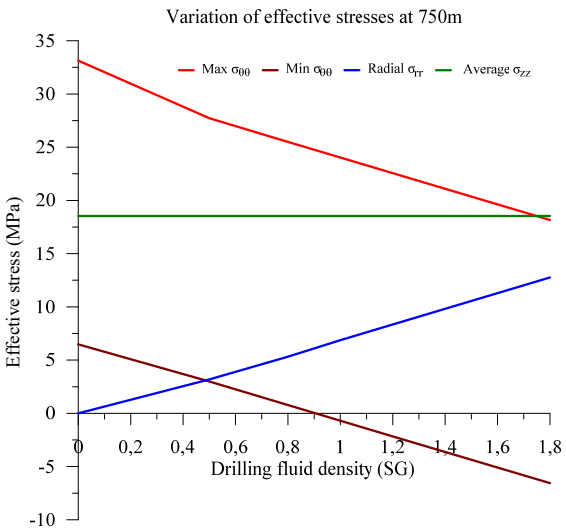

FIGURE 32: Variation of hoop and radial stresses with change of drilling fluid density at 750 m

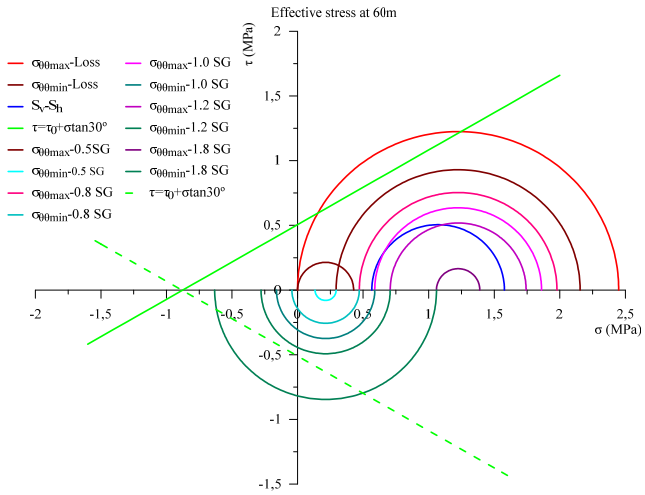

FIGURE 33: Effective stress variation and Mohr-Coulomb failure analysis at 60 m indicating changes in stress conditions with drilling fluid density

Loss of drilling fluid circulation in the well is represented by zero radial stress. At all depths wellbore collapse is likely to occur during loss of circulation in the maximum compressive stress direction since the Mohr's circle envelop plots outside the failure line. In addition, the minimum stress represented by minimum hoop stress is compressive (positive) at all depths and at depths below 1200 to 3000 m (Figures 37 and 39) its failure envelop exceeds the failure. Adjusting drilling fluid density, maximum compressive stress plot below the failure line to a depth 750 m indicating stability improves with increase drilling fluid density. However, at 1.8 SG chances of tensile fracture is possible at all depths.

Above 750 m (Figures 37-39), failure in the maximum compressive stress can take place at 0.8 SG since the circle envelop exceeds the failure line. Well OW-731D drilled directionally at an inclination of 20° in 200°N direction, experienced challenges at 810m and the 8½" hole section was drilled blindly without any returns to surface. Mohr circle plots for depth above 750 m to 3000m correlate high probability of wellbore collapse as evidenced with cuttings fill of 400 m (Table 7). In well RN-33, broken zones at 1550 and 2550m are viewed in the televiewer logs (Figure 29). The well was drilled using water and circulation losses were experienced during drilling (Níelsson, et al., 2014) .

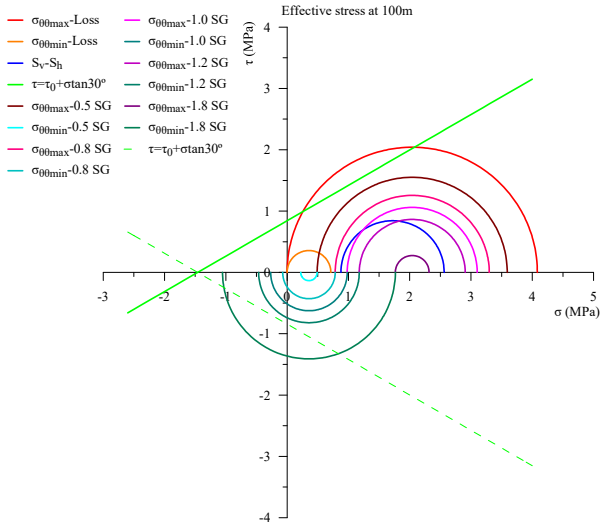

FIGURE 34: Effective stress variation and Mohr-Coulomb failure analysis at 100 m indicating changes in stress conditions with drilling fluid density

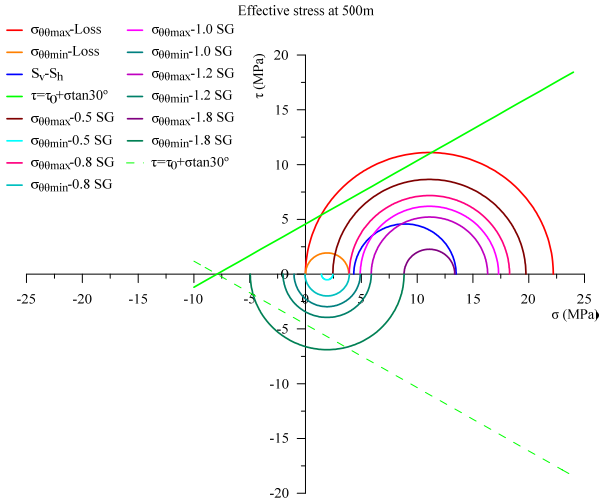

FIGURE 35: Effective stress variation and Mohr-Coulomb failure analysis at 500 m indicating changes in stress conditions with drilling fluid density

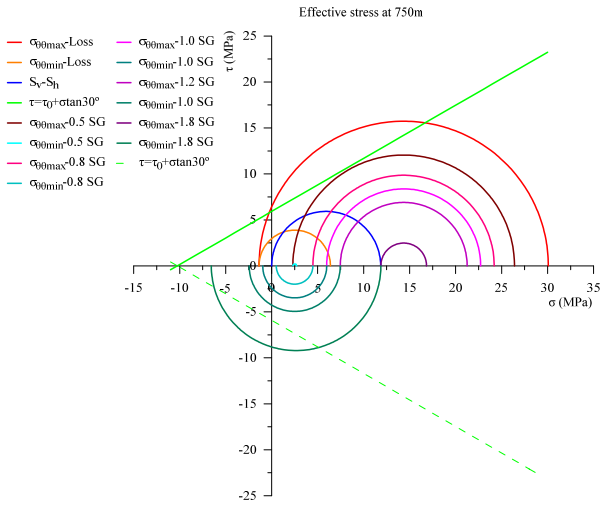

FIGURE 36: Effective stress variation and Mohr-Coulomb failure analysis at 750 m indicating changes in stress conditions with drilling fluid density

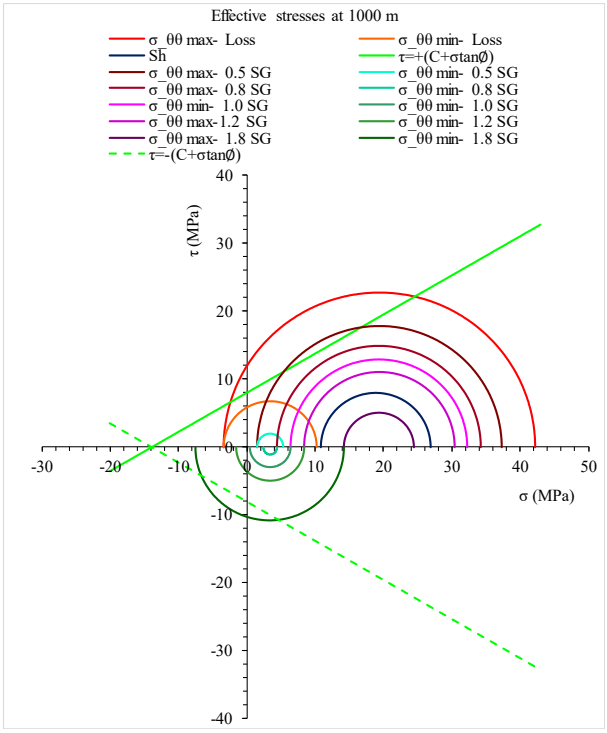

FIGURE 37: Effective stress variation and Mohr-Coulomb failure analysis at 1000 m indicating changes in stress conditions with drilling fluid density

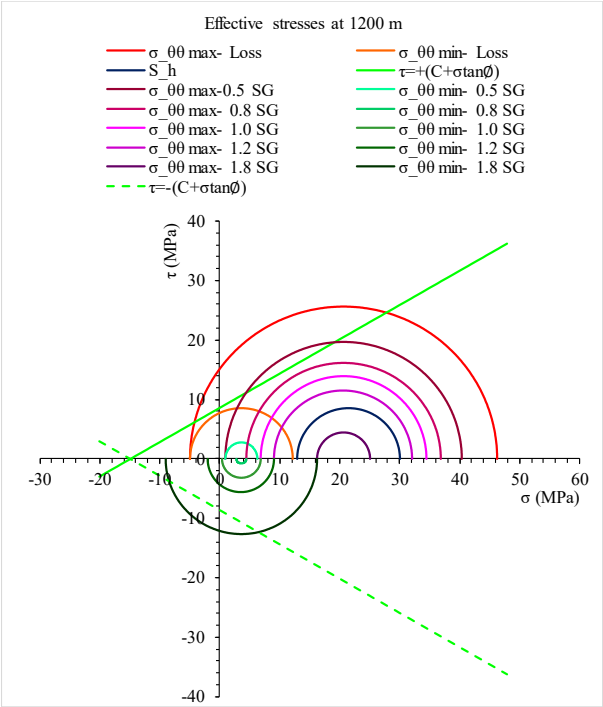

FIGURE 38: Effective stress variation and Mohr-Coulomb failure analysis at 1200 m indicating changes in stress conditions with drilling fluid density

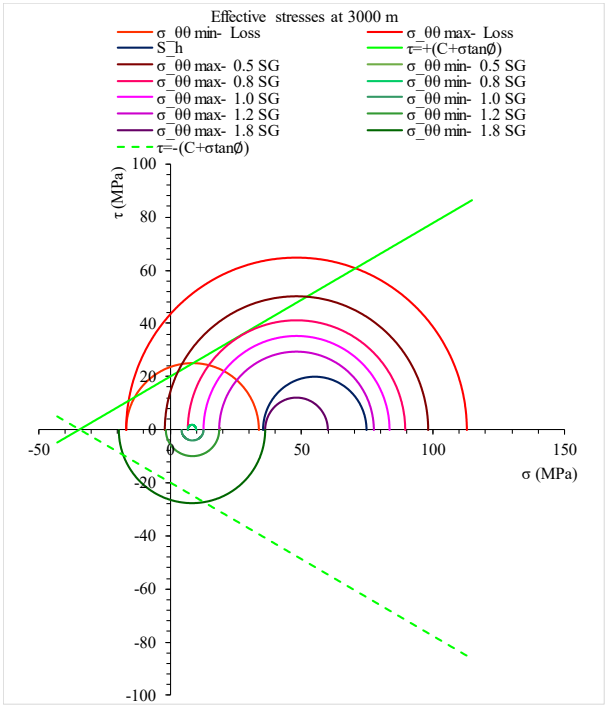

FIGURE 39: Effective stress variation and Mohr-Coulomb failure analysis at 3000 m indicating changes in stress conditions with drilling fluid density

7.3 Average drilling fluid density

The difference between the minimum and maximum drilling fluid densities when drilling at a given depth defines the variation range of drilling fluid density and gives the stability margin. The margin can be varied to by adjusting drilling fluid density to match the condition of the well. In geothermal well drilling, the choice of drilling fluid is limited to bentonite-based mud in the cased and cemented well sections. Water and aerated water is preferred when drilling production reservoir section. Minimum drilling fluid density refers to the fluid density that generates enough well pressure to achieve wellbore stability and prevent borehole collapse or inflow of formation fluid if not required. Maximum drilling fluid density refers to the fluid density that yields maximum well pressure that initiates loss of circulation due to formation fracturing or propagation of fluid into the already existing fractures commonly found in geothermal formations (Fjaer et al., 2008; Zoback, 2010).

Mohr's circle plots (Figure 33-36) indicates stability with drilling fluid density of 0.5 to 1.2 SG but possibilities of tensile fracture at 1.8 SG. Between 750 m and 3000 m (Figures 37-39), stability is between 1.0 to 1.2 SG. The mid-point (Median-line principle) (Mitchell and Miska, 2011) between the fracture pressure and BPD estimates the average drilling fluid density. Figure 40 shows the plot of the estimated minimum stress and BPD from the water level encountered at OW-731 and the average line plot within the stability margin.

Taking a ratio of the midpoint values to the minimum fracture give a value of 0.73 in the 8½" hole. Calculating the ECD using the midpoint gives drilling fluid SG of 0.91 in 8½" hole section. Plotting the midpoint ratio to minimum fracture, ECD and pump pressure (annular pressure loss) from the drilling log show how drilling fluid density varies with pore pressure and calculated minimum formation strength in the wells. Both ECD and midpoint ration decrease to value of below 0.5 below 600m. Pump pressure gives the pressure difference between inlet through the drill string and return through the annulus at surface. Fluctuation of recorded pump pressure shows low pressure when loss of drilling fluid is experienced.

Well OW-731 experienced total loss during drilling of 12¼" hole section corresponding to very low annular pressure loss compared to OW-731B that was drilled with full circulation returns (Table 7). The shape of the pump pressure profile follows the ECD and mid-point values that gradually increases with depth at constant rate. Figure 41 displays the variation of midpoint ratio, ECD and recorded pump pressure in two wells OW-731 and OW-731B in Olkaria.

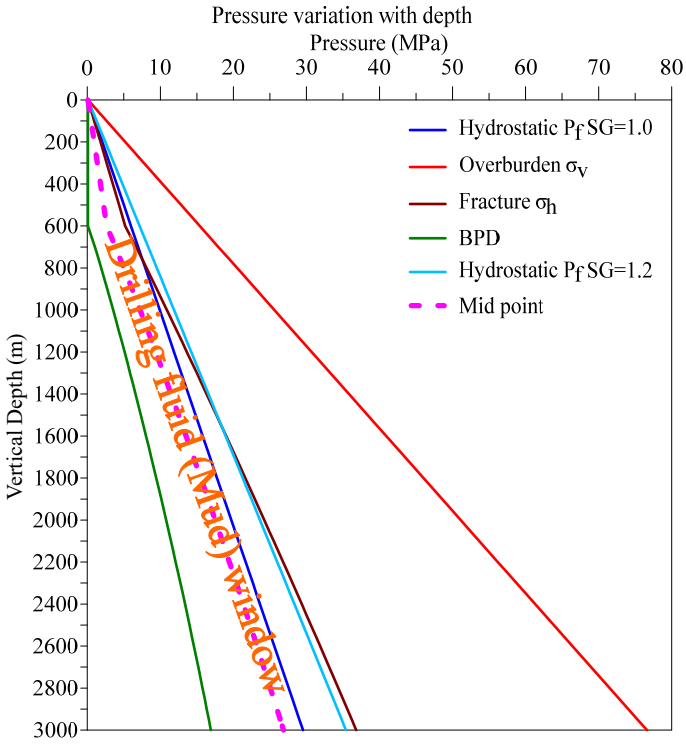

FIGURE 40: Drilling fluid (mud) window showing the mid-point line (Mitchell and Miska, 2011)

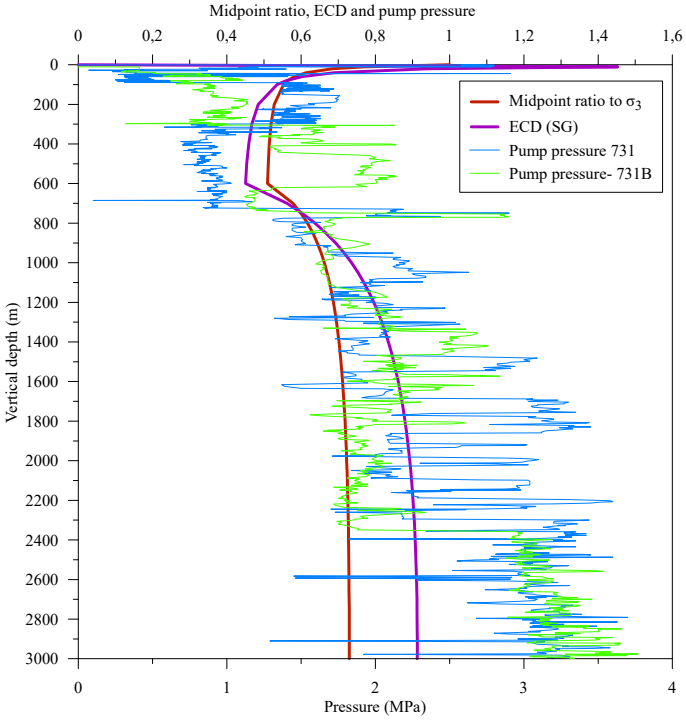

FIGURE 41: Variation of midpoint ratio to fracture pressure, ECD and actual pump pressure recorded during drilling with depth

7.4 Drill bit usage

Analysing the number of drill bits used in drilling Olkaria wells at OW-731, extra number of bits were used in zones that encountered instability challenges. In the 17½" anchor section, OW-731A, B and C had collapsing formations at 200 to 300 m (Table 7) that required cement plugging used extra new bits as opposed to the other two wells that encountered hard formation with only one new bit used. Wells OW-731A and OW-731C experienced loss of circulation and collapsing formation at 400 m in the 12¼" hole section and required six new bits to complete drilling of this section. OW-731B which had a revision of anchor casing depth to 400m used one bit in the 12¼" hole section and had no instability problems encountered.

Drilling of the 8½" hole section indicates more consumption of drill bits from four in the vertical well OW-731 to eight in three directional well OW-731A, B and C. These wells experienced intermittent loss of circulation in the course of drilling. In well OW-731D, instability below the production casing shoe that required fifteen cement plugs combined with complete loss of circulation during drilling of almost entire 8½" hole section coincide with twenty-three 8½" bits used in this well compared to eight in other wells. The drilling progress of OW-731D (Figure 18) show the picks of trips in and out of the well for bit change. Comparing the ROP of the wells, no significant variation noted in 8½" thus linking the high rate of bit wear to lack of cutting removal that increased frequency of bit changes. Table 14 gives a summary of number of drill bits used and the depths drilled. ROP experienced in different sections of the five wells is compared in Figure 42.

TABLE 14: Drilling rate and number of used drill bits in five wells on drill pad 731 in Olkaria, Kenya

Bit (")	Description		Wells at well pad 731				
			OW-731	**OW-731A**	**OW-731B**	**OW-731C**	**OW-731D**
26	Depth	(m)	57	45	45	46	44
	Drilling time (hr)	(hrs)	126	47	32	49	88
	Rate	(m/hr)	0.5	1.0	1.4	0.9	0.5
		(N)	0	0	0	0	0
	Bits used	(RR)	1	1	1	1	1
		Total	**1**	**1**	**1**	**1**	**1**
17½	Depth	(m)	236	239	342	277	245
	Drilling time (hr)	(hrs)	476	91	161	195	208
	Rate	(m/hr)	0.5	2.6	2.1	1.4	1.2
		(N)	1	3	2	3	1
	Bits used	(RR)	3	1	0	1	1
		Total	**4**	**4**	**2**	**4**	**2**
12¼	Depth	(m)	424	460	353	418	456
	Drilling time (hr)	(hrs)	277	100	95	169	151
	Rate	(m/hr)	1.5	4.6	3.7	2.5	3.0
		(N)	2	6	1	6	3
	Bits used	(RR)	1	1	1	1	1
		Total	**3**	**7**	**2**	**7**	**4**
8½	Depth	(m)	2277	2246	2249	2249	2255
	Drilling time (hr)	(hrs)	497	447	462	435	444
	Rate	(m/hr)	4.6	5.0	4.9	5.2	5.1
		(N)	4	8	8	8	23
	Bits used	(RR)	1	1	1	1	1
		Total	**5**	**9**	**9**	**9**	**24**
N-New bit, RR- Re-run bit							

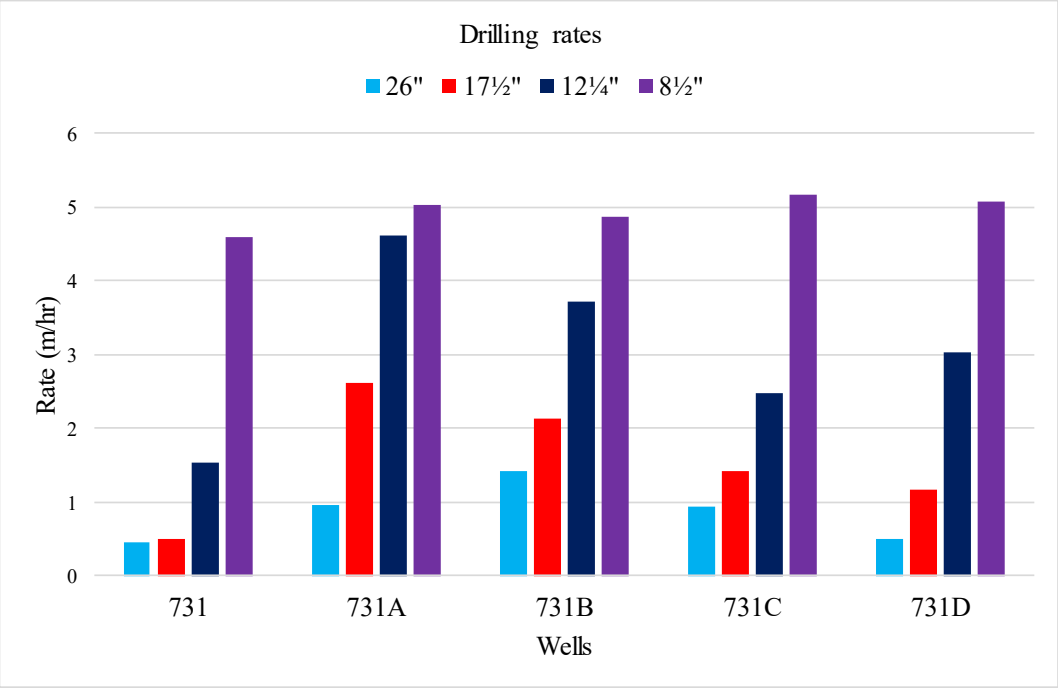

FIGURE 42: Drilling rates in the four well sections of OW-731 wells in Olkaria, Kenya

8. DISCUSSION

Analysing causes of wellbore instability in Olkaria wells, loss of circulation, wellbore collapse and creep in some instances affect most of the wells. Well RN-33 in Iceland experienced loss of circulation and wellbore collapse during drilling of the 26" surface hole and 21" anchor hole sections of the well that slightly affected the drilling progress. These instabilities caused stuck drill string conditions, required use of cement to stabilize, and extended reaming time to either land casing or liner. Drilling progress of wells is affected when wellbore instabilities are encountered extending the time required to complete drilling of the geothermal well. Extra drilling days and materials are used in the wells to cover the loss related to wellbore instabilities.

Reaming and circulation was applied in an effort to maintain wellbore clear of cuttings but resulted increased well completion time as can be seen in OW-731A where over 20% is required in three sections. Drilling of Surface Casing section, two wells (OW-731C and OW-731B) experienced loss of circulation and collapsing borehole that required cement to stabilize and rigging down for well pad repairs. Similar situation occurred in well RN-33 in which air hammer drilling had to be changed to rotary drilling and stabilizing weak formation with cement for drilling to continue (Figure 28). Anchor and Production Casing section instabilities are dominated by total loss of drilling fluid and collapsing formation. Total loss of drilling fluid hampered cutting removal and reduced bit efficiency due to cutting regrinding. Collapsing wellbore walls combined with accumulation of cuttings increased the chances of stuck drill string and needed cement to stabilize. Another impact of loss of circulation was casing cementing required more time for backfill cementing jobs to fill cement up to the surface. Zones between 140m to 400m seem to be highly fractured and consisting of fragmented formation in the Olkaria wells as depicted in the Figure 17. All the five wells had loss circulation and three well required cement to contain borehole collapse. In RN-33 loss of circulation at 131m affected cutting removal and required cement to seal off the zone for drilling to progress.

Loss of circulation during drilling of 8½" section required reaming and longer circulation time to clear the cuttings. In well OW-731D, a zone of collapsing formation between 810m and 850m required cementing to stabilize and loss of circulation occurred entire section making it difficult to obtain geological logs due to lack of cuttings. The well recorded the highest number of drill bits used (24pcs) to complete drilling (Table 14) caused possibly by accumulation of cuttings that increased rate of bit wear compared to the other four wells. Accumulation of cuttings is also evidenced by running of slotted liner that could not go beyond 2600m translating to 400 m column of cuttings from the well bottom at 3010m. Creep causing tight narrowing sections between 1200 and 1360 m in well OW-922 (Figure 14) took over sixty days to contain with use of dispersant and reaming using drilling mud affecting the time for temperature recovery of the well. This well took the highest number of days to complete followed by OW-731D and demonstrate effects of wellbore instability in terms total well cost and flowrates as depicted by pressure and temperature profiles (Figure 22). OW-731D indicates temperatures below 200°C after 30 days compared to the other wells at OW-731 that have temperature above 250°C.

Comparing drilling time is the four well sections for the OW-731 wells (Appendix A), wells that had wellbore instabilities that impacted on drilling progress have less than 50% of the of the total time spent on actual well drilling. In OW-922, reaming in the 8½" took over 50% of the time to contain wellbore instability (Table 6). This situation is also seen in OW-731D with WOC and tripping took 50 % compared to 28% of the drilling time. Well OW-731A which had instability problems in the 17½" and 12¼" hole sections have 15% and 24% of drilling time compared to 71% and 47% of time spent on circulation, reaming and WOC.

Pressure and temperature data (Figures 19 to 23) acquired during completion tests after drilling show the pressure pivot point in OW-731 at 2200m with 130 bar pressure but the pivot point is missing in the other wells. Reassessing the minimum Production Casing depth using the vertical well data, sets minimum casing vertical depth at 1450m using the African Union code of practice (African Union;, 2016) and at 700m using the old New Zealand standard (1991). The difference between the calculated casing depths using the two standard is great and calibration of the fracture gradient using FLOT can be conducted to confirm the right casing depth in conjunction with open hole logging of new wells. Deeper

casing depth for the directional wells would have isolated the unstable zone of between 800 and 850m in OW-731D that affected drilling of the 8½" hole section reducing drilling time and other materials used during drilling. Another benefit would be to isolate low enthalpy fluid inflow into the wells recorded in the well pressure and temperature profiles just below the production casing. Decline in well productivity highlight need for casing depth revision based on the down hole well condition. Comparing the five wells, OW-731D have the lowest mass output and instability problems just below the production casing affected drilling of the 8½" hole section. Total mass flowrate of the five well is shown in Table 15.

TABLE 15: Mass output of drill pad OW-731 wells (KenGen, 2017- Reservoir)

Well	WHP (Bara)	Total Mass output discharging on 8" pc pipe (t/hr)	Enthalpy (kJ/Kg)
OW-731	7.5	91	1923
OW-731A	3	58	1412
OW-731B	6.7	197	1103
OW-731C	6.4	150	1228
OW-731D	3	42	2675
*Vapour enthalpy at 100 °C=2675 KJ/kg			

Caliper logs conducted in well RN-33 in anchor, production and liner sections (Figures 25, 26 and 27) show difference between the drill bit diameter and final wellbore diameter. Sections with high diameter variation indicate zones that the wellbore either collapsed or easily eroded by the drilling fluid. The sections increased the formation materials needed to be transported out of the well by drilling fluid and reduces the flow velocity thus decreasing its ability to clean the well. This required additional reaming and circulation of the well during drilling. Moreover, extra cement was required to fill up the spaces during casing cementing (Níelsson et al., 2014). In the liner section of the well, large diameter were recorded in the caliper log at 1239, 1350, 1556 and 2250 m depth that coincided with the fractured and eroded depths from the televiewer log (Árnadóttir et al., 2014). The fracture form feeder zones during well production and are thus beneficial to well output but are pathways for drilling fluid loss during well drilling process affecting wellbore stability during drilling.

Transforming vertical S_v, maximum horizontal S_H, and minimum horizontal S_h, field stresses into stresses around the wellbore gives the effective hoop, radial and vertical stresses around the wellbore (Table 11, 12, 13). The difference between radial and tangential effective stresses creates shear stresses that induce wellbore failure through either compressive collapse or tensile fracturing. Plotting stress variation around the wellbore indicates high compressive stresses at 90 and 270° and low stresses at 0 and 180° for vertical well (Figure 30) measured from North (0° azimuth). In the directional wells (Figure 31), variation of the stresses is dependent on the inclination angle and azimuth. Directional wells at OW-731 pad are inclined to approximately 20° from the vertical at different azimuths but indicate difference in stress levels. Well OW-731D (200°) has the highest compressive stress followed by OW-731B (225°) then OW-731A (135°) and OW-731C (270°) has the least. This is confirmed in well RN-33 with an inclination angle of 30° at azimuth of 171° which has the highest hoop stresses at 96°/276° referenced clockwise from North (0° azimuth).. Maximum hoop stresses occur in the direction of minimum stress (90° and 270°) for vertical well. Directional well OW-731C drilled in minimum stress direction (270°) indicate less hoop stresses compared to OW-731D (200°). Figure 43 shows stress variation with minimum stress representing the borehole wall.

Mohr's circle diagrams (Figures 33-39) using maximum hoop stress, minimum hoop stress and radial stress at different drilling fluid densities, indicate changes in wellbore stability at different depths. Setting drilling fluid density to zero to represent loss of drilling fluid circulation, chances of compressive (collapse) failure increases with the circle envelop plotting outside the failure line at all depth. Increasing density to 1.8 SG, compressive stresses reduces but tensile failure (fracture) is likely at all depths with minimum hoop stress envelop intersecting the failure line. Effective hoop and radial stresses from surface to a depth of 750 m indicate stability when using drilling fluid density between 0.5 SG to 1.2

SG. Above 750 m, fluid density of 0.8 to 1.2 SG show wellbore stability. This can guide in drilling fluid management to match encountered down hole conditions.

Tensile thermal stresses induced during formation cooling by cold drilling fluid can fracture formation and increase propagation of the existing fractures found in geothermal formations. Expansion can lead to breakout during heating up of the well but this occurs after the well is completed and the casing strings installed during drilling contains the induced stresses. Increase in tensile stress reduces compressive stress in the well that can cause breakouts during drilling. Using a temperature difference of 10° recorded in RN-33 during drilling between 2000 to 2500m (Appendix D) in Equation 41 with Modulus of Elasticity$E = 6.0 \times 10^4 MPa$, Linear coefficient of expansion $\alpha_l = 1.6 \times 10^{-5}/K$ and Poisson's ration of 0.25, (Turcotte and Schubert, 2014; Kearey et al., 2002) (Appendix E), the induced thermal stresses is equivalent to 12.8 MPa. This thermal stress is tensile and when inserted in the hoop stress equation it reduces the magnitude of compressive stresses acting on the borehole wall. Higher temperature differences as expected in geothermal results in higher thermally induced tensile stresses that can cause formation fracturing if they exceed formation strength. Effects of thermal stress on the stresses acting on wellbore wall are demonstrated in Figure 44 using data from RN-33 at a depth of 1395 m. the compressive stress reduces as indicated by $\sigma_{\theta max \Delta T}$ but tensile stress increases with reduction of $\sigma_{\theta min \Delta T}$.curve in the direction of maximum horizontal stress. The directions corresponds closely to the direction recorded in the televiewer image in Figure 29 for fracture direction (6°/186°) and the broken zone at 2279 which is recorded in the direction of the maximum compressive stress (96°/276°) measured from North (0° azimuth).

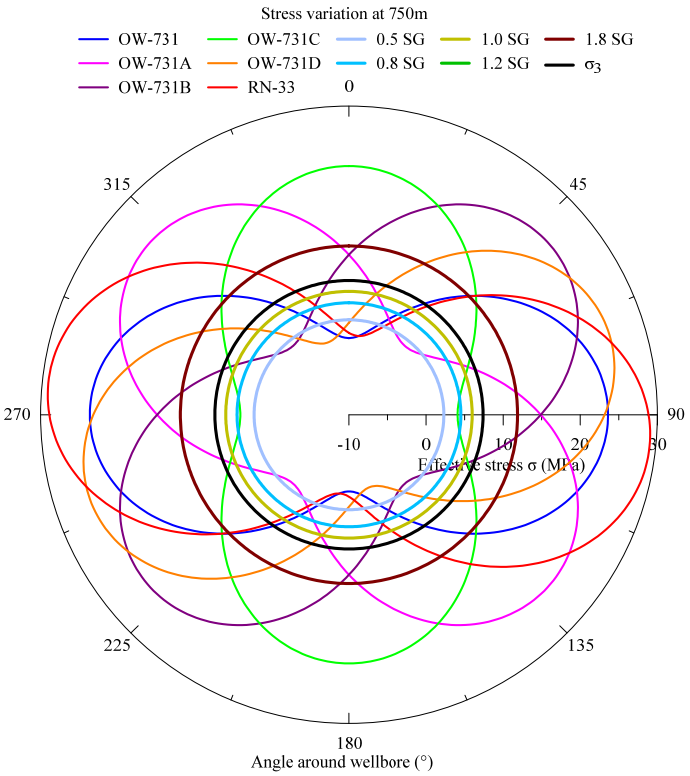

FIGURE 43: Hoop, minimum fracture and radial variation at 750 m indicating angle of maximum hoop stress

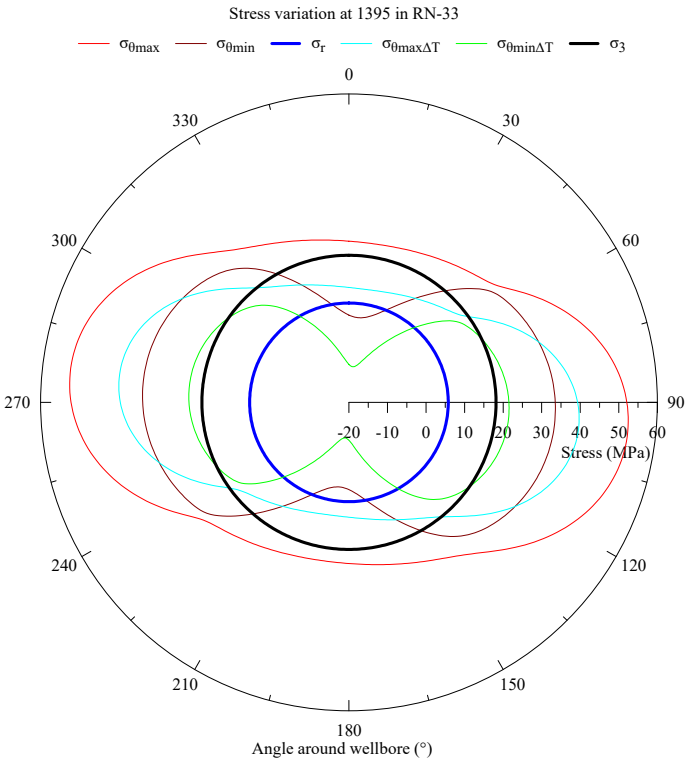

FIGURE 44: Variation of minimum fracture, radial and tangential stresses with inclusion of thermal stresses in well RN-33 at 1395 m

Considering that geothermal fields are highly fractured as seen in (Figure 17) for the Olkaria wells and in the televiewer image Figure 29 of the reservoir section in RN-33, the cooling effects was assumed in this report to be away from the borehole wall propagating the already existing fracture (Grant , 2014). The other aspect of thermal stresses is that

they are also time dependent (Zoback, 2010). With this perceived benefits of improving permeability and but also increasing chances of loss of circulation, thermal stresses were not considered in the stress analysis in this report.

The mid-point of the stability margin (mud window) is less than the water hydrostatic pressure at 1.0 SG. The ratio of the midpoint to minimum fracture increases from 0.60 to 0.73 and ECD from the midpoint values increase from 0.6 to 0.91 from 750m to 3000m. This can be interpreted as need to raise drilling fluid density close to the minimum fracture for better wall support and can be used as a design point in drilling fluid management. This is depicted by the Mohr's Criteria that show the effective stresses plot above the failure line at all depths (Figures 33-39) during loss and at 1.8 SG at all depths. Aerated fluid drilling reduces wellbore pressure to induce flow from formation in subnormal pore pressure conditions found in geothermal fields such as Olkaria but shows less borehole wall support as illustrated by 0.5-0.8 SG. These reduced densities can also be used to illustrate situations of partial losses encountered during drilling where reduced drilling fluid returns is experienced. Water at 1.0 SG plots within the stable region at all depths. Well RN-33 was drilled mainly using water and circulation returns was largely maintained.

9. CONCLUSIONS

The main wellbore instability challenges experienced during drilling of geothermal wells illustrate how drilling problems contributed to deviation of the drilling plan in terms of drilling days, materials required to complete well drilling and overall well cost. Wellbore problems increase significantly the NPT of the rig extending well completion period. Reviewing wellbore stability challenges from drilled wells would help in designing and planning for other wells drilled in similar set up or problematic area.

Loss of circulation, wellbore collapse and tight hole constitute major causes of wellbore stability problems during drilling of geothermal wells in Olkaria. Loss of drilling fluid circulation affects removal of drill cuttings from the well and requires frequent reaming, circulation and working the drill string up and down to avoid accumulation of cuttings above the bottom hole assembly (BHA). Accumulation of cutting in the well during drilling increases the wear rate of the drill bit due to regrinding of the cutting reducing its performance, drilling rate and increase in the quantity of bits required to complete drilling.

Wellbore wall collapse from compressive hoop stresses enlarges well diameter and hinders drilling fluid circulation back to surface. They create cavities in which cuttings accumulate because of reduced fluid velocity in the annulus between the well and the drill string. Collapsed formation material can lead to struck string if the weak zones are large and the formation is composed of large diameter rock materials. Cement is used to seal off loss zones and stabilize weak formation for drilling to advance in cased sections of the well, but not in the reservoir section as it seals off the feeder zones. Cement requires 8 to 12 hour wait on cement (WOC) time for it to set and develop enough strength. This contributes to non-productive time (NPT) of the rig during plug cementing and backfill cementing to the surface in casing cementing. Reviewing well design and drilling practices based on the field well data can help in minimizing chances of potential drilling problems as demonstrated in wells OW-731D and OW-922. Instabilities below the Production Casing in these wells affected the drilling process of the liner section. Data from the vertical well at OW-731 that was initially drilled would have formed an input data for well design and planning of the directional wells that were later drilled on the same well pad. Reviewing of well casing design based on the vertical well indicates need for a deeper casing in the directional wells that would have improved drilling of the well and maybe improve the well productivity.

Analysing effective stresses around the wellbore compressive hoop stresses that causes formation collapse are dependent on the orientation of the wellbore wall. Vertical wellbore has maximum compressive stresses at 90° and 270 ° aligning to the direction of the minimum stress and minimum compressive stress at 0 and 180° clockwise from North (0° azimuth). For directional well, these stresses depend on the inclination and azimuths of the wells relative to North direction. Directional well OW-731C in the azimuth of minimum stress direction (270°) has lower hoop stresses compared to other wells at 731 while OW-731D drilled at azimuth of 200° has the highest hoop stresses. Effective stress, which is the difference between external stresses acting on a rock and the pore pressure (Pp) increases above the water level in the geothermal field. The recorded wellbore pressures are sub normal compared to hydrostatic pressure indicating less formation support and high probability of collapse as recorded wellbore collapse in the wells.

Using the Mohr-Coulomb failure criteria shows compressive failure in the wells is highly likely during loss of drilling fluid circulation at all depths and tensile failure at 1.8 SG. Drilling density between 0.8 to 1.2 SG, show improved wellbore stability with Mohr's circles envelops at these densities falling within the failure line at all depths. The midpoint between the minimum stress and pore pressure (BPD) therefore presents a good basis to design the best fit of the drilling fluid density such as determination of the correct air ratio in aerated drilling, water and foam to maximize hole-cleaning capability.

Open hole logging during drilling for formation temperature, pressure, well geometry through caliper, rock formation through resistivity and imaging in evaluating breakouts, collapsing zones, fractures and formation boundaries, are important in evaluating well instabilities and the best remedial action to apply. The collected data helps in well design revisions, drilling fluid to be used and cement placement method that will not break the formation but on the same time maintain well integrity. From the televiewer the broken zone at 2280m is oriented at 270.21° (Árnadóttir et al., 2014) while from the stress calculation, maximum hoop stress occurs at 276° measured clockwise from North.

10. RECOMMENDATIONS

The stress analysis carried out in this report is based mainly on indirect methods from proposed engineering formulas and analysis for stress calculations and assumptions on various rock properties. To confirm the results direct measurement of field rock parameters would be very beneficial to confirm the results with actual field data. From this report, further study is recommended:

- Rock mechanical study to characterize rock strength and actual rock densities for better understanding of the fracture gradient. Conduct formation leak off test (FLOT) for the cased sections of the wells as per the AU code of practice.
- Study the actual orientations of the fault structure in the field sectors e.g. use televiewer log to image fractures intersected during well drilling to understand the directions of the horizontal stresses, both minimum and maximum, for well trajectories design and optimization.
- Implement well logging during drilling for caliper, borehole imaging, temperature and resistivity for better understanding of well profiles identification of loss zones and stratigraphy. Combined with collected cutting analysis of unstable zones can assist in future well design.
- Revision of casing depth design, especially for the Production Casing, based on actual well conditions encountered during drilling to mitigate instability challenges.
- Measuring the well breakout and mapping of zones prone to instabilities and use information for future well design, planning and execution of the drilling process.
- Study of thermal stresses induced during drilling and their impact of well stability in geothermal well drilling.

REFERENCES

Aadnoy, B.S. and Looyeh, R., 2011: *Petroleum rock mechanics: Drilling operations and well design.* Gulf Professional Publishing, 376 pp.

African Union, 2016: *The African Union Code of Practice for Geothermal Drilling.* Addis Ababa, Ethiopia: African Union Commission, Regional Geothermal Coordination Unit.

Alidi, R, 2017: *Geomechanical analysis to reduce well integrity issues in Eagle Ford drilling.* Department of Petroleum Engineering, Colorado School of Mines, Golden, CO, USA, 89 pp.

Árnadóttir, S., Blischke, A. and Stefánsson, H.Ö., 2014: *Televiewer and spinner logging: results of well RN-33 at Reykjanes geothermal field, SW-Iceland.* Iceland GeoSurvey - ÍSOR, Reykjavík, report ÍSOR-2014/041, 56 pp + app.

Azar, J.J. and Samuel, R.G., 2007: *Drilling engineering.* PennWell Corp., Tulsa, OK, USA, 491 pp.

Baker Hughes, 1995: *Drilling engineering workbook.* Baker Hughes INTEQ, Houston, TX, USA 410 pp.

Blanck, H., 2016: *Seismic methods in geothermal prospecting and utilization of geothermal fields.* Iceland GeoSurvey – ÍSOR, Reykjavik, unpubl. lecture notes.

Bourgoyne Jr., A.T., Millheim, K.K., Chenevert, M.E. and Young Jr., F.S., 1986: *Applied drilling engineering.* Society of Petroleum Engineers, Richardson, TX, USA, 502 pp.

Devereux, S., 1998: *Practical well planning and drilling manual.* PennWell Corporation, Tulsa, Oklahoma, USA, 524 pp.

Economides, M.J., Watters, L.T. and Norman, S.D., 1998: *Petroleum well construction.* John Wiley and Sons Ltd., Chichester, England, 640 pp.

ENGINE Coordination Action., 2008: *Best practice handbook for the development of unconventional geothermal resources with a focus on enhanced geothermal system.* BRGM Editions: Collection Actes/Proceedings, Orleans website: *engine.brgm.fr/Documents/ENGINE_BestPracticeHandbook.pdf.*

European Union, 2015: *2014 JRC geothermal energy status report.* Publications Office of the European Union, Joint Research Centre (JRC), Institute for Energy and Transport, Luxembourg 59 pp.

Finger, J. and Blankenship, D., 2010: *Handbook of best practices for geothermal drilling.* Sandia National Laboratories, U.S. Department of Energy, Livermore, CA, USA 84 pp.

Fjaer, E., Holt, R.M., Horsrud, P., Raaen, A.M. and Risnes, R., 2008: *Petroleum related rock mechanics* (2nd Edition). Elsevier, Amsterdam, Netherlands 514 pp.

Franzson, H., Gudlaugsson, S.Th. and Fridleífsson, G.Ó., 2001: *Petrophysical properties of Icelandic Rocks.* Orkustofnun, Geoscience Division, Reykjavík, Iceland.

Franzson, H., Thordarson, S., Björnsson, G., Gudlaugsson, S., Richter, B., Fridleifsson, G.Ó., and Thórhallsson, S., 2002: Reykjanes high-temperature field, SW-Iceland: Geology and hydrothermal alteration of well RN-10. *Paper presented at the 27th Workshop on Geothermal Reservoir Engineering, Stanford University, Stanford, CA, USA,* 8 pp.

Grant, M.A., 2014: *Lectures on geothermal reservoir engineering.* UNU-GTP, Iceland, report 4, 61 pp.

Grant, M.A. and Bixley, P.F., 2011: *Geothermal reservoir engineering* (2nd ed.). Academic Press, Elsevier, Burlington, MA, USA, 378 pp.

Haraldsdóttir, S.H., 2016: *Well testing – production well testing.* Reykjavik University, Reykjavík, Iceland, Subsurface exploration E-2 course, unpubl. lecture notes.

Harrison, J.P. and Hudson, J.A. (eds.), 2000: *Engineering rock mechanics: part 2: Illustrative worked examples.* Elsevier Science, London, 524 pp.

Hoek, E., Torres, C. and Corkum, B., 2018: *Hoek-Brown failure criterion* (ed. 2002). Rocscience website: *rocscience.com/documents/hoek/references/H2002.pdf*.

Hole, H.M., 2006: *Lectures on geothermal drilling and direct uses.* UNU-GTP, Iceland, report 3, 36 pp.

IADC, 2000: *IADC drilling manual.* International Association of Drilling Contractors (IADC), Houston, TX, USA.

Immerstein, T., 2013: *Wellbore stability and rock mechanics study on the Ula field.* University of Stavanger, Faculty of Science and Technology, Norway, 88 pp.

Jaeger, J.C., Cook, N.G. and Zimmerman, R.W., 2007: *Fundamentals of rock mechanics* (4th ed.). Blackwell Publishing, USA, 488 pp.

Jiménez, J.-M.C., Lara, L.-C.V., Rueda, A. and Trujillo, N.-F. S., 2007: Geomechanical wellbore stability modelling of exploratory wells – study case at middle Magdalena basin. *Ciencia, Tecnología y Futuro, 3-3,* Bogotá, Colombia.

Kearey, P., Brooks, M. and Hill, I., 2002: *An introduction to geophysical exploration* (3rd ed.). Blackwell Science Ltd., London, 272 pp.

KenGen, 2011: *OW-731 well drilling log.* Kenya Electricity Generating Company Ltd, Olkaria Geothermal Development Project, Olkaria, Kenya.

KenGen, 2013-40A: *OW-40A well completion report.* Olkaria, Naivasha, Kenya: Kenya Electricity Generating Company, Ltd., Olkaria Geothermal Development Project, Olkaria, Naivasha, Kenya.

KenGen, 2013-731B: *OW-731B Well Drilling Log.* Kenya Electricity Generating Company, Ltd., Olkaria Geothermal Development Project, Olkaria, Naivasha, Kenya.

KenGen, 2014-731D: *Well completion report for OW-731D.* Kenya Electricity Generating Company, Ltd., Olkaria Geothermal Development Project, Olkaria, Naivasha, Kenya.

KenGen, 2014-731D DDR: *Daily drilling reports for OW-731D.* Kenya Electricity Generating Company, Ltd., Olkaria Geothermal Development Project, Olkaria, Naivasha, Kenya.

KenGen, 2014-922: *Well completion report for OW-922.* Kenya Electricity Generating Company, Ltd., Olkaria Geothermal Development Project, Olkaria, Naivasha, Kenya.

KenGen, 2014-922 DDR: *Daily drilling reports for OW-922.* Kenya Electricity Generating Company, Ltd., Olkaria Geothermal Development Project, Olkaria, Naivasha, Kenya.

KenGen, 2014-OW-49: *OW-49 well completion report.* Kenya Electricity Generating Company, Ltd., Olkaria Geothermal Development Project, Olkaria, Naivasha, Kenya.

KenGen, 2017-Drilling: *Well drilling data base and completion reports.* Kenya Electricity Generating Company, Ltd., Olkaria Geothermal Development Project, Olkaria, Naivasha, Kenya.

KenGen, 2017-Geology: *Daily geological well logging report.* KenGen Geology Section, Kenya Electricity Generating Company, Ltd., Olkaria Geothermal Development Project, Olkaria, Naivasha, Kenya.

KenGen, 2017-Reservoir: *Reservoir well logging data.* Kenya Electricity Generating Company Ltd., Olkaria Geothermal Development Project, Olkaria, Kenya.

Larson, E.W. and Gray, C.F., 2011: *Project management: The managerial process* (5th ed.). McGraw-Hill, Irwin, NY, USA 688 pp.

Mbithi, U.K., 2016: *Interpretation of feed zones to map sub-surface permeability structures and natural state simulation: a case study of Olkaria Domes geothermal system in Kenya.* University of Iceland, MSc thesis, UNU-GTP, Iceland, report 3, 54 pp.

McNamara, D.D., 2017: *Energy geology - lecture notes.* Iceland School of Energy (ISE), Reykjavik University, Reykjavík, Iceland.

Mitchell, R.F. and Miska, S.Z., 2011: *Fundamentals of drilling engineering.* Society of Petroleum Engineers, SPE, Richardson, TX, USA, 696 pp.

Munyiri, S.K., 2016: *Structural mapping of Olkaria Domes geothermal field using geochemical soil gas surveys, remote sensing and GIS.* University of Iceland, MSc thesis, UNU-GTP, Iceland, report 5, 100 pp.

Musonye, X.S., 2015: *Sub-surface petrochemistry, stratigraphy and hydrothermal alteration of the Domes area, Olkaria geothermal field, Kenya.* University of Iceland, MSc thesis, UNU-GTP, Iceland, report 3, 100 pp.

Nelson, E. B., 1990: *Well cementing.* Schlumberger Education Services, Sugarland, TX, USA, 1515 pp.

New Zealand Standard, 1991: *Code of practice for deep geothermal wells.* Standards Association of New Zealand, Wellington, NZ.

New Zealand Standard, 2015: *Code of practice for deep geothermal wells.* Standards New Zealand, Wellington, NZ.

Ngigi, A.N., 2015: Geothermal well design using the new 2015 New Zealand Standard and 1991 Standard: A Case of MW-20A in Menengai, Nakuru county, Kenya. Report 28 in: *Geothermal training in Iceland 2015.* UNU-GTP, Iceland, 607-640.

Níelsson, S., Hardarson, B.S., Stefánsson, H.Ö., Gunnarsdóttir, S.H., Kristinsson, B., Ingólfsson, H., and Stefánsson, S.A., 2014: *Well report - RN-33, drilling of well RN-33 from surface down to 2695 m and geothermal studies of the well during the drilling.* ÍSOR – Iceland GeoSurvey, Reykjavík, report ÍSOR-2014/037, 320 pp.

Otieno, V.O., 2016: *Borehole geology and subsurface petrochemistry of the Domes area, Olkaria geothermal field, Kenya, in relation to well OW-922.* University of Iceland, MSc thesis, UNU-GTP, Iceland, report 2, 84 pp.

Ouma, P., Koech, V. and Mwarania, F., 2016: Olkaria geothermal field reservoir response after 35 years of production (1981-2016). *Papers presented at ARGeo-C6, Addis Ababa, Ethiopia*, 13 pp.

Rabia, H., 2001: *Well engineering and construction.* Entrac Consulting, 650 pp.

Renpu, W., 2011: *Advanced well completion engineering* (3rd ed.). Gulf Professional Publishing, Elsevier, Walthan, USA, 376 pp.

Sanyal, S. K., 2005: Sustainability and renewability of geothermal power capacity. *Proceedings of the World Geothermal Congress 2005,* Antalya, Turkey, 13 pp.

Schoenball, M., Glen, J.M. and Davatzes, N.C., 2016: Analysis and interpretation of stress indicators in deviated wells of the Coso geothermal field. *Proceedings of the 41st Workshop on Geothermal Reservoir Engineering, Stanford University, Stanford, CA*, 12 pp.

Simiyu, S.M., 1999: Seismic velocity analysis in the Olkaria geothermal field. *Proceedings of the 24th Workshop on Geothermal Reservoir Engineering, Stanford University, Stanford, CA*, 7 pp.

Simiyu, S.M., 2000: Geothermal reservoir characterization: Application of microseismicity and seismic wave properties at Olkaria, Kenya rift. *J. Geophys. Research, 105-B6,* 13,779-13,795.

Siratovich, P.A., von Aulock, F.W., Lavallée, Y., Cole, J.W., Kennedy, B.M. and Villeneuve, M.C., 2015: Thermoelastic properties of the Rotokawa andesite: A geothermal reservoir constraint. *J. Volcanology & Geothermal Research, 301*, 1-13.

Steingrímsson, B., 2011: Geothermal well logging: Geological wireline logs and fracture imaging. *Presented at "Short Course on Geothermal Drilling, Resource Development and Power Plants", organized by UNU-GTP and LaGeo, in Santa Tecla, El Salvador,* 11 pp.

Steingrímsson, B. and Gudmundsson, Á., 2006: Geothermal borehole investigations during and after drilling. *Presented at Workshop for Decision Makers on Geothermal Projects in Central America, organized by UNU-GTP and LaGeo in San Salvador, El Salvador*, 10 pp.

Sveinbjörnsson, B.M., 2014: *Success of high temperature geothermal wells in Iceland.* Iceland GeoSurvey – ÍSOR, Reykjavík, report written for Orkustofnun, 40 pp + appendix.

Tariq, A., 2014: *Wellbore stability in shale formations.* Faculty of Science and Technology, University of Stavanger. Stavanger, Norway 93 pp.

Thórhallsson, S., 2017: *Well design and geothermal drilling technology R-E10.* Iceland School of Energy (ISE), Reykjavik University, unpubl. lecture notes.

Tulinius, H., 2016: *Using temperature and pressure logs to determine reservoir condition and well status.* Iceland School of Energy (ISE), Reykjavik University, unpubl. lecture notes.

Turcotte, D., and Schubert, G., 2014: *Geodynamics* (3rd ed.). Cambridge University Press, Cambridge, UK.

Zoback, M. D., 2010: *Reservoir geomechanics.* Cambridge University Press, NY, USA, 461 pp.

Zoback, M.D., Barton, C.A., Brudy, M., Castillo, D.A., Finkbeiner, T., Grollimund, B.R. and Wiprut, D.J., 2003: Determination of stress orientation and magnitude in deep wells. *Intern. J. Rock Mechanics and Mining Sciences, 40*, 1049–1076.

APPENDIX A: Time analysis of wells OW-731, OW-731A, OW-731B, OW-731C and OW-731D (KenGen, 2017 - Drilling)

Activity	Time (Hours)	731
26" (0-64 m)		26" hole section 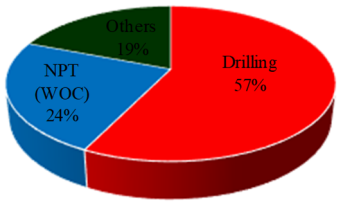
Drilling	126	
NPT (WOC)	52	
Others (casing , cementing, circulating, reaming, rig up, tripping)	42	
Total	**220**	
17½" (64-300 m)		17½" hole section 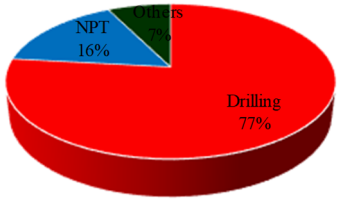
Drilling	489	
NPT (reaming, WOC)	101	
Others (casing, cementing, tripping, WHA)	47	
Total	**637**	
12¼" (300-723 m)		12¼" hole section 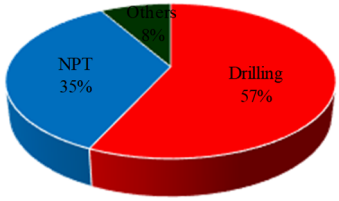
Drilling	296	
NPT (reaming, circulating WOC)	182	
Others (casing, cementing, tripping, WHA)	43	
Total	**521**	
8½" (723-3000 m)		8½" hole section 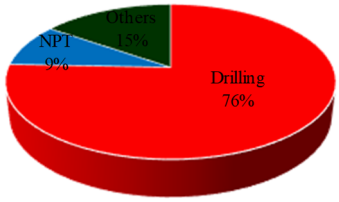
Drilling	509	
NPT (reaming and circulating)	61	
Others (Casing, logging and rig down)	15	
Total	**673**	
Grand total	**2050 (85 days)**	

Activity	Time (Hours)	731A
26" (0-56 m)		26" hole section 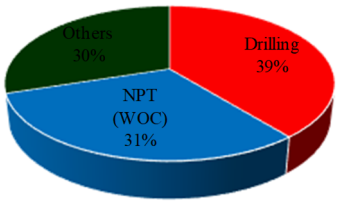
Drilling	47	
NPT (WOC)	37	
Others (casing cementing, Spuding),	36	
Total	**120**	
17½" (56-295 m)		17½" hole section 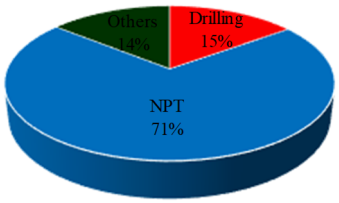
Drilling	117	
NPT (Circulation, reaming, stuck and WOC)	263	
Others (casing, cementing, tripping,WHA and WOW),	23	
Total	**778**	
12¼" (295-754 m)		12¼" hole section 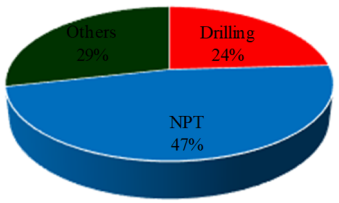
Drilling	174	
NPT (Circulation, reaming, stuck and WOC) Others (Casing, cementing, TOC, WHA and wiper trip) and	53,5	
Total	**720**	
8½" (754-3000 m)		8½" hole section 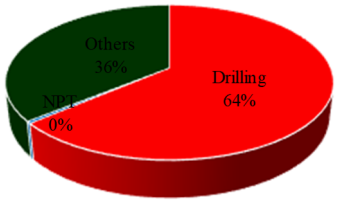
Drilling	453	
NPT (Circulating)	3	
Others (Casing, logging, rig down, tripping and WHA)	255	
Total	**710**	
Grand total	**2328 (97 days)**	

Activity	Time (Hours)	731B
26" (0-56 m)		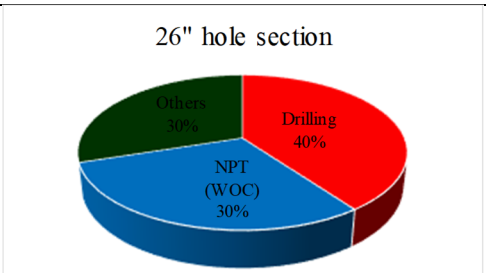
Drilling	32	
NPT(WOC)	24	
Others (casing, cementing, spudding, wiper trip	24	
Total	**80**	
17½" (56- 398 m)		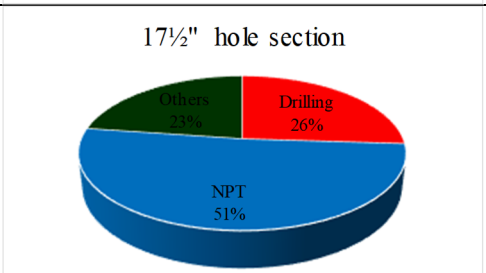
Drilling	222	
NPT (Circulating, reaming, well pad repair, WOC and WOI	437	
Others (Casing, Cementing rig down/ up and TOC)	193	
Total	**852**	
12¼" (398- 751 m)		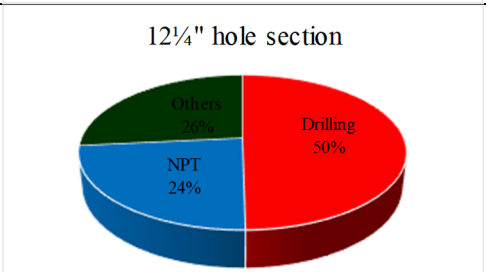
Drilling	103	
NPT (Circulating, reaming and WOC)	3	
Others (casing, cementing, tripping and WHA)	9	
Total	**207**	
8½" (751-3000m)		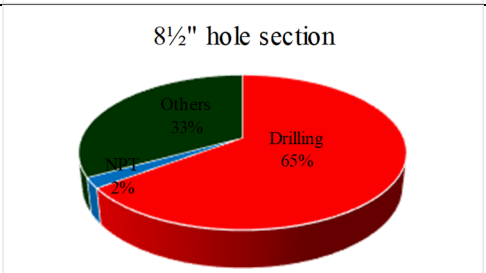
Drilling	475	
NPT (Circulating and reaming)	16	
Others (Casing, logging, Rig down tripping and WHA).	40	
Total	**733**	
Grand total	**1872 (78 days)**	

Activity	Time (Hours)	731C
26" (0-56 m)		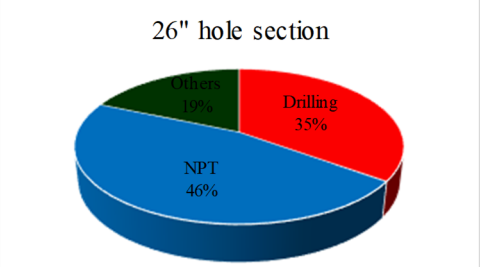
Drilling	49	
NPT (circulating and WOC)	65	
Others (Casing, cementing, spudding and Tripping	26	
Total	**140**	
17½" (56-333 m)		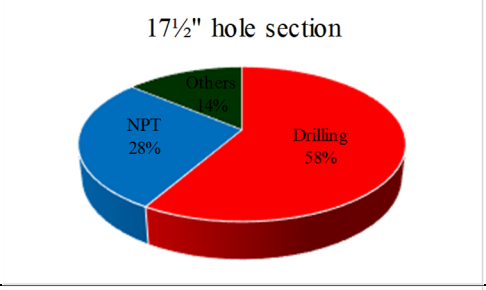
Drilling	206	
NPT (Reaming and WOC)	98	
Others (casing, cementing tripping and WHA	49	
Total	**353**	
12¼" (333-751 m)		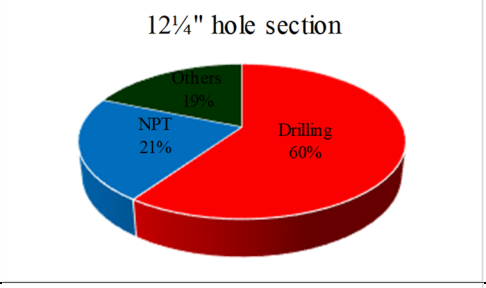
Drilling	185	
NPT (circulation, reaming and WOC)	67	
Others (casing, cementing, tripping and WHA)	58	
Total	**309**	
8½" (751-3000 m)		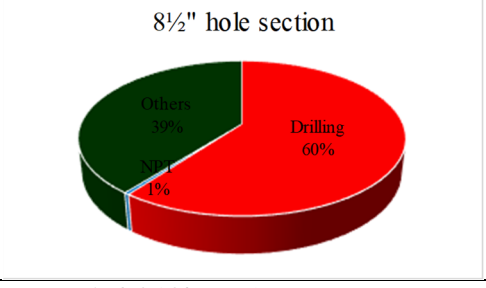
Drilling	442	
NPT (circulating)	3	
Others (casing, logging, rig down, WHA)	289	
Total	**734**	
Grand total	**1536 (64 days)**	

Activity	Time (Hours)	731D
26" (0-55 m)		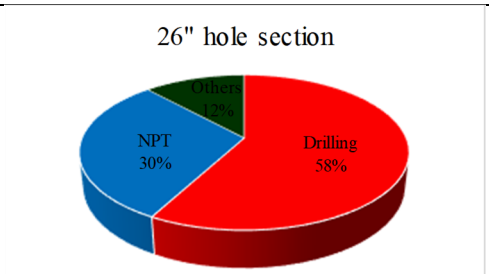
Drilling	88	
NPT (circulating and WOC)	46	
Others (casing, cementing, spud)	18	
Total	**152**	
17½" (55-300 m)		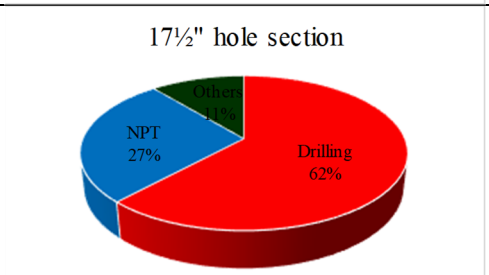
Drilling	213	
NPT (circulating, reaming and WOC)	93	
Others (casing, cementing, tripping and WHA)	38	
Total	**344**	
12¼" (300-755 m)		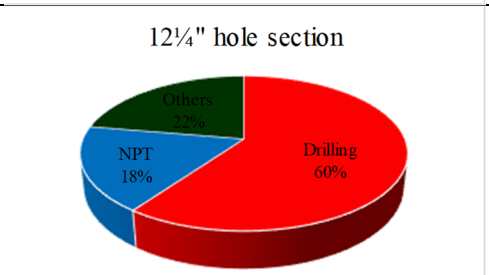
Drilling	172	
NPT (circulating, reaming and WOC)	51	
Others (casing, cementing, tripping, WHA)	64	
Total	**287**	
8½" (755-3010 m)		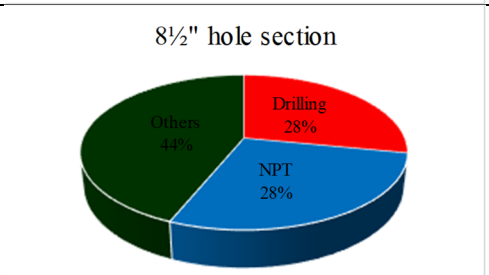
Drilling	495	
NPT (circulating, reaming, stuck casing , TOC, WOC)	495	
Others (casing, cementing, logging, rig down and WHA)	771	
Total	**1761**	
Grand total	**2544 (106 days)**	

APPENDIX B: Stress calculations of wells OW-731A, OW-731B and OW-731C

OW-731A											
Depth (m)		60	100	300	500	750	1000	1200	1500	2000	3000
BPD (MPa)		0.10	0.10	0.10	0.10	1.47	3.54	5.10	7.33	10.80	16.92
P_f (MPa)		0.69	1.08	3.04	5.01	7.46	9.91	11.87	14.82	19.72	29.53
Field stress (MPa)											
S_v		1.58	2.56	7.49	13.49	18.79	26.88	30.00	37.48	49.93	74.85
S_H		1.08	1.74	5.02	9.03	13.02	19.10	21.70	27.43	36.89	55.54
S_h		0.59	0.92	2.56	4.56	7.25	11.32	13.40	17.38	23.84	36.23
Transformed stresses in x, y and z coordinates (MPa)											
σ_x		1.08	1.74	5.02	7.58	11.14	16.58	19.01	24.17	32.65	49.27
σ_y		0.59	0.92	2.56	6.80	10.13	15.21	17.55	22.40	30.37	45.88
σ_z		1.58	2.56	7.49	12.71	17.78	25.52	28.54	35.71	47.65	71.46
τ_{xy}		0.00	0.00	0.00	2.10	2.71	3.66	3.90	4.72	6.13	9.07
τ_{xz}		0.00	0.00	0.00	-2.15	-2.78	-3.75	-4.00	-4.84	-6.29	-9.31
τ_{yz}		0.00	0.00	0.00	0.76	0.99	1.33	1.42	1.72	2.23	3.30
Circular stress components and principal stresses acting on the borehole wall at 0° and 90° (MPa)											
0°	$\sigma_{\theta\theta}$	-0.10	-0.16	-0.48	7.70	10.32	15.61	16.67	20.90	27.93	41.93
	σ_{zz}	1.23	2.05	6.16	11.22	14.79	20.29	21.72	26.50	34.71	51.85
	$\tau_{\theta z}$	0.00	0.00	0.00	1.53	1.97	2.66	2.84	3.44	4.46	6.61
	σ_{tmax}	1.23	2.05	6.16	11.79	15.54	21.50	22.99	28.13	36.92	55.15
	σ_{tmin}	-0.10	-0.16	-0.48	7.13	9.57	14.40	15.40	19.27	25.71	38.63
	σ_r	0.59	0.98	2.94	4.91	5.98	6.37	6.77	7.49	8.92	12.61
90°	$\sigma_{\theta\theta}$	1.87	3.12	9.37	10.84	14.37	21.07	22.50	27.95	37.08	55.49
	σ_{zz}	1.72	2.87	8.62	13.00	16.81	22.66	24.17	29.27	37.99	56.24
	$\tau_{\theta z}$	0.00	0.00	0.00	4.30	5.56	7.50	8.00	9.69	12.58	18.62
	σ_{tmax}	1.87	3.12	9.37	16.35	21.28	29.41	31.38	38.32	50.13	74.49
	σ_{tmin}	1.72	2.87	8.62	7.48	9.89	14.32	15.29	18.90	24.95	37.24
	σ_r	0.59	0.98	2.94	4.91	5.98	6.37	6.77	7.49	8.92	12.61

OW-731B											
Depth m		60	100	300	500	750	1000	1200	1500	2000	3000
BPD (MPa)		0.10	0.10	0.10	0.10	1.47	3.54	5.10	7.33	10.80	16.92
P_f (MPa)		0.69	1.08	3.04	5.01	7.46	9.91	11.87	14.82	19.72	29.53
Field stress (MPa)											
S_v		1.58	2.56	7.49	13.49	18.79	26.88	30.00	37.48	49.93	74.85
S_H		1.08	1.74	5.02	9.03	13.02	19.10	21.70	27.43	36.89	55.54
S_h		0.59	0.92	2.56	4.56	7.25	11.32	13.40	17.38	23.84	36.23
Transformed stresses in x, y and z coordinates (MPa)											
σ_x		1.08	1.74	5.02	7.58	11.14	16.58	19.01	24.17	32.65	49.27
σ_y		0.59	0.92	2.56	6.80	10.13	15.21	17.55	22.40	30.37	45.88
σ_z		1.58	2.56	7.49	12.71	17.78	25.52	28.54	35.71	47.65	71.46
τ_{xy}		0.00	0.00	0.00	-2.10	-2.71	-3.66	-3.90	-4.72	-6.13	-9.07
τ_{xz}		0.00	0.00	0.00	-2.15	-2.78	-3.75	-4.00	-4.84	-6.29	-9.31
τ_{yz}		0.00	0.00	0.00	-0.76	-0.99	-1.33	-1.42	-1.72	-2.23	-3.30
Circular stress components and principal stresses acting on the borehole wall at 0° and 90° (MPa)											
0°	$\sigma_{\theta\theta}$	-0.10	-0.16	-0.48	7.70	10.32	15.61	16.67	20.90	27.93	41.93
	σ_{zz}	1.23	2.05	6.16	11.22	14.79	20.29	21.72	26.50	34.71	51.85
	$\tau_{\theta z}$	0.00	0.00	0.00	-1.53	-1.97	-2.66	-2.84	-3.44	-4.46	-6.61
	σ_{tmax}	1.23	2.05	6.16	11.79	15.54	21.50	22.99	28.13	36.92	55.15
	σ_{tmin}	-0.10	-0.16	-0.48	7.13	9.57	14.40	15.40	19.27	25.71	38.63
	σ_r	0.59	0.98	2.94	4.91	5.98	6.37	6.77	7.49	8.92	12.61
90°	$\sigma_{\theta\theta}$	1.87	3.12	9.37	10.84	14.37	21.07	22.50	27.95	37.08	55.49
	σ_{zz}	1.72	2.87	8.62	13.00	16.81	22.66	24.17	29.27	37.99	56.24
	$\tau_{\theta z}$	0.00	0.00	0.00	4.30	5.56	7.50	8.00	9.69	12.58	18.62
	σ_{tmax}	1.87	3.12	9.37	16.35	21.28	29.41	31.38	38.32	50.13	74.49
	σ_{tmin}	1.72	2.87	8.62	7.48	9.89	14.32	15.29	18.90	24.95	37.24
	σ_r	0.59	0.98	2.94	4.91	5.98	6.37	6.77	7.49	8.92	12.61

OW-731C											
Depth m		60	100	300	500	750	1000	1200	1500	2000	3000
BPD (MPa)		0.10	0.10	0.10	0.10	1.47	3.54	5.10	7.33	10.80	16.92
P_f (MPa)		0.69	1.08	3.04	5.01	7.46	9.91	11.87	14.82	19.72	29.53
Field stress (MPa)											
S_v		1.58	2.56	7.49	13.49	18.79	26.88	30.00	37.48	49.93	74.85
S_H		1.08	1.74	5.02	9.03	13.02	19.10	21.70	27.43	36.89	55.54
S_h		0.59	0.92	2.56	4.56	7.25	11.32	13.40	17.38	23.84	36.23
Transformed stresses in x, y and z coordinates (MPa)											
σ_x		1.08	1.74	5.02	5.61	8.60	13.14	15.34	19.73	26.89	40.75
σ_y		0.59	0.92	2.56	9.03	13.02	19.10	21.70	27.43	36.89	55.54
σ_z		1.58	2.56	7.49	12.45	17.44	25.06	28.06	35.13	46.88	70.33
τ_{xy}		0.00	0.00	0.00	0.00	0.00	0.00	0.00	0.00	0.00	0.00
τ_{xz}		0.00	0.00	0.00	-2.87	-3.71	-5.00	-5.34	-6.46	-8.39	-12.41
τ_{yz}		0.00	0.00	0.00	0.00	0.00	0.00	0.00	0.00	0.00	0.00
Circular stress components and principal stresses acting on the borehole wall at 0° and 90° (MPa)											
0°	$\sigma_{\theta\theta}$	-0.10	-0.16	-0.48	16.37	21.52	30.71	32.79	40.41	53.26	79.43
	σ_{zz}	1.23	2.05	6.16	13.06	17.17	23.50	25.14	30.64	40.08	59.81
	$\tau_{\theta z}$	0.00	0.00	0.00	0.00	0.00	0.00	0.00	0.00	0.00	0.00
	σ_{tmax}	1.23	2.05	6.16	16.37	21.52	30.71	32.79	40.41	53.26	79.43
	σ_{tmin}	-0.10	-0.16	-0.48	13.06	17.17	23.50	25.14	30.64	40.08	59.81
	σ_r	0.59	0.98	2.94	4.91	5.98	6.37	6.77	7.49	8.92	12.61
90°	$\sigma_{\theta\theta}$	1.87	3.12	9.37	2.69	3.84	6.87	7.35	9.62	13.28	20.25
	σ_{zz}	1.72	2.87	8.62	10.64	13.75	18.54	19.78	23.95	31.09	46.02
	$\tau_{\theta z}$	0.00	0.00	0.00	5.74	7.42	10.00	10.67	12.92	16.77	24.83
	σ_{tmax}	1.87	3.12	9.37	13.64	17.72	24.29	25.91	31.55	41.17	61.11
	σ_{tmin}	1.72	2.87	8.62	-0.32	-0.13	1.13	1.22	2.01	3.19	5.17
	σ_r	0.59	0.98	2.94	4.91	5.98	6.37	6.77	7.49	8.92	12.61

APPENDIX C: Olkaria Wells OW-731 area map

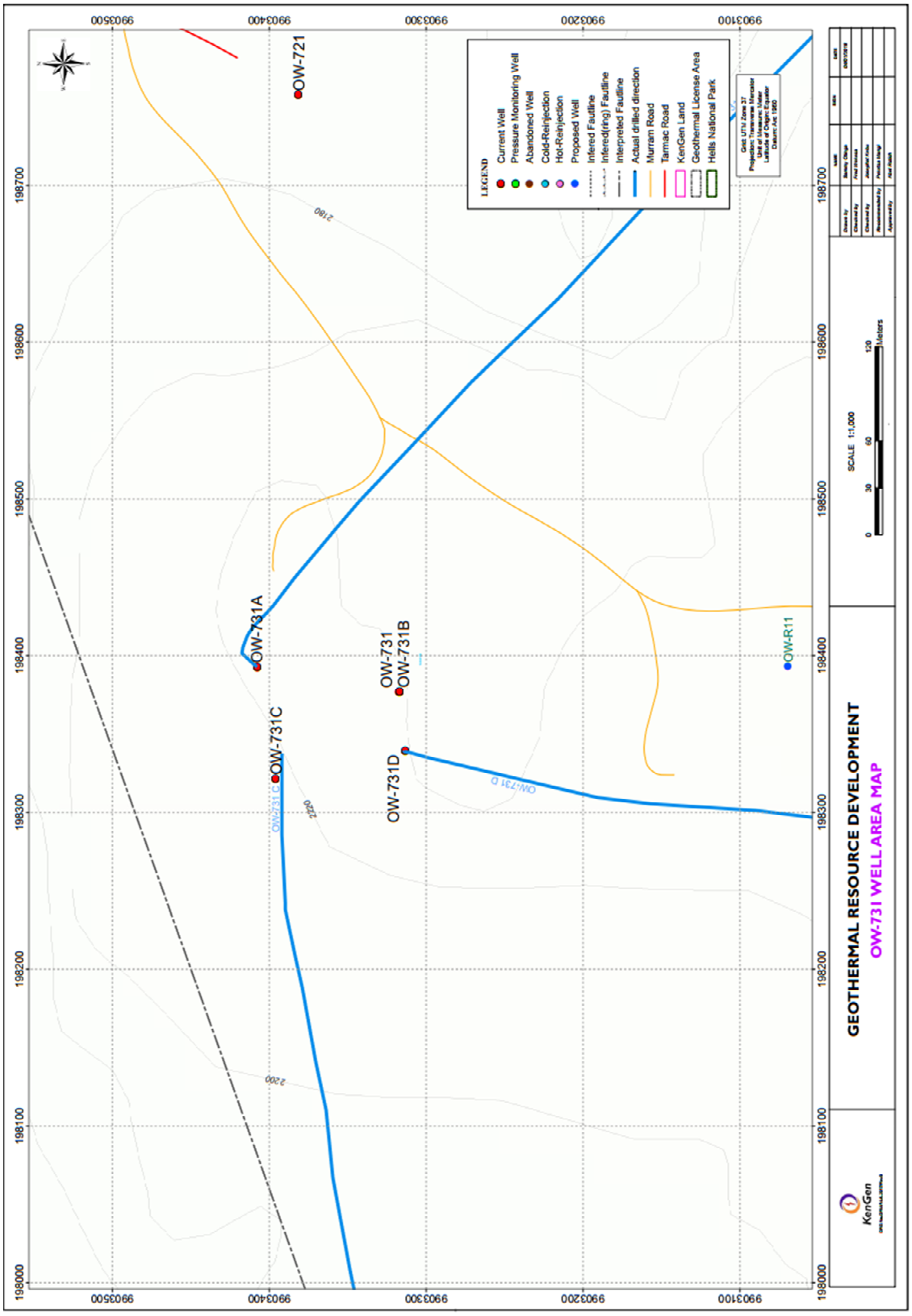

Figure 45: Area map of OW-731 showing location and direction of the wells

APPENDIX D: Drilling parameters recorded in RN-33

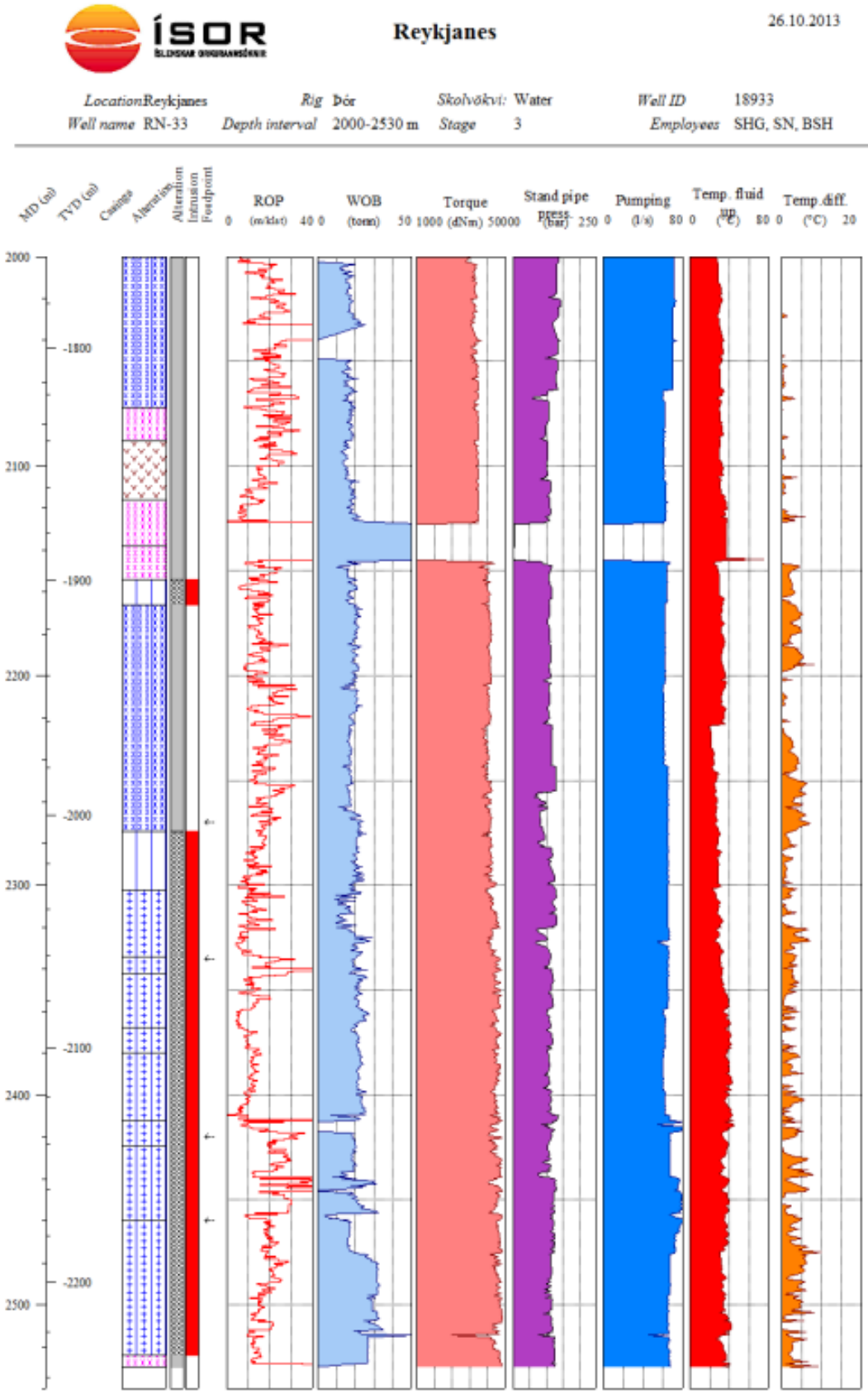

Figure 46: Drilling data compared to lithology at 2000-2530 m depth in RN-33 (Níelsson et al., 2014)

APPENDIX E: Rock properties (Turcotte and Schubert, 2014)

B.5 Properties of Rock

	Density $kg\ m^{-3}$	E 10^{11} Pa	G 10^{11} Pa	ν	k $W\ m^{-1}\ K^{-1}$	α $10^{-5}\ K^{-1}$
Sedimentary						
Shale	2100–2700	0.1–0.7	0.1–0.3	0.1–0.2	1.2–3	
Sandstone	1900–2500	0.1–0.6	0.04–0.2	0.1–0.3	1.5–4.2	3
Limestone	1600–2700	0.5–0.8	0.2–0.3	0.15–0.3	2–3.4	2.4
Dolomite	2700–2850	0.5–0.9	0.2–6.4	0.1–0.4	3.2–5	
Metamorphic						
Gneiss	2600–2850	0.4–0.6	0.2–0.3	0.15–0.25	2.1–4.2	
Amphibole	2800–3150		0.5–1.0	0.4	2.1–3.8	
Marble	2670–2750	0.3–0.8	0.2–0.35	0.2–0.3	2.5–3	
Igneous						
Basalt	2950	0.6–0.8	0.25–0.35	0.2–0.25	1.3–2.9	
Granite	2650	0.4–0.7	0.2–0.3	0.2–0.25	2.4–3.8	2.4
Diabase	2900	0.8–1.1	0.3–0.45	0.25	2–4	
Gabbro	2950	0.6–1.0	0.2–0.35	0.15–0.2	1.9–4.0	1.6
Diorite	2800	0.6–0.8	0.3–0.35	0.25–0.3	2.8–3.6	
Pyroxenite	3250	1.0	0.4		4.1–5	
Anorthosite	2640–2920	0.83	0.35	0.25	1.7–2.1	
Granodiorite	2700	0.7	0.3	0.25	2.0–3.5	
Mantle						
Peridotite	3250				3–4.5	2.4
Dunite	3000–3700	1.4–1.6	0.6–0.7		3.7–4.6	
Miscellaneous						
Ice	917	0.78	0.29	0.31–0.36	2.2	16

Turcotte and Schubert, 2014 – Figure 47